Investigations of the role of the Guanine nucleotide Exchange Factor ‚alpha-Pix' in the development of Marginal Zone B cells and their homeostasis within the Marginal Zone

Thesis

for the degree of

doctor rerum naturalium (Dr. rer. nat.)

approved by the Faculty of Natural Sciences
of Otto von Guericke University Magdeburg

by Dipl. Biochemist Michael Steiner

born on: 29 January 1979 in: Bad Salzungen

Examiner: Prof. Dr. rer. nat. Klaus-Dieter Fischer
Prof. Dr. rer. nat. Klaudia Giehl

submitted on: 18 February 2025
defended on: 29 October 2025

Table of Content

List of Figures

List of Tables

1. Introduction

1.1 The αPix protein is a guanine nucleotide exchange factor for the Rho GTPases Rac1 and Cdc42

1.1.1 Rho GTPases are guanine nucleotide binding proteins

Rho GTPases regulate the actin cytoskeleton, cell cycle and cell division, transcription of genes, phagocytosis, adhesion, migration, polarization, growth and survival of cells and the protrusion and retraction of neurites[3-6]. Abnormal regulation of Rho GTPases can lead to the development of malignant transformations by Ras and other oncogenes[7].

There are two types of guanine nucleotide-binding proteins (G proteins): membrane-associated, heterotrimeric G proteins (so-called large GTPases) and cytosolic Ras-like G proteins (so-called small GTPases). Small GTPases have a size of 21 kDa, therefore also called p21-GTPases. The GTPase Ras (Rat sarcoma) was first characterized in 1981. Since all small GTPases have a homologous tertiary structure to Ras, it was used to name the superfamily. The superfamily of Ras or p21 GTPases comprises over 150 members and is divided into 6 families: Ras-like, Rab-like, Arf-like, Ran-like, Sar-like and Rho-like. The family of Rho (Ras homologous) GTPases consists of 22 members[1]. The 22 members can be divided into 10 groups according to their homologies: Cdc42, Rac1, RhoA, RhoD, Rif/RhoF, Rnd3/RhoE, TTF/RhoH, Chp/RhoV, Miro1/RhoT1 or RhoBTB[2].

1.1.2 Cellular functions of Rho GTPases

Rho GTPases were discovered in all eukaryotes. Most Rho GTPases play a role in the movement of the cellular plasma membrane by regulating the membrane-associated cytoskeleton. The Rho GTPases Rac (Ras related C3 botulinum toxin substrate), Cdc42 (cell division cylce-42) and RhoA (Ras homologous member-A) have been the most intensively studied so far. Their functions have been described in filopodia, lamellipodia and stress fibres, three morphologically different structures that are the

basis for active movement processes of cells. These structures are regulated by different GTPases: Cdc42 and Rac1 regulate peripheral actin-polymerization in filopodia and lamellipodia, whereas RhoA regulates actin polymerization to form stress fibres. Stress fibres enable the build-up of contractile forces with the help of myosin II proteins. Filopodia are long, thin protuberances of a cell formed by long, parallel bundles of actin filaments with the same polarization. In contrast, lamellipodia are broad lamellar protuberances of a cell, the formation of which enables locomotion processes. In 2009, Machacek et al[8]. showed a visualization of the active conformations of the GTPases Rac1, Cdc42 and RhoA in MEF cells (embryonic mouse fibroblasts). In this study the activation of the three GTPases was analysed in a spatiotemporal coordinated manner. Activated RhoA was measured directly at the cell edge. In contrast, Rac1 and Cdc42 were activated 2 µm behind the cell edge. The activation of RhoA and Rac1 and Cdc42 respectively took place with a time shift of 40 sec and was of antagonistic nature. RhoA played a role in the initiation of extensions. Rac1 and Cdc42, on the other hand, played a role in the reinforcement and stabilization of newly formed appendages[8].

Other Rho GTPases, such as RhoG, RhoD, TC10 and Rif are also involved in the formation of actin-mediated protuberances[9-11]. For RhoA, RhoB, RhoD and Cdc42, a function in intracellular transport of vesicles, e.g. in exocytosis or in vesicular transport between the Golgi apparatus and the endoplasmic reticulum, could be shown[12,13].

Rho GTPases regulate the dynamics of cell membranes by interacting with membranes through posttranslational modifications (farnesylation or geranylgeranylation) or by being activated by membrane-associated guanine nucleotide exchange factors at the membrane. The different posttranslational modifications of the different Rho GTPases allow the action of different Rho GTPases at different intracellular loci, which is a prerequisite for directed cell movements[14]. Functional losses or deregulations of Rho GTPases may not only lead to cell degeneration and thus to tumour development, but also to neurodegenerative diseases[15].

1.1.3 The involvement of Rac and Cdc42 in B cell development

The role of Rac and Cdc42 during the development of B cells is not fully understood and still under investigation. Mice lacking the expression of Rac2 develop decreased B1a population and MZB with defective proliferation and calcium flux[1]. Rac2 is differentially expressed by hematopoietic cells and a Rac2 deficiency goes along with decreased IgM-secreting plasma cells and attenuated humoral immune responses. The loss of the ubiquitously expressed Rac1 alone is embryonic lethal[96]. However, the B cell specific impairing of Rac1 and Rac2 function simultaneously leads to a severe block in B cell development at an IgD-negative transitional B cell stage[97]. This is likely due to a survival defect resulting from defective activation of Akt and expression of anti-apoptotic Bcl-xl[96]. The B cell specific deletion of Cdc42 expression leads to a reduction of all splenic B cell populations and B1a cells, similar to Rac1/Rac2 double knock-out, but not to a migration defect as it was reported for Rac-2 ko B cells. Therefore, although both Cdc42 and Rac1/Rac2 are important in late B-cell development in the spleen by mediating B cell survival and proliferation, Rac1/Rac2, but not Cdc42, are required for B cell migration[1]. The B cell specific inactivation of Cdc42 leads to a dramatic reduction of mature recirculating B cells in bone marrow and lymph nodes and spleen. This was due to a reduced egress of immature B cells (IgD^- and IgD^{lo}) from bone marrow into sinusoids[162]. The MZB and B1 cell compartments were completely absent in spleen and peritoneal cavity,

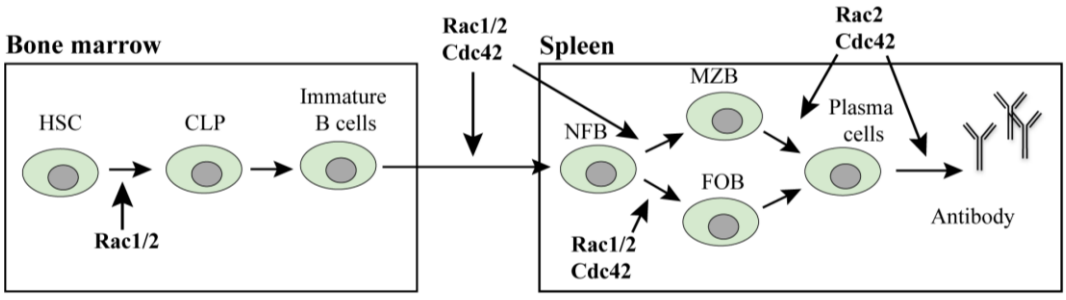

Figure 1: Involvement of Rho GTPases Rac1, Rac2 and Cdc42 in the development of B cells

Rac1 and Rac2 are important for common lymphoid progenitor (CLP) differentiation from hematopoietic stem cells (HSCs) in the bone marrow. Rac1, Rac2, and Cdc42 are critical for multiple stages of B cell development in the spleen, whereas Rac2, Cdc42 also regulate antibody production. Modified according to Mulloy, 2010[1].

respectively. It could be shown that Cdc42 plays also a role in early BCR signalling, antigen presentation and plasma cell differentiation[162]. This shows that Cdc42 participates at different stages during the development of B lymphocytes and their differentiation into effector or antibody secreting cells[162].

1.1.4 The reaction cycle of small GTPases

Rho GEFs activate Rho GTPases by catalysing the exchange of the GDP with GTP bound to the Rho GTPases (Fig. 2). The first Rho GEF was discovered in 1988 as a transforming factor in cells of diffuse B cell lymphoma[17] and was therefore named Dbl. Common to all Rho GEFs is a Dbl homologous (DH) domain, which is followed C-terminally by the so-called pleckstrin homologous (PH) domain (Fig. 3). The specific interaction of a Rho GEF with the Rho GTPase takes place on the surface of these two domains. The cell-specific expression of Rho GEFs enables different functions of a Rho GTPase in different cell types. To date, the family of Rho GEFs has grown to 82 members[121].

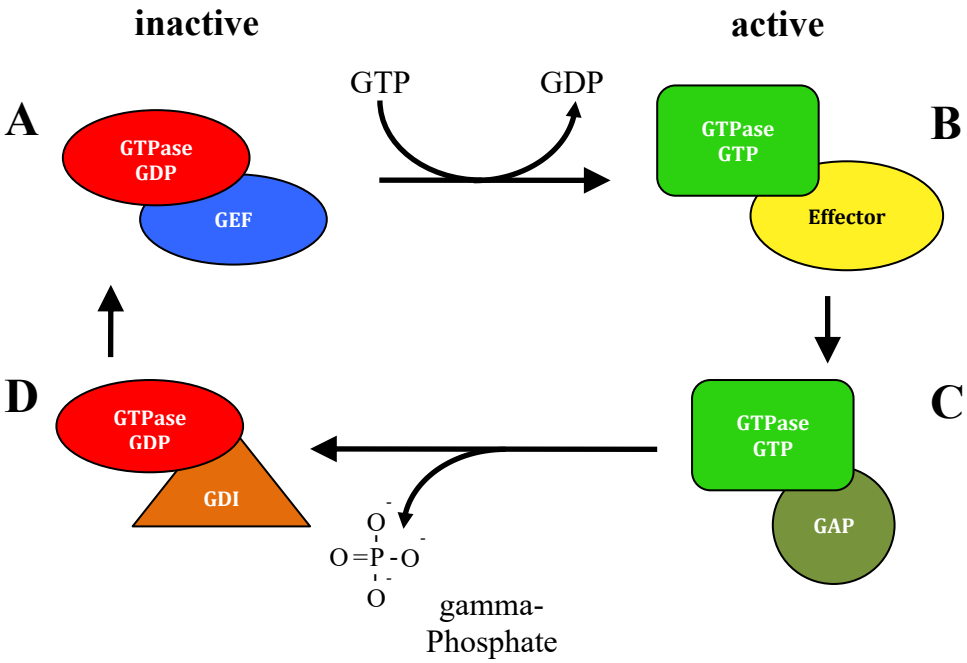

Figure 2: Regulation of the reaction cycle of small GTPases.

*The interaction of GTPases with effector molecules is regulated by the interaction with activating GEFs **(A)** or inactivating factors GAPs and GDIs **(C and D)**. The regulation of effector proteins is achieved by interaction of the GTPase in the active GTP-bound*

*state with the effector **(B)**. The GDP-bound state results from the enzymatic hydrolysis of GTP by the intrinsic GTPase activity and can be accelerated by interaction with GAPs **(C)**. The cleavage of gamma-phosphate from GTP induces a conformational change of GTPase. The GDP-bound conformation is the inactive conformation of GTPase, which can be stabilized by interaction with GDIs **(D)**. As a result, the GTPase can no longer interact with the effector, thus switching off the regulation of the effector by the GTPase*[16].

1.1.5 The Rho GEFs of the PIX family

PIX proteins were described in the late 1990s as direct interaction partners of p21-activated kinases (PAKs)[18, 19, 20], hence their name: PIX = PAK interacting exchange factor. Two genes are known: X-linked alpha-pix (αPix, Cool-2 or ARHGEF6) and beta-pix (βPix, Cool-1 or ARHGEF7), which is encoded on chromosome 8 in the mouse and on chromosome 13 in humans. In contrast to αPix, several βPix-species with different cellular localization have been described[21, 22, 23]. The family of PIX proteins consists of 3 members in total: αPix with a size of 90 kDa, βPix with a size of 85 kDa and p50, a splice variant of βPix with a size of 50 kDa24 (Fig. 3). The different PIX proteins have a different influence on the signalling of PAK. βPix has a stimulatory effect with respect to PAK activation, but is not able to directly activate PAK, whereas p50 has an inhibitory effect regarding the Cdc42/Rac stimulated PAK activation[20]. For αPix a strong PAK activation could be shown[24]. PIX proteins are Rho GEFs, which regulate the activity of the Rho GTPases Rac1 and Cdc42[18, 25]. For the activation of PAK by the Rho GTPase Cdc42 the interaction of PAK with αPix is necessary[26]. After activation of G-protein coupled receptors, PAK associates with the G(beta-gamma) subunit. The PAK-G(beta-gamma) complex stimulates the dissociation of the αPix dimer into the monomers. In the monomeric form αPix has GEF activity towards Cdc42. When activated, i.e. GTP-bound Cdc42 interacts with a monomer of αPix, the induced conformational change leads to an increase in GEF activity towards Rac[27, 28]. This could be a basic mechanism in cellular movement processes that enables the spatiotemporal coordination of the activity of Rho GTPases.

1.1.6 Structure and interactions of PIX proteins

PIX proteins interact with Rho GTPases through their Dbl-homologous (DH) and pleckstrin-homologous (PH) domains typical for Rho GEFs (Fig. 3). Furthermore, both PIX homologous form N-terminal a Src-homologous 3 domain (SH3) and C-terminal a GIT-binding domain (GBD). These domains allow interactions with proteins containing proline-rich sequences or with GIT proteins (see below: "The PIX-GIT complex"). Furthermore, αPix has a calponin-homologous (CH) domain

Symbol	Domain	Interaction partner
CH	Calponin homology domain	unkonwn
SH3	Src homology 3 domain	PAK, Rac, c-Cbl
DH	Dbl homology domain; catalytic domain	Cdc42, Rac
PH	Pleckstrin homology domain	Cdc42, Rac
T1	T1 insert	Src (Y442 (asterics))
PR	Prolin-rich region	POPX1, POPX2
GBD	GIT binding domain	Git-1, Git-2
CC	Coiled-coil regionwith putative leucine zipper	Dimerization
ZB	PDZ domain binding motive	Scribble, Shank
C	Alternative spliced carboxy-terminal region	

Figure 3: Domain structure of PIX proteins

The figure shows the domain structure of αPix (Cool-2), βPix (Cool-1) and a splice variant of βPix (p50Cool-1). All three proteins show the domain tandem typical for Rho GEFs, consisting of the DH and PH domain. This DH-PH cassette is used for the interaction of the Rho GEF with the GTPase. Pix proteins form additional domains for interaction with other proteins (see interaction partners). From Frank & Hansen 2008[29].

with unknown function, which is not present in ßPix[29].

The PIX-PAK interactions play an important role in processes such as morphological changes or migration of cells[30]. This is also shown by the association of αPix with paxillin in focal adhesions[25] and by the high accumulation of αPix in the focal complexes of Rac or Cdc42 overexpressing cells[18]. Focal adhesions are macromolecular protein complexes on the inner plasma membrane of cells that connect the cytoskeleton with the extracellular matrix. In addition, focal adhesions provide platforms for complex bidirectional signalling to control cellular adhesion and migration[31-33].

1.1.7 The PIX-GIT complex

PIX proteins also interact with G-protein coupled receptor kinase interacting (GIT) proteins (Git-1 and Git-2) to form a stable complex called the PIX-GIT complex with a size of 1 to 2 MDa[34,35]. The PIX-GIT complex acts as a macromolecular platform that coordinates the cellular localization and activation of GTPases in focal adhesions[29]. To this end, a number of proteins interacting with the PIX-GIT complex have been described that have important functions in the regulation of the cytoskeleton and vesicle transport or turnover between the plasma membrane and endosomes. These include the G-protein coupled receptor kinases (GRK)[36], which regulate phosphorylation and internalization of receptors, Scribble[37,38], a tumour suppressor that regulates cell movement and adhesion, Paxillin[36] and FAK[39,40] (focal adhesion kinase), focal adhesion proteins and the signal transduction factor phospholipase C gamma[41]. GIT proteins are GTPase activating proteins (GAP) and can stimulate the GTPase activity of Rho GTPases (Fig. 2). This can accelerate the hydrolysis of the GTP bound to the GTPase, resulting in the GDP-bound state of the GTPase and a shutdown of the GTPase-mediated signal transduction.

1.1.8 Cellular functions of PIX proteins

In the mouse, PIX proteins are mainly expressed in thymus, lymph node and spleen tissue, i.e. by hematopoietic cells. Compared to αPix, βPix shows a broader spectrum

and a higher level of expression, besides hematopoietic cells mainly in brain, lung, muscle, testis and ovaries[42].

A role of the PIX/GIT complex in the development and communication of neuronal cells was described. In the morphogenesis of dendrites and formation of synapses, especially βPix and Git-1 play a role[43]. In contrast, αPix is necessary for the differentiation of neurons in the hippocampus[44]. The loss of αPix in humans leads to mental retardation[45-47].

αPix together with Pak4 controls the size and number of podosomes[48] by a locally restricted regulation of actin dynamics in macrophages. Podosomes are typically found in cells that have to overcome tissue barriers (e.g. macrophages, dendritic cells and osteoclasts). Podosomes are highly dynamic ring-like structures that protrude into the extracellular matrix. They are associated intracellularly with actin and actin-regulating proteins and extracellularly with integrins and complement receptors[49, 50].

In neutrophils, cells of hematopoietic origin, αPix and Git-2 are involved in the cell polarization and coordination of chemotactic movement processes[51, 52]. In lymphocytes, αPix plays not only a role in the formation of the immunological synapse between activated B and T cells and in the signalling of activated antigen receptors (BCR and TCR), but also in the control of migration processes[42, 53]. It could be shown, that the loss of αPix[54] and Git-2[55] leads to defects in positive selection during the development of thymocytes. This defect was attributed to an increased motility of αPix and Git-2 deficient thymocytes, which in turn leads to inefficient interactions with other cell types.

αPix is also involved in the negative regulation of the homeostasis of the marginal zone B cell population[42].

1.2 Marginal zone B cells and their differentiation and role in immune responses

1.2.1 Classification of marginal zone B cells

Marginal zone B cells are lymphocytes and represent a subpopulation of the B cell compartment. The B cell population is responsible for the humoral immune response and is therefore an essential part of the mammalian immune system. The B cell compartment can be divided into subtypes, in B1 and B2 cells.

B1 cells mainly occur in the peritoneum and are classified by their CD11b, CD43 and CD5 expression[56, 57]. B1 cells express a highly polyspecific repertoire of B cell receptors with low affinity and therefore recognize a broad spectrum of antigens. They produce the majority of the so-called natural serum IgM and IgA globulins in the gut and contribute mainly to unspecific defence reactions. Interestingly, the neonatal B cell compartment consists of B1 cells, exclusively[58-60].

The population of B2 cells can be further divided into follicular B cells and marginal zone B cells (MZB). MZB differ from follicular B cells in a number of parameters and represent a separate B cell type[61, 62]. The most obvious difference is the localization in the organism, which is the reason for their naming. Follicular B cells are recirculating and fill the majority of all secondary lymphatic organs of the organism. In the mouse, on the other hand, the non-recirculating MZBs are found only in the spleen. There they are mainly located in the marginal zone, a blood-flow-through structure that enables the filtering of antigens contained in the blood[63]. The relative number of MZB in the mouse is 4 - 7% of all splenic B cells (Fig. 14).

The anatomy of the human spleen and the characteristics of human MZB differ in a number of parameters from that of the mouse. Human MZB are recirculating. Since the genes of their B cell receptor carry somatic mutations, they are often referred to as IgM memory cells. In contrast, murine MZB do not show somatic mutations of the B-cell receptor. In the human spleen, the B cell follicles are not separated from the MZ by a marginal sinus. The differentiation of the MZ from the B cell follicle only becomes clearly visible in the course of a germinal centre reaction. Nevertheless, MZB are also exposed to the bloodstream in humans, so the contact of MZBs with blood-borne antigens is also possible[64].

1.2.2 The differentiation of marginal zone B cells

Hematopoietic stem cells assemble the B-cell antigen receptor complex in the bone marrow and differentiate via pre- and pro-B cells into highly self-reactive immature B cells. Only immature B cells with low or no self-reactivity differentiate further into so-called transitional (T) B cells. There are three types based on their CD93 and CD23 expression: T1, T2 and T3 B cells[65]. A quarter of the developing B cells mature into follicular B cells in the bone marrow. The majority, however, migrate into the spleen as transitional B cells and differentiate there into follicular B cells or MZB[66, 67] (Fig. 4). It is assumed that MZB develop from T2 B cells and T2 B cells develop from T1 precursors. Essentially, four mutations are known to lead to an altered development of MZB. This concerns signalling pathways of the B cell receptor, Notch-2 as well as the BAFF receptor and NF-kappaB and mutations that influence adhesion and migration properties of MZB[62, 74] (e.g. ICAM[68], S1PR1[69], CB2[71], CXCR7[72], SWAP70[73], Tab. 1,). A weak signal strength of the B cell receptor leads to the development of MZB, whereas a strong signal of the B cell receptor leads to the development of follicular B cells. B cells from so-called QM mice express a low-affinity transgenic 'quasi-monoclonal' B cell receptor, which is associated with a decreased signalling of the B cell receptor[75]. In these mice the MZB population is highly elevated compared to follicular B cells[76]. In contrast, B cell receptor signalling mutants show decreased relative numbers of MZB. Aiolos is an attenuator of B cell receptor signal strength and Aiolos deficient mice have defective MZB development[77]. CD22 also has an inhibitory function in signalling the B-cell receptor. CD22 deficient mice also form reduced MZB populations[78]. Other stimuli are also important in the development of MZB. MINT is an inhibitor of the Notch-2 signalling pathway and is much more strongly expressed by follicular B cells compared to MZB[79], with other words the Notch-2 signalling pathway is more prominent in MZB. Delta-like-1 (DL-1) is a ligand for the Notch-2 receptor and is formed by the endothelial cells in the venules of the spleen[80] (Fig. 3). The presence of this ligand and the expression of Notch-2 by MZB is essential for the development of MZB[81]. BAFF is a cytokine produced by follicular dendritic cells in the B cell follicle and plays a role in survival rather than differentiation of follicular B cells. The BAFF receptor activates the NF-kappaB signalling pathway and plays a role as survival signal in the differentiation process of T2 progenitor cells[82-84]. p50-REL and p50-RelA are heterodimeric transcription factors of the NF-kappaB signalling

pathway. Mutations of the monomeric components p50 (NFkappaB1), REL (c-REL) and RELA (p65) respectively lead to defective MZB development[85].

In addition, cellular interactions with significance in MZB development have been reported. CD1d is strongly expressed by MZB and is an MHC-I molecule, which is specifically recognized in complex with α-galactosylceramide by the TCR of invariant natural killer T cells of type 1, so-called iNKT cells[86]. Invariant natural killer T cells induce CD1d-mediated apoptosis in MZB and thus regulate the homeostasis of the MZB population in a negative way[87].

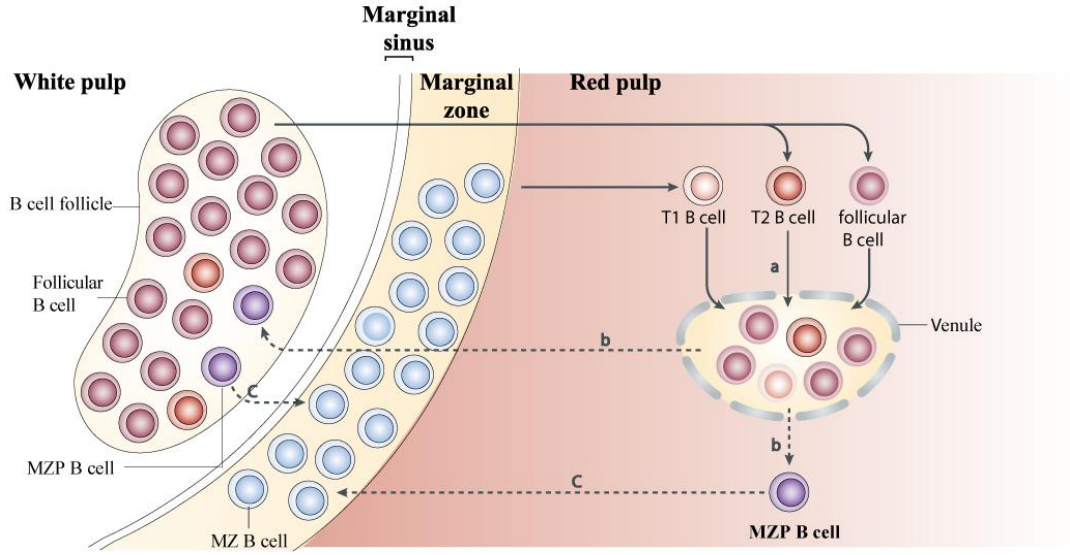

Figure 4: Model for the development of MZ B cells in the spleen

A model for the development of marginal zone (MZ) B cells is shown. (a) T1 B cells, T2 B cells or follicular B cells with weak autoreactivity or BCR signals to endogenous antigens reach the red pulp and the red pulp veins. In the case of T1 B cells, this can happen shortly after leaving the bone marrow by entering via the marginal zone. T2 B cells and follicular B cells coming from the B cell follicle must cross the marginal sinus to enter the red pulp and the red pulp veins via the marginal zone or reach the red pulp veins via the so-called bridging channels. (b) In the fenestrated lumen of the red pulp veins, B cells receive inductive signals from DL-1 (delta-like-1, ligand of Notch-2), causing the precursors to differentiate into MZ precursor (MZP) B cells. MZP B cells remain briefly in the red pulp or enter the B cell follicle via CXCL13. (c) MZP B cells then reach the marginal zone either S1P-mediated from the B cell follicle or migrate directly from the red pulp into the marginal zone where they differentiate into MZ B cells. Modified according to Pillai and Cariappa 2009[62].

Although great progress has been made in recent years in elucidating mechanisms, the development and homeostasis of MZB is still not understood in detail. An overview of mouse models with effects on the MZB population is presented in Tables 1A and 1B.

Table 1A: Mouse models with decreased population of marginal zone B cells relative to follicular B cells

Defective factor	**Description of defective factor Effect on MZB population**
CD19 ko[88]	BCR co-receptor, no MZB in CD19 ko mice
Aiolos[77]	BCR attenuator (enhanced BCR signal in knock out) No MZB in Aiolos ko mice
CD22[78]	BCR co-receptor, inhibitor (enhanced BCR signal in knock out) No MZB in CD22 ko mice
SHIP[89]	Negative signalling inositol phosphatase, macrophages dislocalize in the red pulp No MZB in Ship ko mice
Akt1/2[90]	Serine/threonine kinase, no MZB in Akt1/2 double ko mice
Pyk-2[91]	Tyrosine kinase, regulation of signalling pathways of receptors for chemokines and growth factors with a role in Ras-, MAP kinase-, PKC- und Inositol phosphate pathways Reduced motility of B cells No MZB in Pyk-2 ko mice
Lsc[92]	GEF for Rho, no MZB in Lsc ko mice
SWAP70[73,93]	Expression in B- but not in T-cells, interacts with Rac (actin remodelling) 2-fold reduction of MZB population in SWAP70 ko mice[73]
Rap1b[94]	small GTPase (Ras superfamily) PI3/Akt pathway, MEK/ERK pathway, regulation of activity of all MAPK and JNK 3-fold reduction of MZB population in Rab1b ko mice
RAC[95-97]	Rac1 and Rac2 are Rho GTPases arrest of B cell development at stage of recirculating MZB precursors, which cannot migrate into the spleen[97] 5-fold reduction of MZB population in Rac2 ko mice
Notch-2 – DL-1[80,81,98]	DL-1 (delta-like-1) is a ligand of Notch-2 receptor No MZB in DL-1 mice No MZB in Notch-2 ko mice

Tabel 1A continued from previous page

Defective factor	Description of defective factor Effect on MZB population
CB2[71,99]	CB2 (Cannabinoid receptor-2), holds MZB in spleen 3-fold reduction of MZB population in CB2 ko mice
NF-kappaB[85]	nuclear factor 'kappa-light-chain-enhancer' of activated B-cells is a heterodimeric transcription factor (p50-p65 or p50-cRel) 3-fold reduction of MZB population in p50 ko, p65 ko and c-Rel ko mice
Sly-1[100]	Adaptor protein with SH3 domain in lymphocytes, phosphorylation upon activation of antigen receptor 3-fold reduction of MZB population in Sly-1 ko mice

Table 1B: Mouse models with increased population of marginal zone B cells relative to follicular B cells

Defective factor	Description of defective factor Effect on MZB population
QM mice[75,76]	Low affinity BCR 4-fold increase of MZB population in QM mice
Btk[77,101]	Bruton's tyrosine kinase Increased MZB population in Xid und Btk ko mice
MINT[79]	Inhibitor of Notch-2 pathway 3-fold increase of MZB population in MINT ko mice
Mertk[102]	Mer Tyrosine kinase, expressed by macrophages and dendritic cells 2-fold increase of MZB population in Mertk ko mice, increased immune response
αPix[42]	GEF for Rac and Cdc42, interacts with Git-2 2-fold increase of MZB population in αPix ko mice
S1PR1[69]	S1P receptors 1 2-fold increase of MZB population in S1PR1 ko mice
Foxo1[103]	Transcription factor, CD19-PI3K-Akt-Foxo1 3-fold increase of MZB population in Foxo1 ko mice
Klf-2[104,105]	Transcription factor, expressed by follicular B cells but not by MZB 6-fold increase of MZB population in Klf-2 ko mice
Klf-3[106,107]	Transcription factor No MZB in Klf-3 ko mice[107] Increased MZB population when Klf-3 is over expressed[106]
iNKT cells[87]	Invariant natural killer T cells Negative regulation of MZB homeostasis by iNKTs cells

1.2.3 The biological function of Marginal zone B cells and their role in immune responses

The biological function of B lymphocytes is the production of antibodies and their secretion into the blood. In this way, they ensure humoral immunity against pathogenic antigens. MZB fulfil a special function here. On the one hand, they ensure a certain basic immunity by secreting so-called autoantibodies into the circulation and, on the other hand, they are responsible for a first rapid early defence against blood-borne antigens or pathogens[108, 109]. In contrast to follicular B cells, they are able to do this mainly due to their special localization in the marginal zone of the spleen[108, 110].
Several factors are already known to play a role in the correct positioning of MZB in the spleen and thus in their biological function, e.g. follicular shuttling (Fig. 5). Besides S1PR1, interleukin-7 is also important for the positioning of MZB in the MZ[111]. If the adhesion molecules LFA-1 and VLA-4 are inhibited, MZB are flushed with the blood flow from the MZ into the periphery[68]. This is also true for the cannabinoid receptor-2 (CB2)[99, 112]. Pharmacological inhibition of the chemokine receptor CXCR7 also leads to a reduction of the MZ population in the spleen[72]. CXCR7 is expressed by MZB but not by follicular B cells and recognizes the chemokine CXCL12. However, the role of blood-flow induced shear stress in the MZ was not investigated yet.
MZB are significantly involved in thymus-independent (TI) immune responses, but also play a role in the initiation of thymus-dependent (TD) immune responses (see below). For an efficient immune response, interactions of MZB with other cell types are required with respect to their function within a defence reaction (Fig. 4). Without marginal zone macrophages (MZM) in the MZ, MZB are not able to localize in the MZ[89]. MZB regulate the SIGN-R1 expression of marginal zone macrophages, which in turn is necessary for antigen binding by MZB[113]. Antigen binding by MZB is also supported by blood-exposed dendritic cells[114]. MZB filter complement-associated immune complexes from the blood and pass them through cell-cell interactions on to follicular dendritic cells[115] located in the B cell follicle[127]. Furthermore, in contrast to follicular B cells, MZB have the potential to directly activate CD4 T cells[116]. Support of the CD8 T cell response against blood-borne viruses by MZB could also be shown[117].

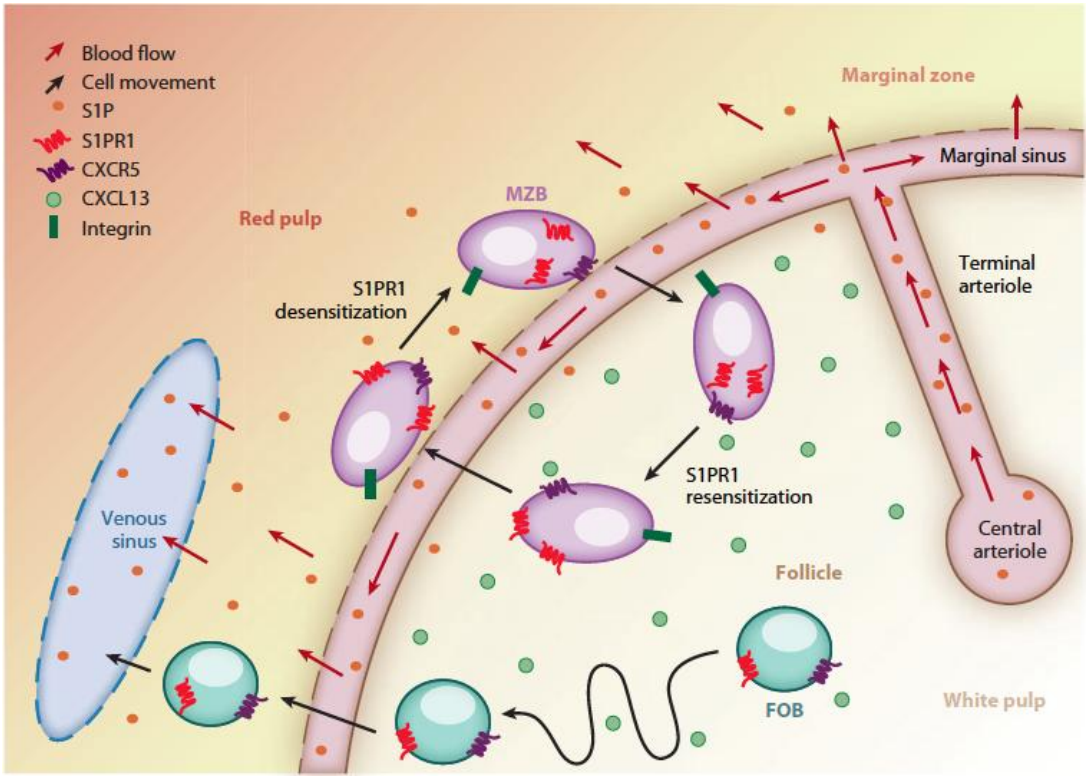

Figure 5: Molecular mechanisms underlying the shuttling of marginal zone B cells between the marginal zone and the B cell follicle.

The figure shows a schematic section of the white pulp with the adjacent marginal zone and red pulp. The red arrows show the direction of blood flow and the black arrows show the direction of cell movement.
The blood reaches the marginal sinus and the marginal zone through the central arteriole. In the blood-flowing compartments of the spleen, the concentration of S1P is higher compared to the bloodless compartments (white pulp). The concentration of CXCL13 is highest in the B-cell follicle.
Marginal zones B cells localize in the marginal zone due to their strong S1PR1 expression. Due to the ligand-induced internalization of S1PR1, MZB become desensitized to the S1P stimulus after a certain period of time and become sensitive to CXCL13, whereupon marginal zone B cells migrate into the B cell follicle in response to the CXCL13 stimulus. Due to the low concentration of S1P in the B cell follicle, S1PR1 is resensitized. MZB then migrate back into the marginal zone where they reposition themselves due to integrin-mediated adhesion. Follicular B-cells that are near the marginal sinus can also migrate S1PR1-directed into the marginal zone. Due to their lower expression of integrins, follicular B cells are flushed into the red pulp and enter the circulation. S1P: sphingosine-1 phosphate; S1PR1: S1P receptor-1; CXCR5: chemokine (C-X-C motif) receptor 5; CXCL13: chemokine (C-X-C motif) ligand 13, modified according to Cyster & Schwab, 2012[131].

The transport of complement-associated immune complexes from the blood into the blood-free B cell follicles of the spleen is realized by MZB in a process called 'follicular shuttling'[126] (Fig. 6). In the B cell follicle, the antigens are transferred to follicular dendritic cells for antigen presentation[115, 118, 124]. In this way, MZB fill the gap between innate and adaptive immunity. Antigens are differentiated according to the type of immune response they trigger. A distinction is made between thymus-independent (TI) and thymus-dependent (TD) antigens. TD antigens are proteins and hapten-protein conjugates. TI antigens are e.g. components of encapsulated bacteria such as lipopolysaccharides (LPS) or lipids and are further subdivided into TI-1, e.g. LPS and TI-2 antigens, e.g. Ficoll. The different immune responses occur with the participation of different cell types. Thus, different mouse models with different cellular defects show different or even no immune responses to corresponding antigens. The formation of an immune response in so-called Nu/Nu and Xid mice is the basis for this classification. Nu/Nu mice do not develop a thymus, thus this strain is T cell-deficient, whereas no B cells are formed in Xid mice. Nu/Nu mice are not able to respond immunologically to TD antigens. Nu/Nu and Xid mice are able to respond to TI-1 antigens. In contrast, the TI-2 immune response is also defective in B cell-less Xid mice.

Follicular B cells have their biological function in the defence against TD antigens. For the processes of class change and affinity maturation of immunoglobulins MHC-II restricted costimulatory signals of T2 helper cells in the course of a TD immune response are essential. In contrast, MZB are more involved in the immune responses against TI antigens. This is possible due to their special properties compared to follicular B cells. MZB show in comparison to follicular B cells a lowered threshold for their activation. Furthermore, localization in the MZ brings the MZB into direct contact with antigens contained in the blood, which is not possible for B cells residing the B cell follicle. Due to their localization in the blood perfused marginal zone and the increased expression of the complement receptor 1/2 (CD21/CD35), MZB are able to bind antigens contained in the blood efficiently and to respond to them rather unspecifically but very quickly. In this respect, the secretion of IgM and IgG3 globulins is the typical TI-2 immune response. Class change and somatic hypermutation of immunoglobulins is a typical characteristic of follicular B cells in the course of the germinal centre reaction. It is assumed that murine MZB are not capable of this. It could be shown that a strong MZB-mediated IgG3 production occurs

only in the presence of all spleen cells, i.e. with participation of follicular B cells and T cells[61, 119].

Since MZB is only found in the spleen, the spleen is the lymphoid organ responsible for defence against TI antigens. However, the detailed cellular and molecular mechanisms of this MZB-induced and/or -associated immune responses are not yet fully understood. For example, the cellular source of IgG3 has not yet been clearly identified.

1.2.4 The marginal zone – the anatomy and its importance for the function of MZ B cells

The marginal zone of the spleen represents an anatomically unique niche in the organism, which makes the immunological function of MZB possible. It is a discrete compartment of the spleen, which separates the white pulp from the red pulp (Fig. 3 and 5).

The white pulp resembles the anatomy of lymph nodes and is a bloodless compartment. It consists mainly of B and T lymphocytes, which are spatially separated in the T cell zone and B cell follicle (Fig. 4 and 5). The so-called marginal sinus consists of endothelial cells and represents the outer boundary of the white pulp and the inner boundary of the MZ. Towards the outside the MZ transitions into the red pulp. The red pulp is a reticular fibre network through which blood flows and in which the mechanical filtering of old or dying erythrocytes takes place.

The central arteriole crosses the white pulp, branches and ends openly after the marginal sinus (MS), so that the blood pours into the lumen of the MZ. That means similar to red pulp the blood flows also through the MZ. This does not apply to the B cell follicles, which are part of the white pulp of the spleen and not exposed to the blood (Fig. 6). Thus, in contrast to follicular B cells, MZB come constantly into direct contact with antigens contained in the blood. Cells localized in the white pulp are involved in adaptive immune responses, whereas cells localized in the MZ are specialized in the initialization of innate immune responses. One of the most important properties of the marginal zone is the adjustment of the optimal speed of the blood flow for antigen binding by MZB. This is based on a physical effect that is caused by

the change of the volume during the transition from blood vessel to MZ, while blood pressure remains constant. Only this creates conditions in the MZ that enables MZB the binding of antigens contained in the blood[63, 110].

For antigen presentation and therefore for induction of immune responses MZB transport blood-borne antigens into the white pulp by a process called follicular shuttling (Fig. 6). It is hypothesized that MZB are able to modulate the chemotactic potential of CXCL13 through the S1P-S1PR1 interaction, allowing MZB to shuttle between the marginal zone and the B cell follicle[126]. In the proposed model, S1PR1 functions one receptor hierarchy higher than CXCR5, i.e. the presence of S1PR1 on the surface of MZB overcomes or suppresses CXCR5 function. The binding of S1P in the marginal zone to S1PR1 of MZB results in its internalization into MZB. This ligand-mediated inactivation of S1PR1 increases the sensitivity towards the

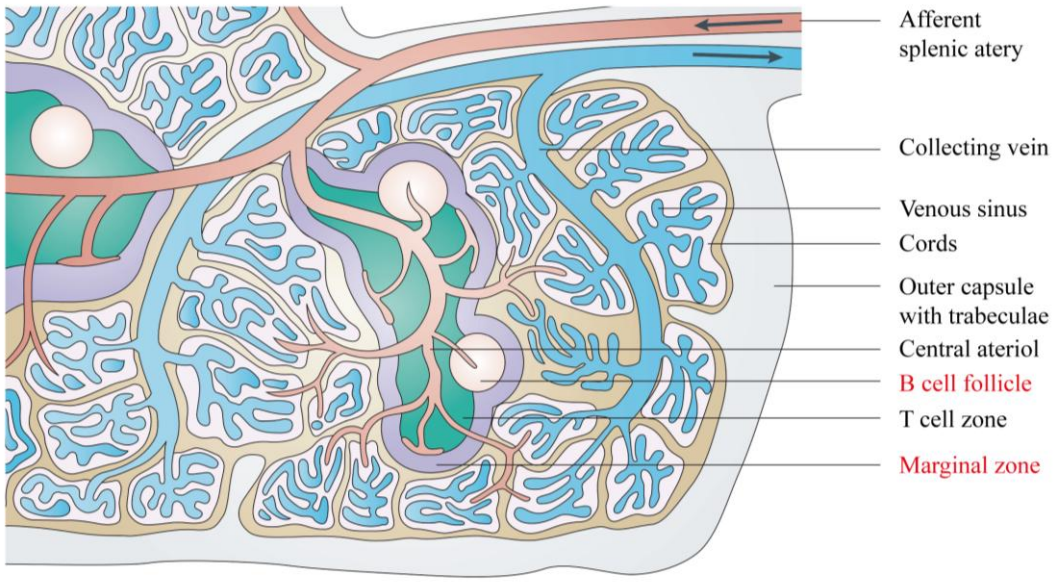

Figure 6: Anatomy of the murine spleen

The arterial blood vessel branches out into the central arterioles. The central arterioles are surrounded by the white pulp. The white pulp consists of the B cell follicles and the T cell zone (also known as periarteriolar lymphoid sheath or PALS). The arterioles end in the connective tissue of the red pulp. From the connective tissue, the blood passes through the venous sinus into the venous blood vessels. The larger arterial and venous blood vessels run together in the outer capsule of the spleen. Modified according to Mebius and Kraal, 2005[120].

chemotactic potential of MZB towards CXCL13, causing a CXCR5-mediated migration of MZB into the B cell follicle. How MZB can detect the CXCL13 secreted by FDC in the B cell follicle despite the presence of blood flow and the MS as physical barrier and if the blood flow plays a role at all in this process is still unclear. However, due to the much lower S1P concentration in the lymphoid tissue, S1PR1 re-accumulates at the MZB surface, causing MZB to relocalize into the marginal zone by its chemotaxis against the S1P gradient. Although it could be shown that GRK-2 plays a role in ligand-induced S1PR1 internalization[132], the molecular mechanisms in the regulation of cell positioning during the follicular shuttling process and the role of blood flow of MZB still needs to be described.

It could be shown that S1PR3 is involved in the regulation of splenic cells generating the MZ architecture[70]. Compared to FOB S1PR3 is highly expressed by MZB[69]. S1PR3 deficient MZB are not able to sense S1P gradients in vitro, since in transwell assays MZB cannot be attracted by S1P gradients[70]. Although, S1PR3 deficient MZB localize normal into the MZ in vivo[70], due to their normal S1PR1 function, they show increased activation induced migration from MZ into the B cell follicle[69]. However, the role of S1PR3 in the MZ localization and the follicular shuttling of MZB in vivo is still not understood.

2. Aims of the project

The basis for an effective clearance of blood-borne antigens are fine regulated processes during the differentiation, homing, activation and communication of immune cells. These fine regulated processes lead to the induction of directed effector functions, like the activation of B lymphocytes and their maturation to antibody secreting plasma cells. The cells of the lymphoid tissue are highly motile even between organs, since they develop in the bone marrow, home via the blood and lymphoid vessel systems to their special locations in secondary lymphoid organs. The underlying migratory processes are crucial to get immune cells activated at the optimal location and time to finally contribute to an effective immune response. The motility of cells is realized by their polarization through the spatiotemporal regulated action of Rho GTPases and asymmetric assembly and disassembly of integrin complexes. Thereby, Rho GTPases regulate the activity of p21 activated kinase (PAK) and PAK signalling affects cytoskeletal rearrangements and gene expression. The activity of the Rho GTPases Rac and Cdc42 is regulated by the RhoGEF αPix, which is mainly expressed by cells of the hematopoietic system.

Since mice lacking the expression of αPix develop increased relative numbers of marginal zone B cells (MZB) in the spleen, the developmental stages of MZB progenitor cells in bone marrow and spleen should be investigated in a first approach to discover a stage of MZB differentiation at which αPix is involved in the negative regulation of the MZB development.

It could be shown that lymphocytes lacking αPix are highly motile. However, data for MZB are not available so far. Since MZB are known to be highly dynamic in vivo for example during their positioning in the marginal zone and the process of follicular shuttling between the marginal zone and the B cell follicle, the impact of αPix deficiency on MZB motility and the homeostasis of the MZB population in the marginal zone should be investigated in vivo in a second approach.

3. Materials and Methods

3.1 Materials

3.1.1 Devices

Device	Designation	Company
Flow cytometer	BD FACSCanto™ II	BD Bioscience
Cell sorter	AutoMACS Pro Separator™	Miltenyi Biotech
Tissue dissociator	GentleMACS Dissociator™	Miltenyi Biotech
Microscope	Leica DMI6000B	Leica Microsystems
Flow generating pump	Ibidi Pump System	Ibidi
Microtome	Leica CM3050 S	Leica Microsystems
Irradiation device	Biobeam8000	Gamma-Service Medical GmbH
Centrifuge	Heraeus Multifuge 3SR+	Thermo Scientific
Shaker mixer	NeoLab 7-2020	NeoLab
Cell incubator	HERAcell 150	Thermo Scientific
sterile work bench	HERAsafe KS	Heraeus
Pipette	1000, 200 and 20 µl	Gilson Inc.
Pipette	250 and 100 µl	Eppendorf
Pipette	2,5 µl	Carl Roth
Weight	Kern PLG (360 – 3 Nm)	Kern & Sohn GmbH

3.1.2 Plastic articles and cell culture materials

Article	Company
Pipette tips 1000, 200 and 10 µl	Eppendorf and Sarstedt
Pipettes 10 ml	Greiner Bio-One
Reaction vials 1.5 ml	Eppendorf
Reaction vials 15 ml and 50 ml	Greiner Bio-One
Tubes for flow cytometry 5 ml, 75 x 12 mm	Sarstedt
24-well transwell-plates 5 µm pore size	Corning

Syringes, 1 ml (Omnican F 0.01 with integrated needle)	B. Braun
Tissue dissociation tubes for GentleMax™	Miltenyi Biotech
Sterile filter, 0.2 µm	Millipore
Cell suspension filter, 30 µm (PreSeparation Filters™)	Miltenyi Biotech
Cell strainer, 40 and 70 µm	BD Bioscience
Flow migration slide: µ-Slide VI 0.4	Ibidi

3.1.3 Reagents

Reagent	**Company**
anti-CD43-microbeads	Miltenyi Biotech
BSA, fatty accid free (powder)	PAA Laboratories
BrdU	Sigma-Aldrich
BrdU Kit	BD Bioscience
CXCL13	R&D Systems
FCS (fetale calf serum)	Gibco, Life Technologies
ICAM	R&D Systems
Ketamine hydrochloride (Ketavet 100 mg/ml)	Pharmacia GmbH
Mounting medium (ImmunoMount)	Thermo Scientific
Marginal Zone and Follicular B Cell Isolation Kit	Miltenyi Biotech
Penicillin/Streptomycin	Gibco, Life Technologies
Sphingosine-1-Phosphate (S1P)	Cayman Chemicals
Streptavidin-PromoFluor 405	PromoCell
Streptavidin-Alexa Fluor 488	Molecular Probes
Streptavidin-Phycoerythrin	BD Bioscience, USA
Streptavidin-Alexa Fluor 660	Invitrogen
Tissue freezing medium	Leica Microsystems
Xylazinehydrochloride (Rompun 2%)	Bayer Vital GmbH

3.1.4 Buffers and Media

Buffer	Composition / Company
PBS	Dulbecco's Phosphate buffered Salin (without $CaCl_2$, without $MgCl_2$) Gibco, Life Technologies
PBS/BSA	PBS 0.25% BSA, fatty acid-free, Gibco, Life Technologies, UK
Histology buffer	PBS 10% donkey serum 0.1% NaN3
Block buffer (migration)	PBS 2% BSA, fatty acid-free
Erythrocyte lysis buffer, pH 7,5	0.01 M $NaHCO_3$ 0.155 M NH_4Cl 0.1 mM EDTA
Cell culture medium	RPMI 1640, Gibco, Life Technologies
Transwell migration medium	RPMI 1640 Penicillin/Streptomycin (1:100) 0.2% BSA, fatty acid-free
Anaesthetic solution	20 mg ml^{-1} Ketamine hydrochloride 0.1% Xylazine hydrochloride
Flow migration medium	HBSS (Hanks' balanced salt solution) 10 mM HEPES 0.2% fatty acid-free BSA

3.1.5 Antibodies

Explanatory note: *anti-‚Antigen'-‚Dye' ‚(clone, company)'*

anti-B220-V450 (RA3-6B2, BD), anti-CD1d-Fitc (1B1, BD), anti-CD16/CD32 (own lab), anti-CD21-Fitc (7G6, BD), anti-CD21-PE (7G6, BD), anti-CD21-APC (7G6, BD), anti-CD23-PE (B3B4, BD), anti-CD35-Bio (8C12, BD), anti-CD45.1-PeCy7 (A20, Biolegend), anti-CD45.2-PerCP (104, Biolegend), anti-CD93-PeCy7 (AA4.1, eBioscience), anti-CXCR5-Bio (2G8, BD), anti-IgD-V450 (11-26c.2a, BD), anti-IgM-V450 (R6-60.2, BD), anti-IgM-APC (X-54, Miltenyi, Deutschland), anti-MadCAM-1-Alexa Fluor 488 (Meca-367), anti-F4/80-Alexa Fluor 488 (BM8, Biolegend), anti-LFA-1 (M17/4, Affymetrix eBioscience), anti-α4-FITC (R1-2, BD), anti-αL-PE (2D7, BD), anti-β2-FITC (C7116, BD), anti-β1-FITC (HMB1-1, Santa Cruz), anti-αPix (Cell Signaling, C23D2), anti-ßPix (cone 23, BD), rabbit-anti-VCAM-1 (H-276, Santa Cruz), goat-anti-mouse ICAM-1 (AF796, R&D), donkey-anti-goat IgG (H+L)-Alexa 488 (polyclonal, Invitrogen), donkey-anti-rabbit IgG-Cy3 (polyclonal, Dianova, 711-165-152), rabbit-anti-Phycoerythrin (Rockland 200-4199).

3.1.6 Software

Application	**Company**
Adobe Illustrator	Adobe
Diva	BD Bioscience
Ibidi Chemotaxis Tool	Ibidi
ImageJ plugin Mtrack2	open source
Endnote	Thomson Reuters
FlowJo	Tree Star Inc.
GraphPad Prism 6	GraphPad Software Inc.
LasAF	Leica Microsystems
Microsoft Office	Mircosoft
Metamorph	Leica Microsystems

3.1.7 Statistical Analysis

All statistical tests were performed with Graphpad Prism 6. For wildtype alone, statistical analyses were made with one-way ANOVA with Dunnett post hoc test performed relative to initial value. For more than one genotype, two-way ANOVA was used with Sidak post hoc tests. t tests were used where indicated in figure legends. To avoid pseudoreplication, the values of 100 - 200 cell tracks from one mouse were averaged per experiment. Statistically significant differences are indicated on the figures according to this legend: *P < 0.05, **P < 0.01, ***P < 0.001, ****P < 0.0001.

3.2 Mice and Methods

3.2.1 Mice strains

The wild type mice of the strain "C57BL/6JCrl" (C57BL/6) as well as "B6.SJL-Ptprca Pepcb/BoyCrl" (Ly5.1) from Charles River (France) were commercially acquired and accordingly mated under specific pathogen-free conditions in the Central Animal Laboratory of the Medical Faculty of the Otto-von-Guericke University for maintenance. The strain "B6.SJL-Ptprca Pepcb/BoyCrl" congenic to "C57Bl/6JCrl" carries the allele from the SJL mouse "Ptprca" or "CD45.1" or "Ly5.1" in the Ptprc gene locus and is therefore referred to as "Ly5.1" in the following. The alpha-pix deficient strain[42] (αPix ko) and the S1P receptor-3 deficient strain[70] (S1PR3 ko) were a gift from J. Chun[158] to Prof. Dr. rer. nat. Klaus-Dieter Fischer and made available for the experiments of this work. The alpha-Pix/S1P-receptor-3 deficient strain (αPix/S1PR3 double ko) was generated by crossing αPix ko mice with S1PR3 ko mice. All strains used in this work were crossed back to the "C57BL/6JCrl" strain for at least 10 generations and kept under specific pathogen-free conditions in the Central Animal Laboratory of the Medical Faculty of the Otto-von-Guerike University and propagated accordingly. The experiments were performed with age- and sex-matched animals according to state and institutional guidelines.
Animal experiment approval number: IBZ-G-02-977-10.

3.2.2 Purification of bone marrow cells, spleen cells and marginal zone B cells

For the purification of bone marrow cells, the posterior thighs were prepared from the corresponding mice and the muscle tissue was removed. Then the bone marrow was washed out with a syringe and collected in a 50 ml reaction tube. For bone marrow reconstitution after the lethally irradiation of mice, the bone marrow was filtered (30 µm pores) and transferred with the appropriate cell density for intravenous injection into 1.5 ml reaction vessels. For the flow cytometric analysis, the erythrocytes were first removed by a 2-minute procedure in ice-cold erythrocyte lysis buffer. After filtering the cell suspension, the cells were labelled for 15 min at 4°C in the FACS tube. After wash step cells were read into the flow cytometer.

For the purification of splenocytes, spleens were prepared from the corresponding mice and placed in tissue dissociation tubes together with PBS/BSA buffer. Then the spleen cells were separated using GentleMACS (Miltenyi) according to the manufacturer's instructions. After pelleting the single cell suspension, the erythrocytes were removed by resuspension of the cell pellet in the erythrocyte lysis buffer and 2-minute incubation. The erythrocyte lysis buffer was removed by 10-fold dilution with PBS/BSA and a centrifugation step. The cell pellet was resuspended in PBS/BSA and transferred through a 30 µm cell filter to a 15 ml reaction tube to remove aggregated cell debris. After this step cell density purified splenocytes was adjusted as needed.

For MZB purification by flow cytometry, splenocytes from male and female age matched wild-type and knockout mice were purified by FACS sorting (FACS Aria III (BD Bioscience) of CD43-depleted splenocytes (negative B cell isolation kit (anti-CD43), Miltenyi) with gating on CD43− CD21+ B cells and on CD21hi CD23low MZB. For MZB purification by MACS columns[133], MZB were purified using a negative isolation kit for MZB (Marginal Zone and Follicular B Cell Isolation Kit, Miltenyi) that keeps MZB unstained. In both cases, erythrocytes were lysed in a standard $NH_4Cl/KHCO_3$/EDTA lysis buffer at room temperature for 2 min after spleen dissociation. Cells were subsequently kept cold for all remaining steps of the purification, and their migration potential was analysed immediately in a flow chamber. For MZB preparation using the kit, cells were purified in two negative isolation steps over columns in an AutoMacs (Miltenyi). The initial step of removing

non-B cells from the cell suspension included biotinylated antibodies against CD43, CD4, CD93 and Ter119 to remove any remaining erythrocytes from the suspension. During the second step MZB were finally isolated by negative selection of CD23 expressing cells. During the isolation, cells were maintained and washed in PBS containing 0.4% fatty acid-free BSA and were never exposed to serum or any other BSA. The final purity of the $B220^{+}$ $CD21^{hi}$ $CD23^{lo}$ MZB was over 90%.

3.2.3 Bone marrow chimeric reconstituted mice

For bone marrow chimeric reconstituted mice, C57Bl/6 Ly5.1 8–12-week-old male and female host mice were lethally irradiated at 10 Gy with BioBeam 8000 providing gamma irradiation (^{137}Cs), then injected intravenously with 2 x 10^6 bone marrow cells derived from sex- and age-matched Ly5.2 donor mice. Recipient mice were immobilized by anaesthesia with intraperitoneal injection of 100 µl ketamine (10 mg ml^{-1}) and xylazine (2 mg ml^{-1}) solution. Ly5.1 recipient mice (six per genotype) were reconstituted with bone marrow derived from two independent donors and analysed 8–12 weeks later.

3.2.4 Flow cytometry

The fluorescence activated cell sorting (FACS^{TM}) method, which has been in existence since 1968, is based on the excitation of cell-specific fluorescent molecules by a laser and enables the analysis of cells at the single cell level at high speed, i.e. up to 10,000 cells in one second. The fluorophore specificity is guaranteed by monoclonal antibodies conjugated with fluorophores. The labelled cells (see below) are separated in a hydrodynamic fluid stream. This makes it possible to irradiate the cells successively with different lasers, which stimulates the fluorophores to fluorescence. The light emitted by the fluorophores passes through a band-pass filter system into the corresponding detectors, which allows the identification and quantification of the fluorophores previously used. In this work the FACSCanto II flow cytometer was used, which was equipped with three different lasers: 405 nm (InGaN), 488 nm (Ar+) and 633 nm (HeNe) laser. Furthermore, the excitation light is scattered by the cells.

The scattered light of the 488 nm laser is collected in two further detectors. The forward scattered light (FSC) with a scattering angle of 3-10° or the cell shadow is used to determine the cell size and the sideways scattered light (SSC), which is reflected 90° from the cell surface, is used to analyse the cell surface or the granularity of cells. The emitted light was generally recorded in the scattered light channels (FSC and SSC) with linear amplification and that in the fluorescence channels with logarithmic amplification.

3.2.5 Cell labelling for FACS analysis

For staining of epitopes on the cell surface 1 to 3 x 10^6 filtered cells (30 µm pores) were transferred into a FACS tube. First the Fc-receptors were blocked for 15 min with monoclonal anti-CD16/CD32 (own production) antibodies. Afterwards the antibody containing buffer was added to the cells without washing and incubated for 20 min at 4°C. Cells were incubated in the secondary staining reagents for 15 min at 4°C followed a washing step. Depending on the analysis, between 1 x 10^5 and 2 x 10^6 cells were read in the flow cytometer. Diva Software (BD Bioscience) was used to acquire the data and the evaluation of the measured data was performed using FlowJo Software (Treestar Inc.).

For intracellular detection of αPix and ßPix, cells were stained for surface markers as above, fixed with 4% paraformaldehyde, permeabilized with BD Perm/Wash solution (BD Biosciences), and incubated with anti-αPix or anti-ßPix antibodies for 30 min at 4°C. After two wash steps, cells were read into the flow cytometer.

3.2.6 LFA-1 blocking in vivo

For treatment with anti-LFA-1, mice were injected with either control IgG or with 100 µl (100 µg) anti-LFA-1 (M17/4) (Affymetrix, eBioscience; 16–0111) 30 min before double in vivo labelling.

3.2.7 Transwell migration

For Transwell migration assay splenocytes were erythrolysed and CD43 expressing cells were removed using the negative B-cell isolation kit (Miltenyi). 2 x 10^6 CD43-depleted spleen cells (resting B cells) of C57BL/6 (WT) and αPix ko mice were loaded in the upper cavity of the Transwell system with 5 µm pore size. After 4 h of migration time, migration rate was determined in the lower well at indicated concentrations of S1P and CXCL13. The migration rate is the percentage of MZB migrated into the lower well (migrated) in relation to the MZB previously added to the upper well (input).

3.2.8 Static adhesion assay

For MZ B cell static adhesion assay purified MZ B cells were incubated at 37°C for 1 h in 96-well plates coated with ICAM-1 (10 µg ml^{-1}, R&D Systems). Poly-L-lysine (0.01%, Sigma)-coated wells were used as a measure of input. Non-adherent cells were dislodged by gently inverting the assay plates for an additional 30 minutes. Attached cells were fixed in the wells with the addition of 4 % (w/v) formaldehyde for 15 minutes at room temperature. Adherent cells were quantified with crystal violet staining and absorbance reading in a Tecan Infinite M200 plate reader. Background crystal violet staining was subtracted, and the percentage of attached cells was determined by comparison with the number of adherent cells found in poly-L-lysine coated wells (set to 100%).

3.2.9 In vivo labelling

For double in vivo labelling mice were anaesthetized by intraperitoneal injection with 100 µl PBS containing ketamine (10 mg ml^{-1}) and xylazine (2 mg ml^{-1}) and placed on a warming pad. Anaesthetized mice were intravenously injected with 1 µg of αCD35-bio, followed 15 min later (unless stated otherwise) with 1 µg αCD21-PE or αCD21-PE and αF4/80-Alexa Fluor 488. Five minutes later, mice were sacrificed, spleens

were rapidly removed and dissected into 2 halves for histology and flow cytometry analysis.

The half spleen for flow cytometry was combined with a half spleen from an unlabelled CD45.1 mouse in order to determine extent of signals from non-specific binding of antibodies to dissociated splenocytes. Spleens were dissociated using a gentleMACS tissue dissociator (Miltenyi). Single cell suspensions were depleted of erythrocytes and resuspended in FACS buffer (PBS + 0.4% fatty-acid free BSA). Cells were stained for flow cytometry using first anti-Fc blocking antibodies, then anti-CD45.1 PE-Cy7 (Biolegend), anti-CD45.2 PerCP (Biolegend), anti-CD1d Fitc (Becton-Dickinson), anti-IgM-APC (Miltenyi) and SA-405 (Invitrogen).

For histological read-out second half of spleens was immediately embedded in Tissue Freezing Medium (Leica) and shock-frozen in isopentane (-40 to -50°C). Sections (12 µm) were cut with a cryostat, air-dried, and fixed with 2% PFA for 10 minutes. Sections were pre-incubated for 10 minutes in 10% normal donkey serum/0.1% NaN_3 in PBS, then incubated for 90 minutes with rabbit-anti-PE (1:500) and streptavidin-Alexa Fluor 488 (1:500) in 10% normal donkey serum/0.1% NaN_3 in PBS. Sections were then washed 3x for 10 minutes each in PBS, pre-incubated in 0.1% BSA in PBS for 10 minutes, incubated for 1 hour with Cy3-conjugated donkey-anti-rabbit (1:500) and streptavidin-Alexa Fluor 488 (1:500) in 0.1% BSA in PBS, washed in PBS for 3x for 10 minutes each, and mounted in ImmunoMount (Thermo Scientific).
For ICAM/VCAM staining, sections were stained as above with rabbit-anti-VCAM-1 (1:50) (Santa Cruz, H-276) and goat-anti-mouse ICAM-1 (R&D AF796) followed by Cy3-conjugated donkey-anti-rabbit (1:500) (Dianova 711-165-152) and Alexa 488-conjugated donkey-anti-goat.
For IgM staining, sections from mice injected with anti-CD21-PE for 5 minutes were pre-incubated in 3% BSA in PBS for 15 minutes, incubated overnight at 4°C in V450-conjugated anti-IgM in PBS, washed 3x for 10 minutes each in PBS, then mounted in ImmunoMount. Slides were visualized using a Leica DMI6000 inverted wide-field microscope with a 10x objective and processed with Leica Application Suite software.

3.2.10 Flow chamber migration assays

Ibidi flow chamber slide (µIV-0.4) (Ibidi, Martinsried, Germany) channels were coated overnight at 4°C with indicated amounts of ICAM-1 or VCAM-1 (R&D Systems), blocked for 1 hour at room temperature with 2% fatty acid-free BSA (Roth, Germany) in PBS, then washed 2x in PBS and filled with migration medium (HBSS containing 0.8 mM Mg^{2+}, 1.26 mM Ca^{2+}, 0.4% BSA, 10 mM HEPES). For S1P treatment, S1P (Caymen Chemical) was resuspended in methanol, sonicated, then dried under a stream of nitrogen gas. Aliquots were resuspended in PBS + 0.4% BSA, then added to migration buffer in the fluidics unit of the Ibidi pump system at a concentration of 200 nM. Purified MZB cells (1.5×10^5) were added to channels and incubated at 37° for 30 minutes before tubing assembly was attached to the slides and to an Ibidi pump system filled with pre-warmed migration medium. Images were acquired at 10x on a Leica DMI 6000 inverted wide-field microscope. Cells were tracked using the ImageJ plugin Mtrack2. Migration parameters were calculated using the Ibidi Chemotaxis tool. The migration index was calculated as the ratio of the projected y-coordinate of a cell's endpoint to its track length. Straightness was calculated as the ratio of the cell's path length to its track length. Velocity was calculated as the ratio of a cell's track length to elapsed time. The values of 100-200 cell tracks from one mouse were averaged per experiment.

4. Results

4.1 Analysis of the Development of MZB cells in αPix deficient mice

The effects of the αPix deficiency on the murine immune system were described before[42]. Besides normal B cell development in bone marrow, a significant increase in the relative number of MZB in the spleen of αPix ko mice was reported. MZB precursor cells begin to differentiate in BM, emigrate in the periphery and further differentiate in the spleen from so-called T2 progenitor cells (T2 MZP)[134]. Since a data set regarding the development of MZB precursor cells in the spleen of αPix ko mice was not available, the B cell development in the bone marrow and in the spleen of αPix ko mice was analysed here in more detail. For this purpose, in bone marrow the absolute and the relative number of the different developmental stages of B cell precursors in BM were determined. In the spleen, a quantitative analysis of the B cell precursor populations and mature B cells was performed.

4.1.1 B cell progenitors in bone marrow of αPix ko mice

The determination of the absolute number of bone marrow cells showed no differences between wildtype (WT) and αPix ko mice as an average of 13.5 million for WT and 13.8 million for αPix ko bone marrow cells were counted per femur (Fig. 7A). The flow cytometric analysis of the B cell precursor populations in the bone marrow of αPix ko mice, showed also no differences in their relative numbers compared to WT mice (Fig. 7B and Fig. 7C). This result is consistent with the data reported by Missy et al, 2008[42].

4.1.2 MZB and their progenitors in the spleen of αPix ko mice

The examination of the spleen mass showed a 1.8-fold enlargement of αPix ko spleen with a mean of 134 µg compared to WT with a mean of 74 µg per spleen (not shown). This phenomenon is reflected in the total number of spleen cells: on average 37 million cells per spleen were counted in the WT and 67 million cells per

Figure 7: Normal number of B cell precursors in bone marrow of αPix ko mice.

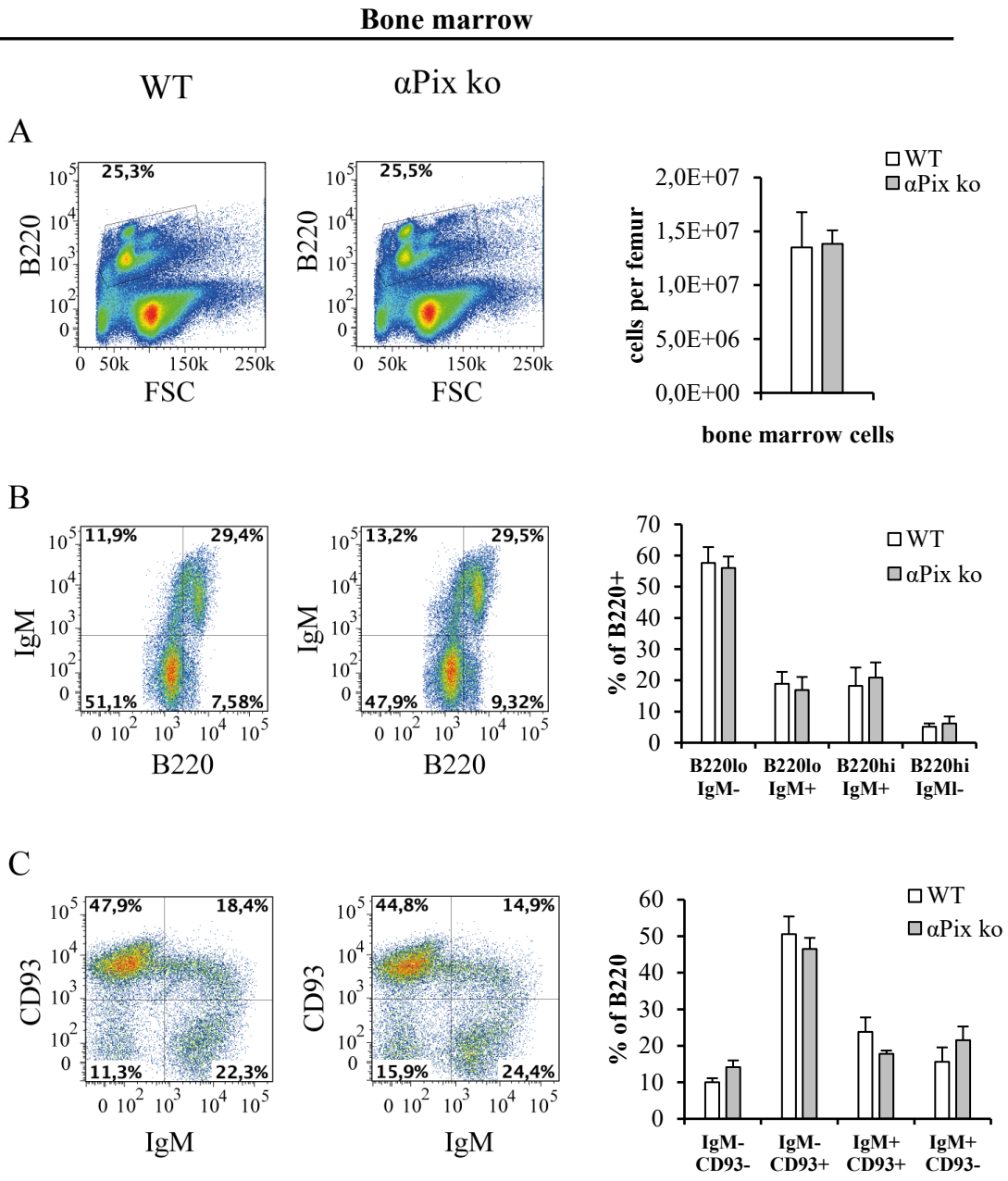

Fig. 7: *The result of the flow cytometric measurement of B cells from the bone marrow of 12-week-old C57BL/6 (WT) and αPix ko mice is shown. Bone marrow cells were labelled with anti-B220, anti-IgM, anti-CD93. Age of mice: 12 weeks. WT: n = 3 and αPix ko: n = 3.* ***(A)*** *Left: relative number of B220 expressing BM cells. Right: absolute number of bone marrow cells of a murine femur after removal of the erythrocytes.* ***(B)*** *Left: Analysis of B cell precursors ($B220^+$) in BM by their B220 and IgM expression. Right: Statistics of subpopulations as indicated.* ***(C)*** *Left: Analysis of $B220^+$ B cell precursors in BM by their CD93 and IgM expression. Right: Statistics of subpopulations as indicated. Bars show mean ± SEM.*

spleen in the αPix ko mouse (Fig. 8A). This is also an increase by factor 1.8. The relative number of B cells with about 60% of splenocytes was in the αPix ko spleen at the same level as in WT (Fig. 8B and Fig. 8C left). The total number of splenic B cells was increased by a factor of 1.9 from 22.5 for WT to 43 million for αPix ko (Fig. 8D), which was related to the increased total number of splenocytes.

When the relative number of immature B cells in the spleen was determined by their CD93 expression (here: $B220^{+}CD93^{+}$, Fig. 9A), it amounts to 6% of the B cell population similarly in WT and αPix ko spleens, whereby the total number in the case of αPix ko was increased by a factor 1.8 from 1.3 million for WT to 2.4 million (Fig. 9B). Since MZB differentiate from T2 B cells, an analysis of the transitional B cells in the spleen was carried out (Fig. 9C). Within the CD93-expressing or immature B cells, the transitional B cells were identified by their IgM and CD23 expression as follows[134]: T1: $IgM^{hi}CD23^{-}$, T2: $IgM^{hi}CD23^{+}$ and T3: $IgM^{lo}CD23^{+}$. The analysis of the relative numbers within the B cells revealed the following mean values for T1 B cells: WT 23.9% and αPix ko 20.6%, for T2 B cells: WT 32.4% and αPix ko 35.8% and for T3 B cells: WT 20.9% and αPix ko 20.1% (Fig. 9D). This means that no significant differences could be measured. The calculation of the total numbers showed in αPix ko spleens an increase of the T1 population by factor 1.6 (WT: 320,000, αPix ko: 500,000), T2 B cells were increased by factor 2 (WT: 420,000, αPix ko: 870,000) and T3 B cells by factor 1.8 (WT: 270,000, αPix ko: 480,000).

The mature subpopulations of splenic B cells can be identified by their CD21 and CD23 expression: marginal zone B cells (MZB: $CD21^{hi}CD23l^{o}$), follicular B cells (FO: $CD21^{lo}CD23^{hi}$) and immature B cells (IM: $CD21^{-}CD23^{-}$). Such an analysis showed in αPix ko mice an increase of the relative number of MZB by factor 1.9 (WT: 6.7%, αPix ko: 12.4%) (Fig. 10A and Fig. 10B). The quantitative determination in Fig. 10C showed an increase of the number of MZB by factor 3.5 (WT: 1.5 million, αPix ko: 5.3 million), for follicular B cells by factor 1.8 (WT: 17 million, αPix ko: 31 million) and for immature B cells also by factor 1.8 (WT: 1.4 million, αPix ko: 2.6 million). The relative number of immature B cells (here: $CD21^{-}CD23^{-}$) in the αPix ko spleen (6.0%) did not differ from the WT (6.3%). Thus, the alternative quantification of immature B cells by the CD21/CD23 expression ($CD21^{-}CD23^{-}$, Fig. 10C) confirms the examination via the CD93 expression (CD93+, Fig. 9A and Fig. 9B), since consistent for both WT and αPix ko.

Figure 8: αPix deficiency leads to enlarged spleen (splenomegaly).

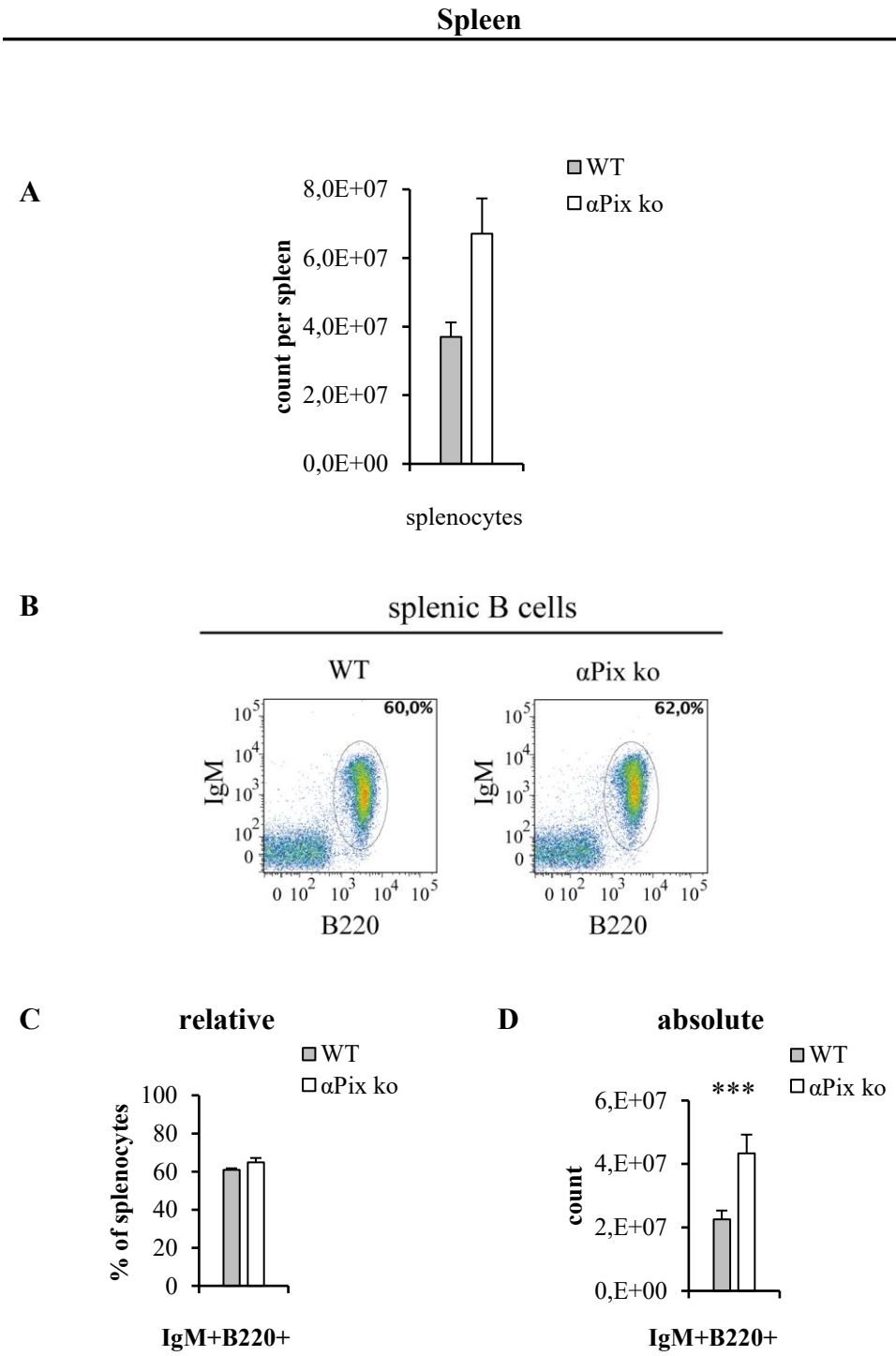

Fig. 8: *The quantitative analysis of B cells in αPix ko spleens is shown.* ***(A)*** *The total number of WT (grey bars) and αPix ko (white bars) spleen cells (without erythrocytes) was determined using the flow cytometer.* ***(B)*** *Relative number and* ***(C)*** *absolute numbers of $B220^{+}IgM^{+}$ cells in spleens from WT and αPix ko mice. WT: n = 3 and αPix ko: n = 10. Bars show mean ± SEM. ***P < 0.001 by t-test.*

Figure 9: Quantification of transitional B cells (T1, T2 and T3) in αPix ko spleen.

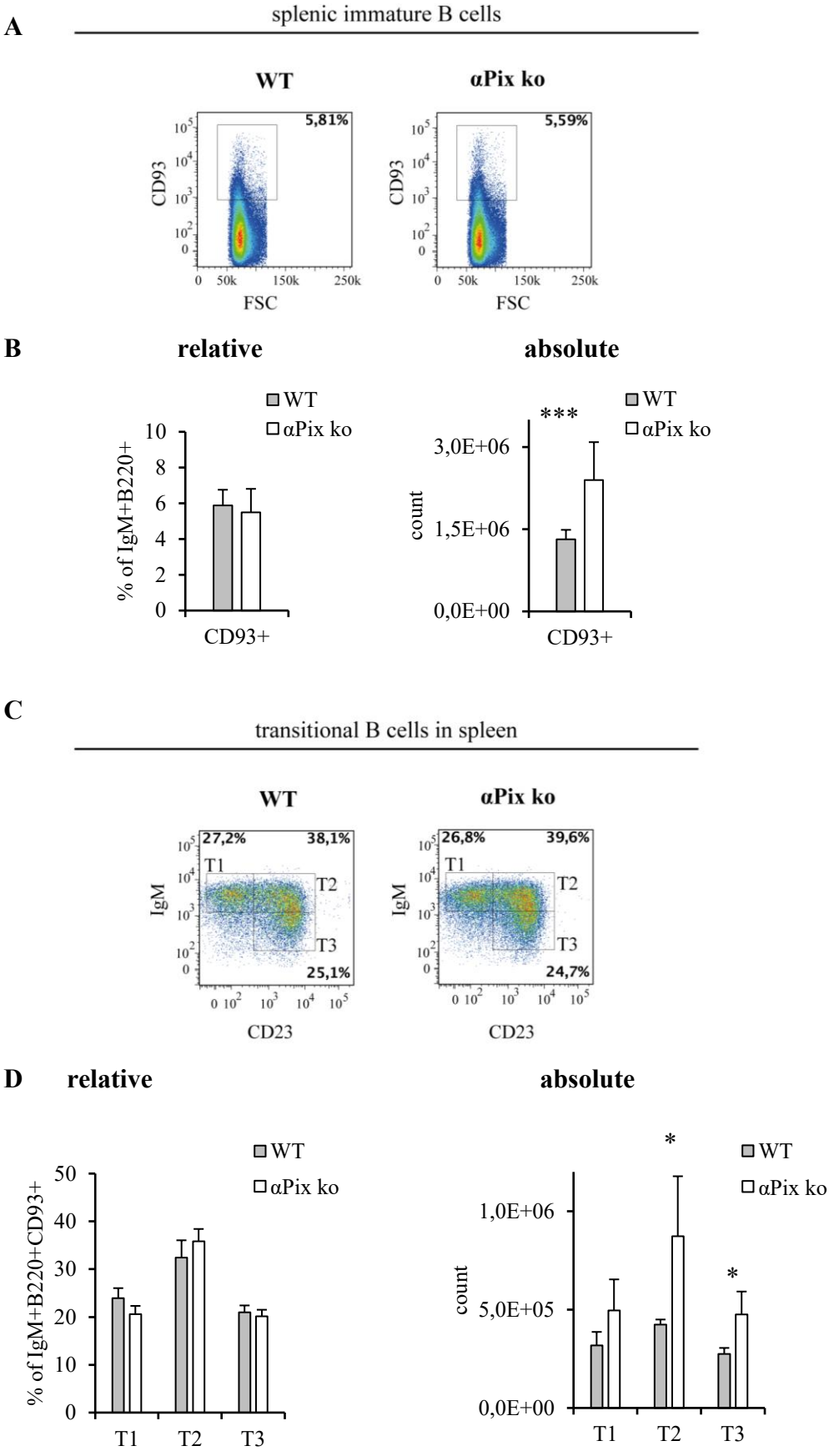

Fig. 9 (on previous page): *Splenocytes from C57BL/6 (WT) and αPix ko mice were labelled with anti-B220, anti-CD93, anti-CD23 and anti-IgM and analysed by flow cytometry[134]. Age of mice: 12 weeks. WT: n = 3 and αPix ko: n = 10.* ***(A)*** *Representative FACS plots of WT and αPix ko immature B cells ($B220^+CD93^+$) in spleen.* ***(B)*** *Statistics of relative (left) and absolute (right) numbers of immature splenocytes ($B220^+$ $CD93^+$).* ***(C)*** *Representative FACS plots of WT and αPix ko transitional B cells ($B220^+$ $CD93^+$) determined by their IgM and CD23 expression.* ***(D)*** *Statistics of relative (left) and absolute (right) numbers of transitional B cells. T1: transitional B cells-1 ($CD23^-IgM^{hi}$), T2: transitional B cells-2 ($CD23^+IgM^{hi}$), T3: transitional B cells-3 ($CD23^+IgM^{lo}$). Bars show mean ± SEM. *P < 0.05, ***P < 0.001 by t-test.*

Figure 10: B cells subsets in spleen of αPix ko mice

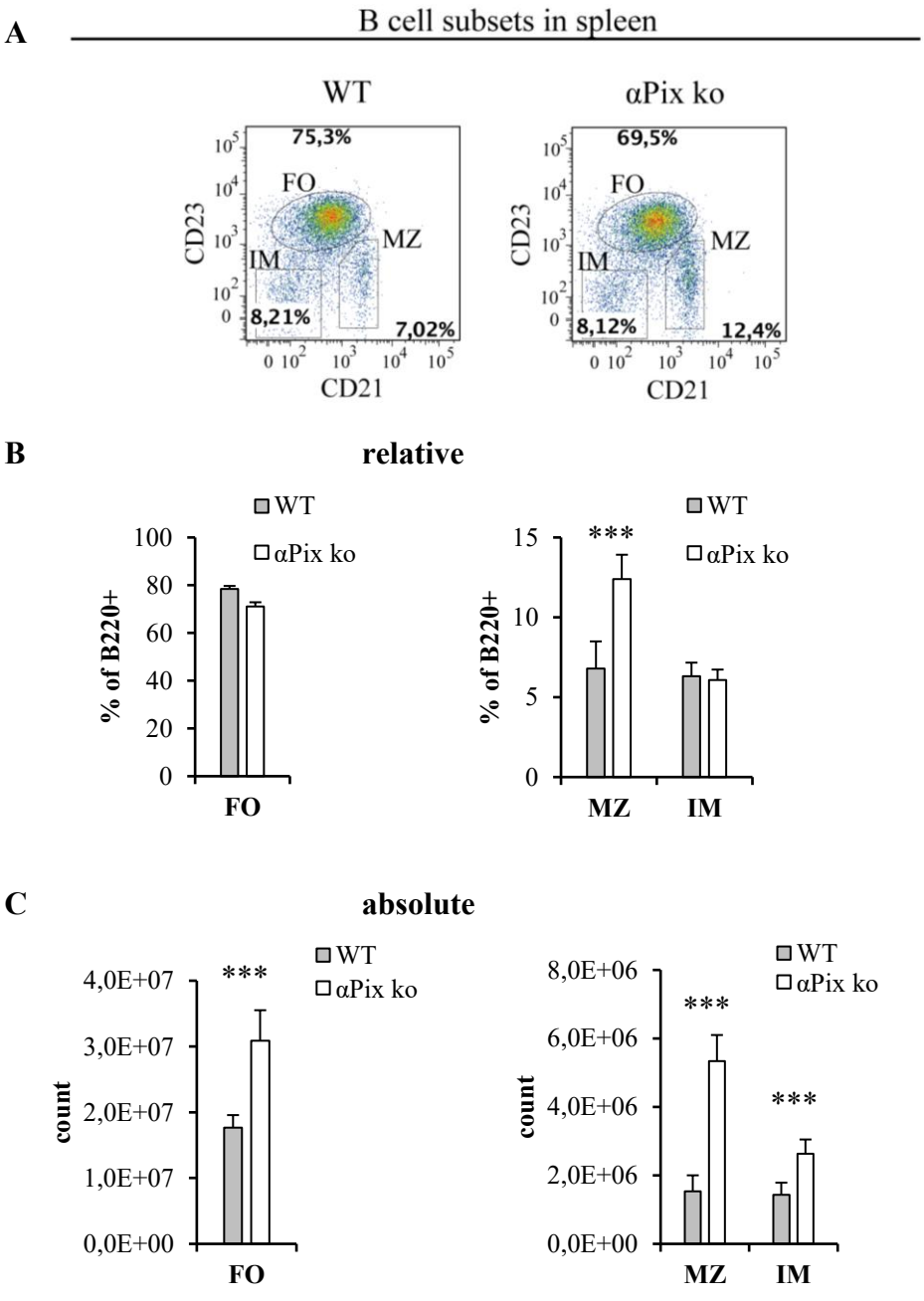

Fig. 10 (on previous page): *The analysis of the splenic B cell subpopulations of C57BL/6 (WT, white bar) and αPix ko (grey bar) is shown. Spleen cells were labelled with anti-B220, anti-CD21 and anti-CD23 and analysed by flow cytometry. Age of mice: 12 weeks. WT: n = 3 and αPix ko: n = 10.* ***(A)*** *Representative FACS plots of splenic B cells ($B220^+$) analysed by their CD21 and CD23 expression.* ***(B)*** *Relative numbers of follicular B cells (left, FO: $B220^+CD21^{lo}CD23^{hi}$), marginal zone B cells (right, MZ: $B220^+CD21^{hi}CD23^{lo}$) and immature B cells (right, IM: $B220^+CD21^-CD23^-$) in WT and αPix ko spleens.* ***(C)*** *Absolute numbers of follicular B cells (left, FO: $B220^+CD21^{lo}CD23^{hi}$), marginal zone B cells (right, MZ: $B220^+CD21^{hi}CD23^{lo}$) and immature B cells (right, IM: $B220^+CD21^-CD23^-$) in WT and αPix ko spleens. Bars show mean ± SEM. ***$P < 0.001$ by t-test.*

4.2 In MZB αPix deficiency leads to an increase in basal motility and adhesion under static conditions

An increased motility of αPix ko B and T cells was reported in the presence and absence of the chemokine CXCL12[42]. Based on this, an increased migration rate of αPix ko MZB compared to WT MZB was also suspected. The most important chemokines for MZB and their biological function are S1P and CXCL13. The fine-tuned regulation of these chemotactic responses is a basic prerequisite for the process of follicular shuttling of MZB[126, 132]. In order to gain insight into the possible consequences of αPix deficiency on biological mechanisms of MZB, the S1P and CXCL13 induced migration rates of αPix ko MZB compared to WT at different chemokine concentrations were determined using the so-called transwell migration assay.

In general, αPix ko MZB show an increased migration rate compared to WT after a 4 hour migration period at each chemokine concentration including basal migration (basal: 4 to 6-fold increase, Fig. 11). In the case of S1P-induced migration, the greatest differences in migration rate were measured at concentrations of 50, 500 and 1000 nM S1P with an increase up to a factor of 2 (Fig. 11A), at 50, 500, 1000 nM for WT: 8.1, 7.8, 3.9% and for αPix ko: 12.9, 13.1, 7.6%). In the presence of CXCL13, αPix ko MZB show an increased migration rate by a factor 2 - 4 compared to WT at concentrations of 25 and 100 nM (Fig. 11B), at 10, 25, 100 nM for WT: 0.3, 1.8, 7.3% and for αPix ko: 1.8, 6.9, 16.9%).

Since S1P is essential for the localization of MZB in the MZ[69] and therefore for their biological function, the idea that S1P affects MZB cell adhesion and this is

Figure 11: S1P and CXCL13 induced migration rates and ICAM-1 mediated adhesion of WT and αPix ko MZB under static conditions.

A S1P

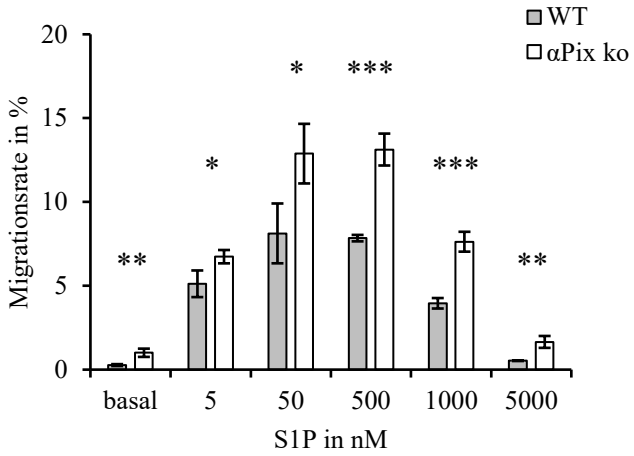

B CXCL13

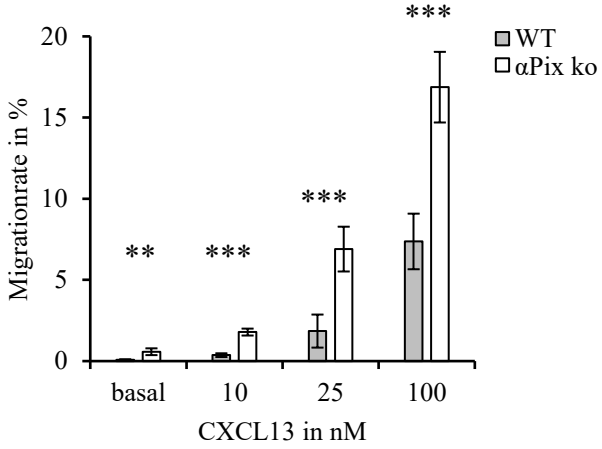

C Migration

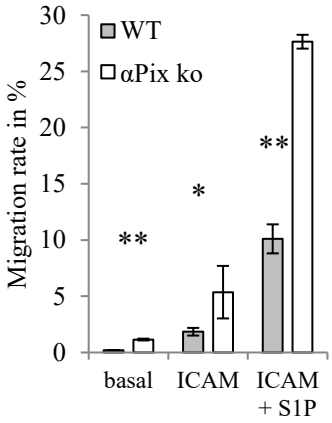

Static adhesion

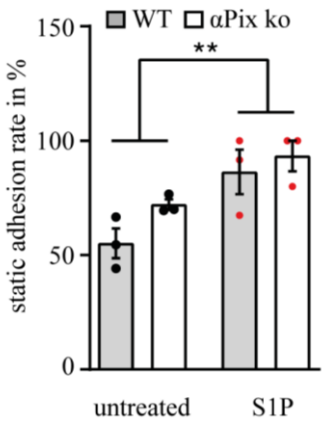

Fig. 11 (on previous page): *The S1P* ***(A)*** *and CXCL13* ***(B)*** *induced migration rates of WT and αPix ko MZ B cells were analysed in vitro. For this purpose, 2 x 10^6 CD43-depleted spleen cells (resting B cells) of C57BL/6 (WT) and αPix ko mice were placed in the upper cavity of the transwell system with 5 µm pore size and the migration rate was determined at* ***(A)*** *S1P concentrations of 0, 5, 50, 500, 1000 and 5000 nM and at* ***(B)*** *CXCL13 concentrations of 0, 10, 25 and 100 nM after 4 h migration time. The migration rate is the percentage of MZB from the lower well (migrated) in relation to the MZB previously added to the upper well (input). Triplicates were measured for each concentration. In* ***(A)*** *is a representative result from 8 independent experiments and in (B) is the result of the mean values from 3 (10 and 25 nM) and 4 (100 nM) independent experiments respectively.* ***(C) Left****: Transwell migration to S1P (200 nM) through ICAM-1-coated (2.5 µg ml^{-1}) membranes after 4 h migration time. Increased migration of αPix ko MZB in transwells in all conditions.* ***Right****: Static adhesion of WT and αPix ko MZB cells treated with S1P (200 nM) on ICAM-1 (2.5 µg ml^{-1}), relative to total adhesion on poly-lysine (n = 3). Data are representative of 5 experiments with 1 mouse per genotype each. Bars show mean ± SEM; *p<0.05, **p <0.01, ***P < 0.001 by t-test.*

modulated by αPix was tested. For this a static adhesion assay with WT and aPix ko MZB was performed. WT and αPix ko MZB were treated with S1P (200 nM) on ICAM-1 (2.5 µg ml^{-1}) coated surface. The number of adhered MZB was determined relative to the total adhesion on poly-lysin. The mean of percentages are shown in Fig. 11C. In the absence of S1P a fraction of 55% of WT MZB was adherent on ICAM-1. αPix ko MZB showed an increase of the percentage with 72% by factor 1.3. When S1P was added the adhesion rate was significantly increased for WT MZB by factor 1.6 to 87% and for αPix ko MZB by factor 1.3 to 94%. That means, in the absence of αPix the basal MZB adhesion on ICAM-1 is increased and that S1P significantly increased MZB cell adhesion by about 30-50% (Fig. 11C left). Combined with the S1P induced migratory response on ICAM-1 (Fig. 11C left), there were observed plausible data for WT MZB: about 10% migrated on ICAM and about 90% were adherent. These values are also consistent with data reported for follicular shuttling of MZB[126]. However, for αPix MZB it was difficult to interpret the measured data: although 94% of αPix ko MZB were determined as adherent, but 30% of αPix ko MZB could migrate through the pores of the ICAM coated transwell membrane into the lower well. Although with this result, αPix ko MZB show stronger adhesion despite higher migration rates, it is difficult to interpret the huge difference of the S1P induced migratory response of αPix MZB compared to WT (Fig. 11C right), However, this

result suggested a role of αPix in the regulation of the migrational response of MZB on ICAM-1.

4.3 Expression of chemokine receptor CXCR5, integrins and βPix in αPix ko MZB

Since there was measured an altered in the cellular motility due to the absence of αPix[42, 54] (Fig. 11), it was focussed on cellular factors which are known to play an important role in migratory processes of lymphocytes: integrins control cellular adhesion[68], chemokine receptors control the directional migration and homing of cells[69, 128] and βPix is a GEF involved in the regulation of Rho-GTPases[14, 136, 137]. Rho-GTPases regulate intracellular processes, needed for migratory processes, e. g. remodelling of cytoskeleton and polarization of cells[135].
Since only poor cell numbers of MZB are available (Fig. 10C), analysis of expression levels is very difficult via the standard procedure called Western Blot. On one hand the factors to be analysed are not reaching the detection border to produce processable signals. On the other hand, another hurdle was, that during the time of the conduct of these experiments, specific antibodies suitable for the Westen Blot analysis were not available. Therefore, as read-out an experimental setup using flow cytometry was established in order to identify αPix deficiency induced changes of expression levels of the chemokine receptor 5 (CXCR5), integrins (α4, αL, ß1 and ß2) and βPix (intracellular).

4.3.1 Normal CXCR5 expression on αPix ko MZB

A flow cytometric analysis of the CXCR5 expression of splenocytes was performed to clarify whether an altered receptor expression on αPix ko MZB could deliver an explanation for the increased CXCL13 induced migration rate. B220 signals were used to differentiate between B cells ($B220^+$) and non-B cells ($B220^-$), with the $B220^-$ population serving as the internal negative control for staining. In Fig. 12A, the low signal strength for $B220^-$ cells indicated that non-B cells ($B220^-$) in the spleen do not express the CXCR5 receptor, which shows the specificity of the used

Figure 12: Gene expression of CXCR5, integrins and βPix in αPix ko MZB

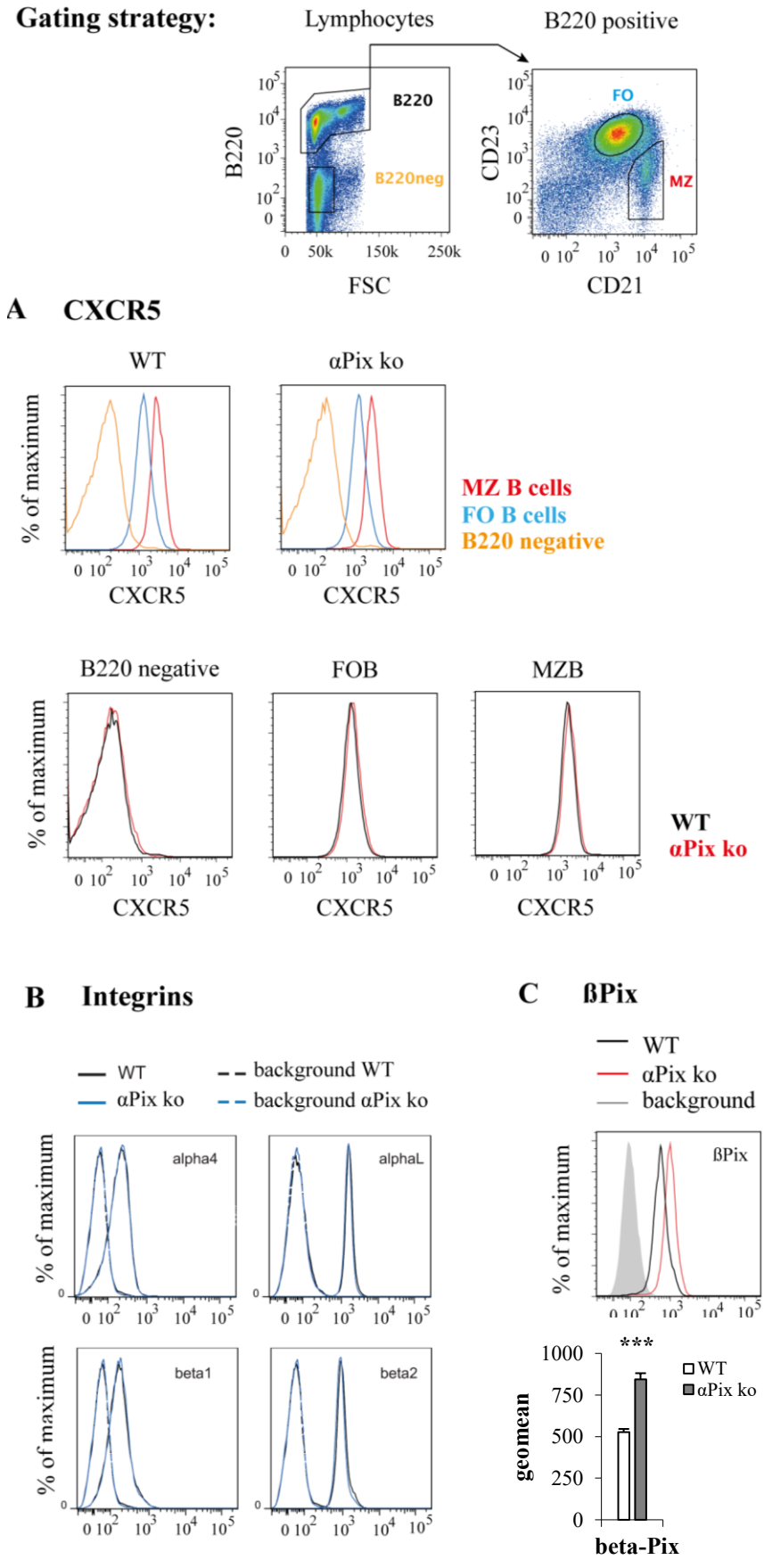

Fig. 12 (on previous page): *Spleen cells from C57BL/6 (WT) and αPix ko mice were labelled with anti-B220, anti-CD21 and anti-CD23. The B cell subpopulations were distinguished as follows: marginal zone B cells (MZ B cells): $B220^{+}CD21^{hi}CD23^{lo}$; follicular B cells (FO B cells): $B220^{+}CD21^{lo}CD23^{hi}$ and non-B cells (B220 negative): $B220^{-}$.* ***(A)*** *Upper panel: CXCR5 expression of the subpopulations MZ B cells, FO B cells and non-B cells from WT and αPix ko mice, analysed by flow cytometry. Lower panel: comparison of the CXCR5 expression on the surface of non-B cells, FO B cells and MZ B cells from WT and αPix ko spleens. Data represent 1 experiment with 3 mice.* ***(B)*** *Expression of the integrins αL, β2, α4, β1 on the surface of WT and αPix ko MZB analysed by flow cytometry (αLβ2 = LFA-1 and α4β1 = VLA-4). Data represent 1 experiment with 3 mice.* ***(C)*** *Intracellular expression of βPix of WT and αPix ko MZ B cells ($B220^{+}CD21^{hi}CD23^{lo}$). Data represent 1 experiment with 3 mice. Bars show mean ± SEM. ***P < 0.001 by t-test.*

antibody. Within the B cells ($B220^{+}$) the CXCR5 receptor expression was analysed on MZB ($CD23^{lo}/CD21^{hi}$) and follicular B cells ($CD23^{hi}/CD21^{lo}$). The result of the measurement showed that MZB have an increased CXCR5 expression level compared to follicular B cells (Fig. 12A). Comparing the signals from WT and αPix ko samples, no differences in CXCR5 expression were found on all subpopulations of the examined spleen cells (Fig. 12A). This result allows the conclusion that the cause for the increased CXCL13-induced migration rate of αPix ko MZ B cells is more likely to be found in deregulated intracellular signalling pathways than in altered expression of the chemokine receptor.

4.3.2 Normal expression of integrin on αPix ko MZB

The flow cytometric analysis of the expression of integrins α4, αL, ß1 and ß2 on the surface of MZB showed also no differences between WT and αPix ko MZB as shown in Fig. 12B. This observation encourages the hypotheses of deregulated intracellular signalling pathways, when αPix is not expressed.

4.3.3 Increased βPix expression in αPix ko MZB.

Since αPix deficient thymocytes express increased levels of the it's homolog βPix and show also increased motility, the increased migration rates of αPix ko MZB could also

reflect abnormal activation of GTPases in MZB. It was reported that the increased motility was caused by an enhanced Rac activation level, due to increased amount of the GEF βPix[54]. Therefore, the level of βPix expression in αPix ko MZB was tested by flow cytometry. Indeed, the intracellular βPix levels were strongly increased in the absence of αPix (geometric mean: WT = 500, αPix ko = 800, factor 1.6 (Fig. 12C). This suggested that the loss of αPix is compensated by MZB with enhanced expression of βPix.

4.4 Design and establishment of a innovative live cell imaging system to investigate migrational behaviour of MZB under flow conditions (Flow Assay)

During the above-described research, the following issues or hurdles were discovered. The limitations experienced were as follows:

- Low cell count of MZB to prepare samples with sufficient amount of targets in the sample to be analysed.
- Lack of available antibodies with needed specificity for flow cytometry or immunofluorescence microscopy.
- The Transwell Assay used for migrational analysis represents only poorly the biologic environment of MZB, since the MZ is exposed to blood flow and shear stress has an effect on cellular migrational behaviour.
- The literature provides no data regarding the behaviour of MZB under flow and only very poor MZB data available in the literature.
- Due to the design of so far described flow systems, it is not possible to apply a constant flow direction in one direction over time or to apply constant shear stress. Peristaltic pumps exert a fluctuating pressure and systems with installed syringes as medium reservoir can hold the flow in one direction in only a limited time window, until the medium filled syringe is empty.
- The laminar flow is essential for the analysis of cellular migration, to be able to calculate the shear stress and to apply constant flow condition across the whole sample to be analysed. This is a requirement for the calculation of the shear force exposed to the cells. With non-calibrates systems (slides, connecting lines, pump) it is very difficult to apply a defined laminar flow and therefore to calculate precisely the resulting shear stress exposed to the cells.

4.4.1 Design of the system

The importance of shear stress as parameter for directed cellular migration is illustrated for example by the trans-endothelial migration of leucocytes, which is promoted by flow induced shear stress and not by the chemokine gradient[122]. Due to the absence of flow, the adhesion process in blood vessels e.g. the MZ is poorly simulated by the assays shown in Fig. 11. To investigate and observe for the first time the migratory behaviour of MZB under flow conditions a innovative live cell imaging system was established. The setup included the installation of the ibidi pump in a Leica DMI6000B widefield microscope with live cell imaging setup (Fig. 13). The installation of the innovative ibidi pump opened the possibility to apply constant flow in one direction with no time limits[159]. This is special, since this was not possible with other pump systems before, e.g. peristaltic pump produces fluctuating pressure or pumps with syringe-based reservoirs limit the experimental time by their volume. Since the slides and lines available at ibidi are calibrated and programmed into the provided software, with this system it becomes possible to apply defined conditions in the flow chamber regarding laminar flow strength exerting the shear stress and surface parameters of the flow chamber. This advantage ensures besides a high flexibility a very precise and sensitive adjustment, which leads to a high reproducibility and high measure sensitivity of this setup. The live cell imaging system was equipped with a with a temperature control and the buffering of cell culture or migration medium. The wide field microscope contained a time lapse recording function within the software. The combination of the flow system (ibidi) with the live cell imaging system (Leica DMI6000B) offered the possibility to observe and analyse the samples with living cells under constant and defined flow conditions even on a single cell level.

Figure 13: Flow chamber system: Setup of the fluidics system, pump, microscope and incubation chamber.

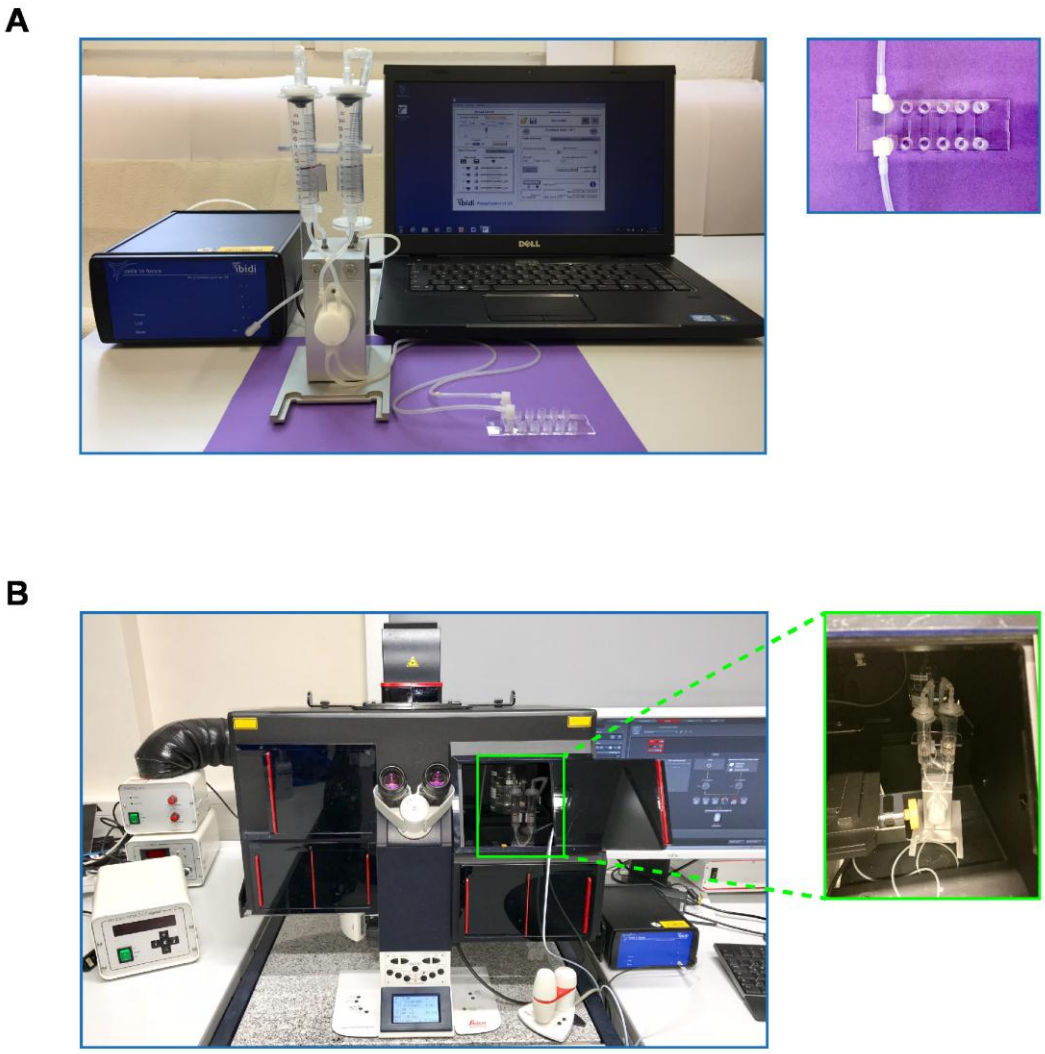

Fig. 13: (A) *Image of the pump system consisting of a pump with connected fluidics unit and laptop running the software to control the pump. Higher magnification image: the flow chamber slide with 6 flow chambers, the first of which is attached to the tubing of the fluidics unit.* ***(B)*** *Typical setup for measuring in vitro migration of MZB against flow. A microscope equipped with a heating chamber (black box) containing the fluidics unit connected to a pump outside the microscope (blue square object to the lower right of the microscope). Higher magnification image: the fluidics unit inside the microscope heating chamber*[141].

4.4.2 Functionality of the designed system

4.4.2.1 Comparison of migratory behaviour of MZB with FOB under flow

Under static conditions MZB adhere more than follicular B cells (FOB) to ICAM-1 and VCAM-1[68]. Positioning of MZB in the MZ is mediated via LFA-1-ICAM adhesion[68] and MZ residing MZB are exposed to the blood flow[110]. To rule out here for the first time, if this increased adhesion of MZB to ICAM-1 under static conditions also enables them to adhere under shear stress, ibidi slides were coated with ICAM-1 (2 µg ml^{-1}), VCAM-1 (2 µg ml^{-1}) or ICAM-1 & VCAM-1 (= mix, 1 µg ml^{-1} each) over night at 4°C. A cell count of 1,5 x 10^5 MZB or FOB were loaded into the coated channels of the ibidi slide. Loaded ibidi slides were incubated for 30 min at 37°C to allow the acclimatisation of the MZB in the migration medium. The tubing to connect the ibidi pump was installed on the slide and the slide was installed into the microscope of the live cell imaging system.

Under flow MZB stay attached, FOB are washed out. To show the cell density loaded into the ibidi slide the first image was taken before the flow was started (Fig. 14A, 100%). This image shows all loaded cells including the non-adherent. In the next step a shear stress of 3 dyn cm^{-2} was applied for 10 seconds. The low shear stress was chosen to allow also the adhesion of FOB, which are known to show lower adherence to ICAM-1[68]. After 10 seconds of flow start at 3 dyn cm^{-2}, only about 20% of the FOB stayed attached and could resist the flow on ICAM-1. In contrast more than 60% of MZB were still adherent on ICAM-1 after 10 sec at 3 dyn cm^{-2}. Since all non- or weak adhesive cells are washed out, this percentage shows the adherence capacity of loaded MZB and FOB on ICAM-1 under a shear stress of 3 dyn cm^{-2}. After 30 minutes of flow, the numbers of MZB (55% of loaded) still adhering to the slide surface exceeded those of FOB (8% of loaded) by about 7-fold (Fig. 14A). This increased adhesion capacity of MZB compared to FOB is in line with published data derived from static assays[68] and indicates that the system is functional. The adherence of MZB under flow and a comparison with FOB was described here for the first time.
To further investigate and describe the different adhesion behaviour of MZB and FOB over time, the adhesion rate of MZB on ICAM-1 and/or VCAM-1 under flow

Figure 14: MZB are more resistant than FOB to detachment under shear flow.

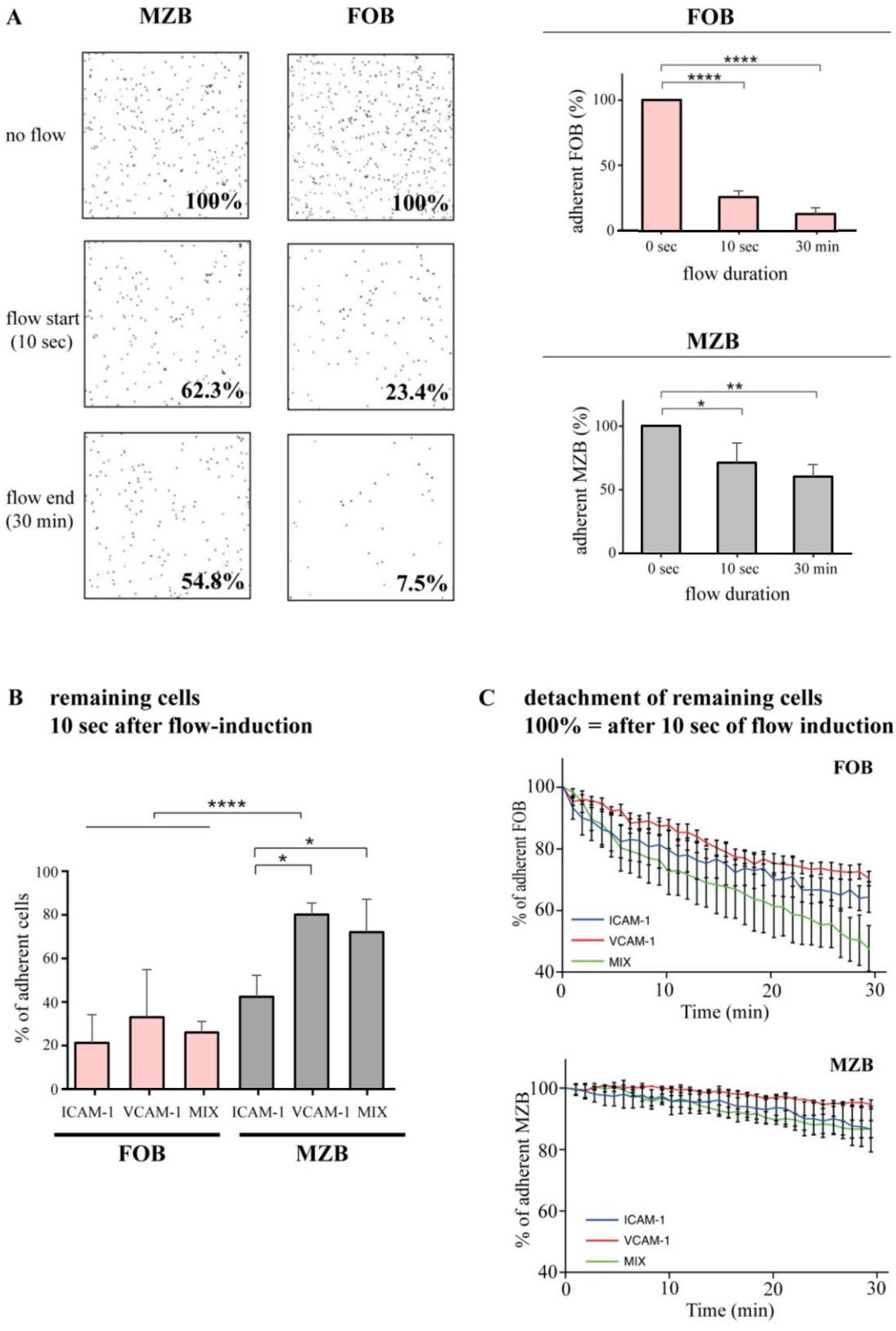

Fig. 14 (on previous page): *(**A**) Comparison of detachment at start and end of flow application to MZB and FOB cells. Representative microscopy field of view of MZB (left) and FOB (right) cells in flow chamber on ICAM-1 (2 µg ml^{-1}) before flow (3 dyn cm^{-2}) (t = 0), at flow start (t = 10 sec), and flow end (t = 30 min), with percentages of remaining cells relative to the before flow number shown below (left panels). Quantification shown on the right (n = 3). Bars correspond to means and symbols represent the average of 100 - 200 cells from one mouse. (**B**) Comparison of detachment after start of flow (t = 10 sec) to starting numbers on ICAM-1 (2 µg ml^{-1}), VCAM-1 (2 µg ml^{-1}), or ICAM-1 and VCAM-1 (1 µg ml^{-1} each) mixed. (n = 3). (**C**) Detachment over time of marginal zone B cells (MZB) and follicular B cells (FOB). Percent attachment based on number of cells after flow (3 dyn cm^{-2}) start (t = 10 sec), mean ± SEM on ICAM-1 (2 µg ml^{-1}), VCAM-1 (2 µg ml^{-1}), or ICAM-1 and VCAM-1 (1 µg ml^{-1} each) mixed (n = 3). *P < 0.05, **P < 0.01, ****P < 0.0001.*

was analysed and compared to the adhesion rate of FOB. Cell-loaded ibidi slides were installed into the microscope. The first image was taken before the flow was started. This cell count was set to 100%. After the flow was started for 10 seconds a second image was taken (Fig. 14B). Fig. 14B shows the percentage of cells, which were still adherent on ICAM-1, VCAM-1 and the mix of ICAM-1 and VCAM-1 after an initial push of flow for 10 seconds at 3 dyn cm^{-2} relative to the count of all loaded cells before the flow was started. The initial force of the shear stress with a duration of 10 seconds was enough to dislodge the majority of the FOB cells on all three surfaces as opposed to the MZB (Fig. 14B), suggesting that the basal adhesion of MZB cells on the integrin ligands ICAM-1 and VCAM-1 is higher compared to FOB cells. Adhesion rate of MZB was highest on VCAM-1 (MZB: 80%, FOB: 30%) followed by the adhesion on the mix of ICAM-1 and VCAM-1 (MZB: 70%, FOB: 22%). On ICAM-1 alone 40% of adherent cells remained after 10 seconds for MZB and 20% for FOB (Fig. 14B). The remaining adherent cells after the initial 10 sec push shown in Fig. 14B were monitored under flow with the live cell imaging system for further 30 minutes. Fig. 14C shows their detachment under flow with time at 3 dyn cm^{-2}. The graphs show that the rate of loss for the FOB over time was much higher than for the MZB on all three ligand-coated surfaces (Fig. 14C). After 30 minutes of flow MZB showed under all three conditions a loss of maximal 15% of initial adherent cells after 10 sec of flow. The loss of MZB on VCAM-1 was lowest (95% adherent), compared to ICAM-1 and ICAM-1 & VCAM-1, on which the loss was almost similar with 86% remaining cells (Fig. 14C). Compared to MZB, FOB showed an increased loss under these conditions with 70% remaining FOB on VCAM-1, 65% on ICAM-1 and 39% adherent FOB on the mix of ICAM-1 & VCAM-1 after 30 min.

4.4.2.2 Characterization of the migratory behaviour of MZB under flow on the Integrin Ligands ICAM-1 and VCAM-1

MZB migrate up to the flow on ICAM but not on VCAM. Since there was no data available in the literature describing the migratory behaviour of MZB under shear stress, the migratory response of MZB was investigated under flow in more detail. To test the response of MZB cells to increasing flow strength on ICAM-1, several parameters of migratory behaviour were assessed: the migration index, cell velocity, and the straightness of the migration tracks. To get a picture of the MZB motility characteristics, 5 different strengths of shear stress were applied: 0, 1, 3, 6, 10 dyn cm^{-2}. To observe and track the MZB, a time-lapse recording with 1 image every 10 seconds was applied for 30 minutes. Resulting track plots are shown in Fig. 15A, and the statistics of velocity, migration index and straightness are shown in Fig. 15B. With no flow (0 dyn cm^{-2}), MZB cells spontaneously migrated about 75 µm in all directions, which could be seen in the approximately equal number of tracks that terminated above the x-axis (black tracks) and below the x-axis (red tracks) (Fig. 15A). Additionally, the values for migration index centred around zero, indicating no net gain in directional movement (Fig. 15A, 0 dyn cm^{-2}). With the introduction of a relatively low shear stress at 1 dyn cm^{-2}, MZB cells continued to migrate equally in all directions (Fig. 15A and Fig. 15B). At a flow strength of 3 dyn cm^{-2}, a majority of the MZB cell tracks appeared as black, indicating that the MZB cells could detect the flow and respond by migrating up to or against it (Fig. 15A, 3 dyn cm^{-2}). As flow strength increased to 6 dyn cm^{-2} and 10 dyn cm^{-2}, velocity remained constant at all 5 conditions between 4 – 5 µm min^{-1} while migration index and straightness increased (Fig. 15B). These data showed that MZB cells are able to sense flow induced shear stress and re-orient their migration polarity complexes in its direction, with the efficiency of this process increasing with the strength of the flow. To investigate the role of integrin ligand composition on the migratory behaviour of MZB under flow, we tested MZB migration at a flow of 8 dyn cm^{-2} on an inverse gradient of ICAM-1 and VCAM-1 ranging from 5 µg ml^{-1} alone to 0 µg ml^{-1}. The track plots showed that

Figure 15: MZB cells are not flushed out by flow but migrate up to it.

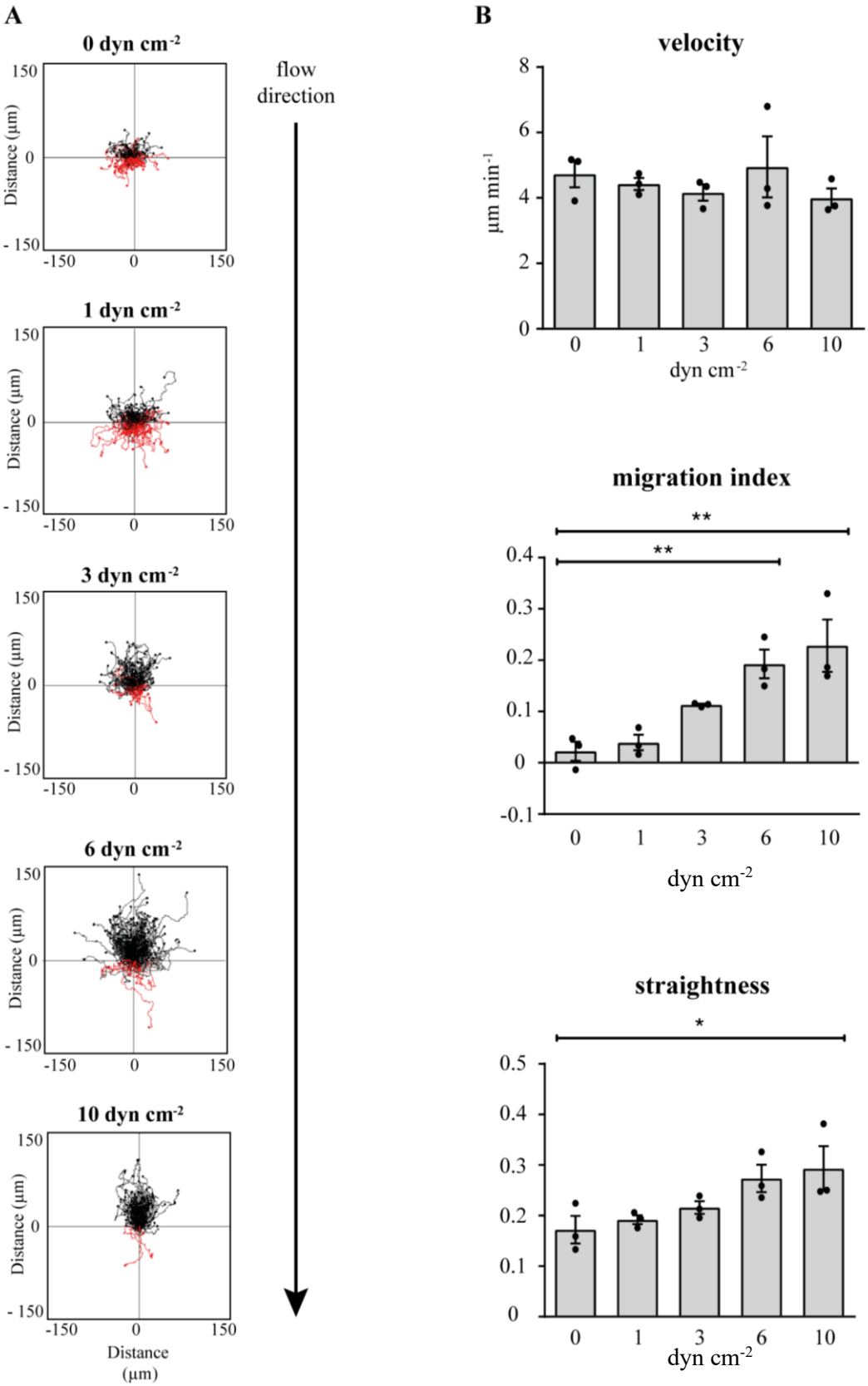

Fig. 15 (on previous page): (A) *Representative track plots of MZB cell migration against flow on ICAM-1 (7 µg ml^{-1}). Flow strengths indicated in dyn cm^{-2}; flow direction indicated by arrow. Tracks with endpoints above the horizontal axis are shown in black; tracks below are shown in red.* ***(B)*** *Quantification of velocity, migration index, and straightness for the indicated flow strengths. All three graphs show different parameters from the same set of experiments with one mouse each. Bars correspond to means ± SEM. Data are form three experiments with one mouse each. Symbols in one condition group denote the three replicates and represent the average of 100 - 200 cells from each individual mouse. *P < 0.05, **P < 0.01, one-way ANOVA with Dunnet post hoc tests comparing all flow strengths to 0 dyn cm^{-2}.*

MZB migrated well against the flow on ICAM-1 alone but were inhibited by VCAM-1 alone (Fig. 16A). The inclusion of VCAM-1 did not affect the migration index when it was half the mixture or less. However, when the proportion of VCAM-1 in the mix was 75% to 100%, the velocity, migration against flow, and straightness parameters were reduced by about half (Fig. 16B). Also, the proportion of cells that could migrate more than 10 µm away from their start position (displacement > 10 µm) dropped from about 80% on ICAM-1 alone to about 35% on VCAM-1 alone (Fig. 16B). To identify any in vivo relevance to MZB responses to ICAM-1 and VCAM-1, spleen sections were stained for these integrin ligands and observed that ICAM-1 is strongly expressed in the MZ, consistent with Lu et al[68]. However, it was observed that VCAM-1 is virtually absent in the MZ even though present in the red pulp (RP) along with ICAM-1 (Fig. 16C).

Figure 16: MZB cell directional migration against flow on ICAM-1 is arrested by VCAM-1.

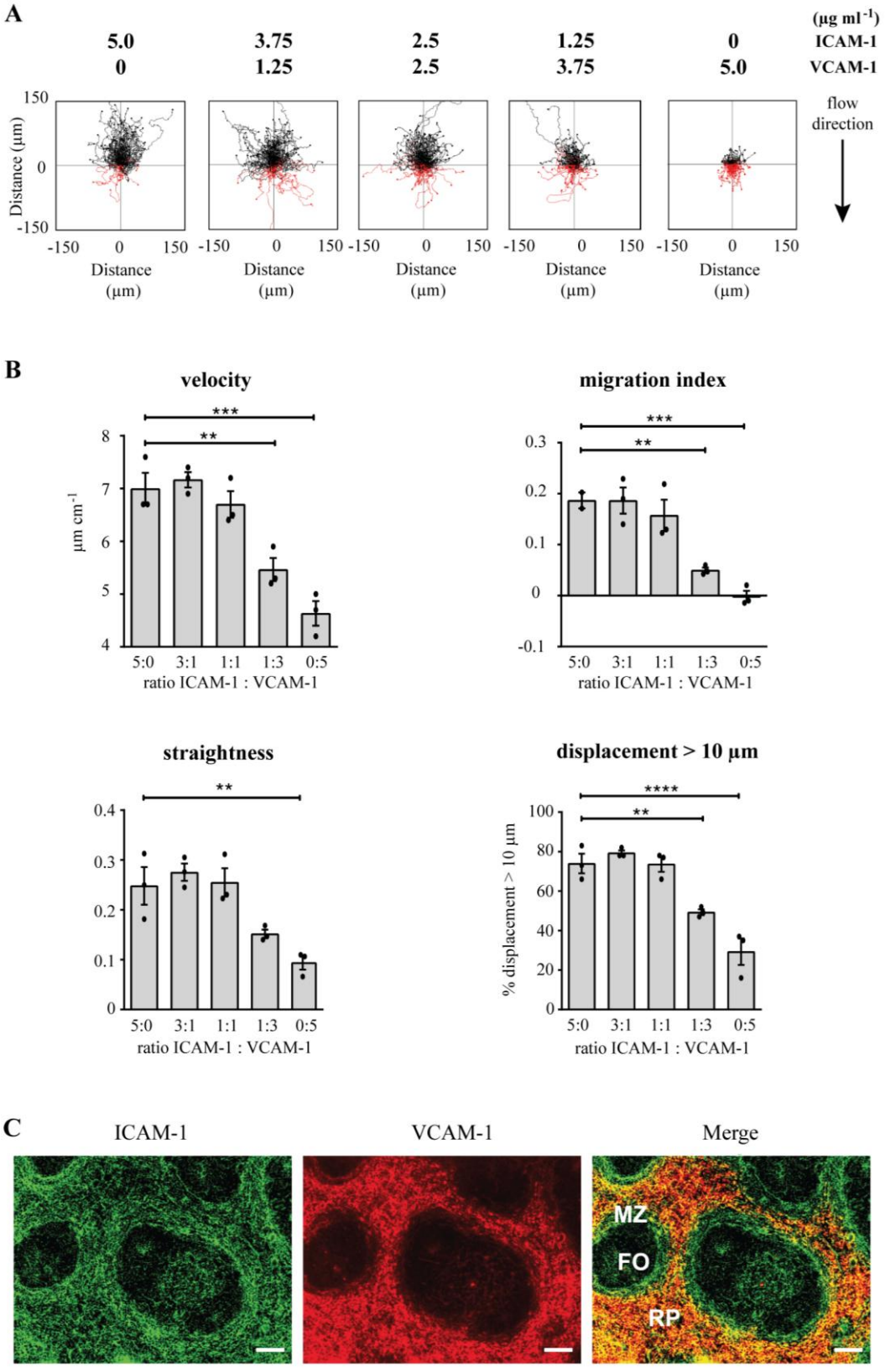

Fig. 16 (on previous page): (A) *Representative track plots of MZB cell migration against flow (8 dyn cm^{-2}; direction indicated by arrow) on coatings of ICAM-1/VCAM-1 ratios as indicated: 5:0, 3:1, 1:1, 1:3 and 0:5.* ***(B)*** *Quantification of velocity, straightness, migration index, and percentage of cells with displacement more than 10 µm for the MZB migration on the ICAM-1/VCAM-1 ratios shown in (A). All four graphs show different parameters from the same set of experiments. Bars show means ± SEM. Data are from three experiments with one mouse each. Symbols in one condition group denote the three replicates and represent the average of 100 - 200 cells from each individual mouse. **P < 0.01, ***P < 0.001, ****P < 0.0001 one-way ANOVA with Dunnett post hoc tests comparing all ICAM-1/VCAM-1 mixtures to ICAM-1 alone.* ***(C)*** *IF microscopy of ICAM-1 (green), VCAM-1 (red), and the merge (orange) in the spleen, showing follicles (FO), marginal zone (MZ), and red pulp (RP). Representative of n = 2. Scale bars = 100 µm.*

4.5 Analysis of migratory behaviour of αPix deficient MZB under flow

4.5.1 Under flow αPix deficiency leads to enhanced motility and to defective ICAM and VCAM mediated adhesion

MZB cells from αPix ko mice show increased migration in transwell assays (Fig. 11). To investigate the role of αPix in the migratory behaviour of MZB on the integrin ligands ICAM-1 and VCAM-1, purified αPix deficient MZB were applied to the above-described flow assay. The migrational parameters under different shear stress conditions (3, 5 and 10 dyn cm^{-2}) were analysed in comparison to WT MZB.

Under flow αPix deficiency leads to an enhanced motility. Results in Fig. 17A and Fig. 17B show that αPix ko MZB migrated about 50% faster than WT MZB under all three flow conditions, resulting in a higher number of longer tracks as shown in Fig. 17A. WT MZB cells moved with a speed of 4 - 5 µm min^{-1}. The speed of αPix ko MZB was increased on ICAM-1 under all three flow conditions by factor 1.5 to 6 - 8 µm min^{-1} (Fig. 17B). αPix ko MZB showed also a significant increase of the migration index (directness) and straightness compared to WT MZB. This shows that in the absence of αPix MZB can still sense shear stress but αPix expression has an inhibitory effect on the ICAM-1 mediated MZB migration up the flow.

Figure 17: MZB cells lacking αPix migrate faster than WT MZB and show increased detachment under flow.

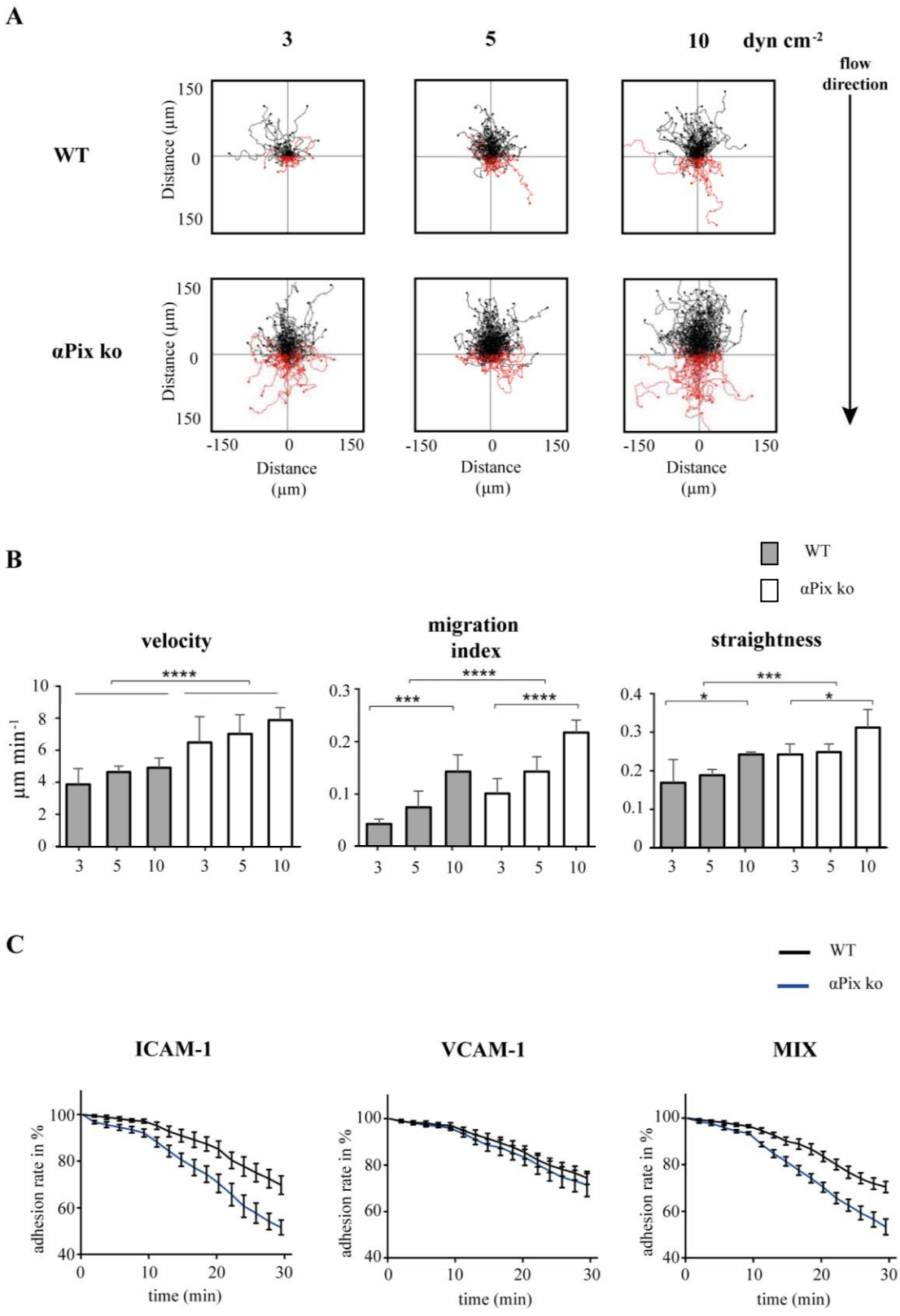

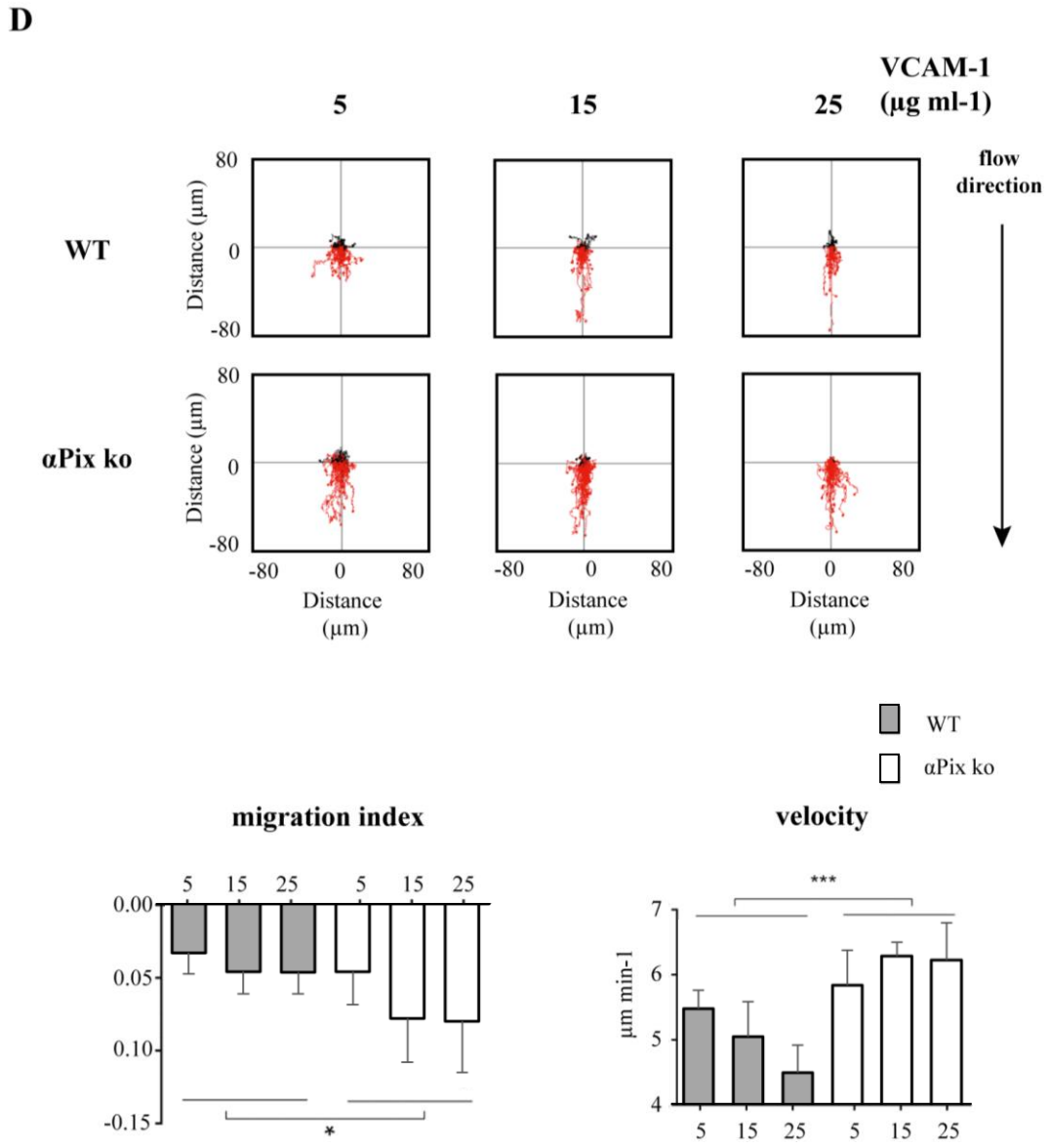

Fig. 17 (A - C on previous page): (A) *Representative track plots of wildtype (WT) and αPix ko MZB cells migrating on ICAM-1 (7 µg ml^{-1}) against flow at a shear stress as indicated: 3, 10 and 15 dyn cm^{-2}.* ***(B)*** *Quantification of velocity, migration index and straightness for the flow strengths shown in (A). Data are from three experiments with one mouse each. Symbols in one condition group denote the three replicates and represent the average of 100 - 200 cells from each individual mouse. Data are expressed as mean ± SEM. *P < 0.05, **P < 0.01, ***P < 0.001, by two-way ANOVA for velocity on ICAM-1, by t-test for migration index on ICAM- and by one-way ANOVA for straightness (comparison of values to WT).* ***(C)*** *Detachment of WT and αPix ko MZB. Fraction of remaining cells calculated as a percentage relative to the number of cells after start of flow on ICAM-1 (1.5 µg ml^{-1}), VCAM-1 (1.5 µg ml^{-1}), or ICAM-1 and VCAM-1 together (0.75 µg ml^{-1} each) under flows of 3 dyn cm^{-2} (0 to 10 min), 9 dyn cm^{-2} (10 to 20 min), and 15 dyn cm^{-2} (20 to 30 min) (n = 5 mice per genotype, 5 experiments total).* ***(D)*** *Data was kindly provided by Dr. Kerry Tedford. Representative track plots of WT and aPix ko MZB cells migrating on increasing VCAM-1 concentrations as indicated (5, 15 and 25 µg ml^{-1}) under flow (8 dyn cm^{-2}). Quantification of migration index and velocity is shown below the track plots. Bars show means ± SEM. *P < 0.05, ***P < 0.001 by two-way ANOVA. 3 mice per genotype in 3 experiments with 1 genotype each.*

Under flow αPix deficiency leads to increased ICAM mediated detachment. Given that cell speed is a function of adhesion[160], the effect of αPix deficiency on the adhesion of MZB on ICAM under static conditions (Fig. 11C) was compared with the effects on adhesion under flow. As described above, under static conditions αPix ko MZB showed an increase of adhesion on ICAM-1 by factor 1.3 (Fig. 11C, WT: 55%, αPix: 72%). In contrast, in the flow adhesion assay designed to measure detachment of MZB under increasing flow strengths, αPix ko MZB showed an increased detachment rate on ICAM-1 alone or on an ICAM-1/VCAM-1 mix compared to WT (Fig. 17C). After 30 min (0 - 10 min: 3 dyn cm^{-2}, 10 - 20 min: 9 dyn cm^{-2} and 20 - 30 min: 15 dyn cm^{-2}) 70% of WT MZB but only 50% of αPix MZB could resist the flow. This increased detachment rate was not observed on VCAM-1 alone, since 80% of both WT and αPix ko MZB were still attached after 30 min. However, this detachment was measured on low amounts of VCAM-1 (1.5 µg ml^{-1} in Fig. 17B).

VCAM induced stop signal is impaired in αPix ko MZB. To investigate the effects of higher VCAM-1 concentrations, MZB migration under flow was tested on slides coated with 5, 15 or 25 µg ml^{-1} of VCAM-1 at a constant shear stress at 8 dyn cm^{-2}. In contrast to the response on ICAM-1, the tracks from WT and αPix ko MZB cells showed a downwards trend on the track plots at all VCAM-1 concentrations (Fig. 17D). That was confirmed by a negative migration index (Fig. 17D, right), indicating that the MZB migrated with the direction or down the flow (Fig. 17D). With increasing VCAM-1 concentrations both WT and αPix ko MZB showed a slight trend of increased negative migration index (Fig. 17D, right). The migration index for αPix ko MZB was increased compared to WT as follows: on 5 µg ml^{-1} increase by factor 1.5, on 15 µg ml^{-1} increase by factor 1.67 and on 25 µg ml^{-1} VCAM-1 an increase by factor 1.73. The velocity of WT MZB on high VCAM-1 concentrations decreased with the increase of VCAM-1 concentrations as follows: 5 µg ml^{-1} VCAM-1: 5,4 µg ml^{-1}; 15 µg ml^{-1} VCAM-1: 5,0 µm min^{-1} and on 25 µg ml^{-1} VCAM-1: 4,4 µm min^{-1}, indicating that WT MZB were trapped with increasing VCAM-1 concentrations. Interestingly, this reduction of velocity by high VCAM-1 concentrations was not observed for αPix ko MZB (Fig. 17D, right). Compared to WT, αPix ko MZB showed on VCAM-1 an increase in velocity of about 30-50% similar to their migration on ICAM-1 (Fig. 17D), and increased migration down the flow (Fig. 17D). This suggests that a VCAM-1

mediated adhesion can trap WT MZB under flow. In the absence of αPix this trapping is reduced. Taken together, these data indicate that on VCAM-1 the αPix deficiency in MZB leads to a wash-out effect, driven by the increase of the velocity, which goes along with a decreased flow-resistance that pushes the cells in direction with the flow.

4.6 In vivo-effect of αPix deletion on follicular shuttling of MZB

The finding that under artificial flow conditions αPix ko MZB cells detached more than WT suggested that not all αPix ko MZB cells would be retained in the MZ in vivo, as many would be washed out and pushed into the direction of the RP. To test the impact of these findings the role of αPix in the follicular shuttling of MZB was investigated in vivo. Therefore, an assay adapted from Cinamon, 2008[126] was established in our lab. Briefly, since MZB scan in the MZ the blood for antigens, it is possible to tag MZB residing the MZ by an injection of a monoclonal antibody (mAb) into the tail vein. A sequential in vivo staining technique including the injection of a second mAb 15 min after the first shows not only the MZB residing MZ but also those MZB cells which shuttled from MZ into B cell follicle.

4.6.1 αPix deficiency leads to altered follicular shuttling of MZB.

The follicular shuttling of MZB was analysed in WT and αPix ko mice by using this in vivo double labelling technique. Splenocytes were counter stained in vitro to quantify the in vivo stainings on MZB with a flow cytometer. The final FACS plot in Fig. 18A visualizes the migratory behaviour of the whole MZB population of the analysed spleen: MZB in B cell follicle = unstained, MZB shuttled from MZ to B cell follicle = single stained (motile), MZ residing MZB = double stained. The read-out by immunofluorescence microscopy delivers the localization of in vivo labelled MZB (Fig. 18A).

Flow cytometry plots of wildtype and αPix ko MZB cells and its statistics (Fig. 18B) showed that the fraction of MZ-localized MZB was decreased in αPix ko mice from WT with 60% to αPix ko with 40%, while the fraction of shuttlers was increased

Figure 18: MZB cells lacking αPix migrate away from the follicle in direction to the red pulp.

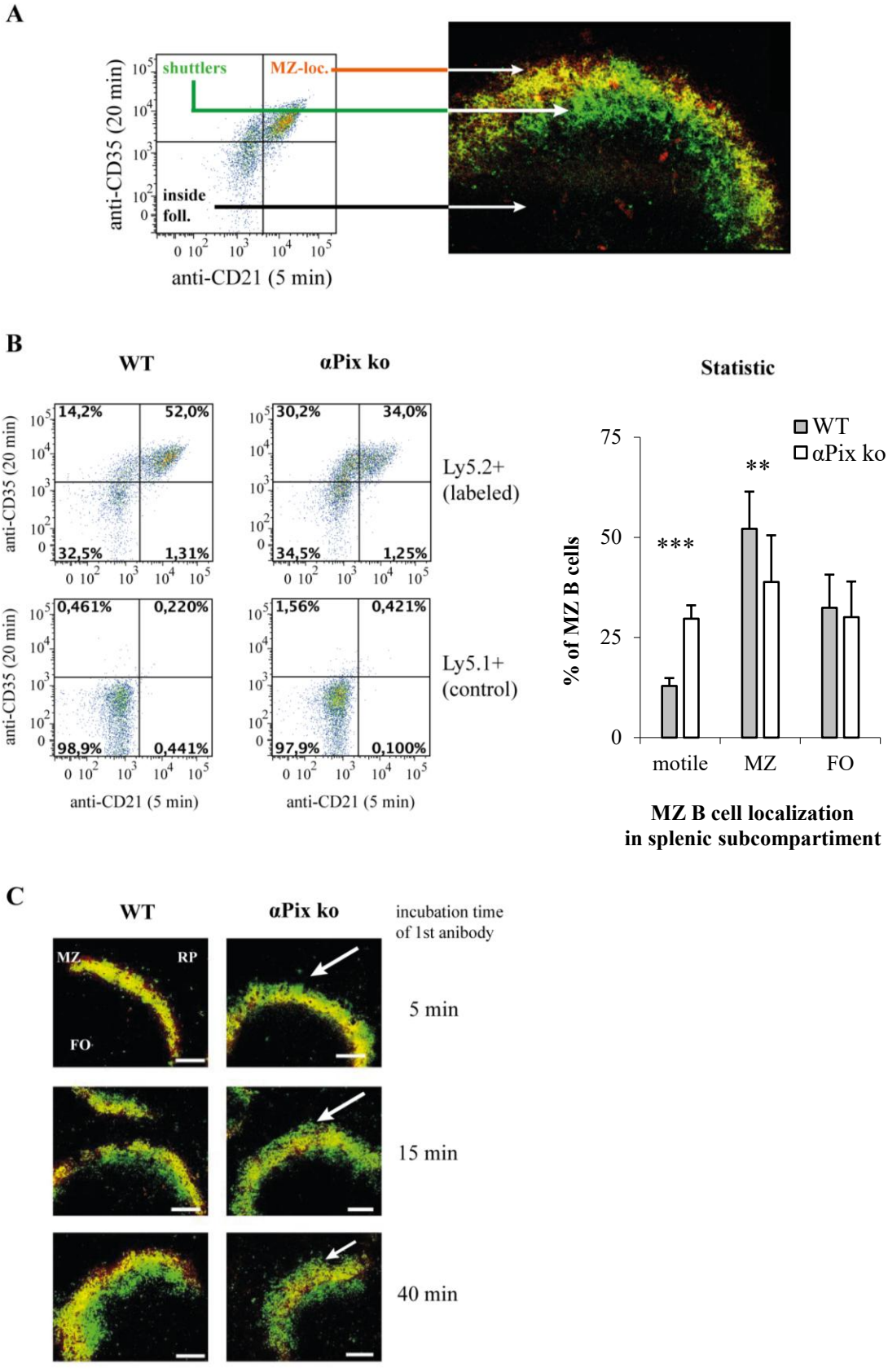

Fig. 18 (on previous page): (A) *Example of FACS and histology staining results for double in vivo labelling of MZB cells. Cells that are labelled with first antibody (anti-CD35) only are called "shuttlers", cells that are doubly labelled with both antibodies (anti-CD21 and anti-CD35) are called "mz-loc.", and cells that are unstained by either antibody are called "inside foll.".* ***(B)*** *Flow cytometry analysis of MZB cells after in vivo labelling of Ly5.2$^+$ WT and αPix ko mice with numbers corresponding to percentage of cells in each quadrant. Ly5.1$^+$ controls (lower panels) show the extent of non-specific binding of iv-injected antibodies during sample processing in vitro. Bars show mean ± SEM. **P < 0.01, ***P < 0.001 by t-test.* ***(C)*** *Microscopy of spleen sections from WT and αPix ko mice. Time course of double in vivo labelling indicated on right (5, 15, and 40 minutes intervals between the two antibody injections). First antibody (anti-CD35) shown in green, second antibody (anti-CD21) shown in red, merged colours appear yellow. Bar = 100 µm.*

with 15% of WT and 30% of αPix ko MZB (Fig. 18B). The unstained MZB fraction was not significantly altered in αPix ko mice.

To view a time course, which should visualize the distribution of cells in vivo, mice were injected with the second antibody after 5, 15 or 40 minutes after the injection of the first antibody. IF images of spleen sections showed in αPix ko mice an abnormally high distribution of single-labelled MZB (green) that were found unexpectedly in the opposite direction of MZ meaning in the direction of the red pulp during the time course (Fig. 18C, white arrows). These data showed that the increased single-labelled population in αPix ko mice, nominally "shuttlers", were not all actually shuttling between MZ and B cell follicle but that some were traveling from the MZ in direction to the red pulp. This suggested an impact of αPix function on the regulation of the correct localization of MZB in the MZ.

4.6.2 αPix deficiency mediated localization defect is MZB intrinsic.

To test if the 'shuttling defect' of αPix MZB cells is intrinsic to the MZB, the advantage of female mice heterozygous for αPix (αPix$^{+/-}$ mice) could be taken, since the gene for αPix (ARHGEF6) is located on the X-chromosome. The random inactivation of X-chromosomes in female mice creates a pseudo-chimeric mouse with half WT cells (αPix$^+$) and half αPix ko cells (αPix$^-$). During the analysis of the flow cytometric data, the distinguishing of the αPix genotypes was done by

Figure 19: αPix deficiency induced mis-localization of MZB is cell intrinsic

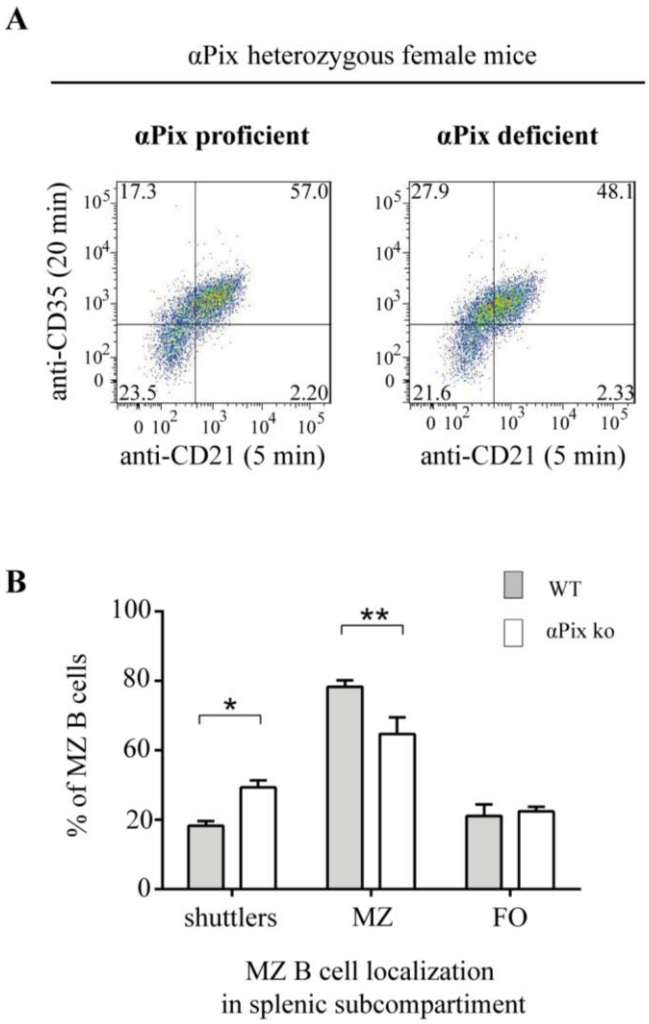

Fig. 19: (A) *In vivo double labelling of MZB in αPix heterozygous female mice (αPix$^{+/-}$). Representative plots of flow cytometric analysis of in vivo double labelled αPix proficient and αPix deficient MZB cells from the same mouse, distinguished by their intracellular αPix expression as indicated.* ***(B)*** *Quantification of relative numbers of shuttlers, MZ-localized, and cells inside follicles (n = 2 mice). Bars show mean ± SEM. *P < 0.05, **P < 0.01 by t-test.*

quantification of the intracellular staining of αPix and separate analysis of the in vivo labelling in αPix expressing and non-expressing MZB.

Double in vivo labelling of the αPix^{+} MZB cells from these mice showed that αPix proficient MZB shuttled normal like WT MZB (Fig. 19), confirming that the defects in the follicular shuttling of αPix ko MZB are intrinsic to the MZB cells and not an environmental effect due to mutation of αPix in other cells. The αPix deficient MZB

from these mice showed the expected significant increase in shuttlers and concomitant decrease in the MZ-localized MZB (Fig. 19).
Altogether, the results derived from the analysis of WT and αPix ko individuums (Fig. 18B) were reproduced and confirmed by the analysis of the follicular shuttling of MZB in the female mice heterozygous for αPix. This indicates that the localization defect of αPix deficient MZB is caused by cell intrinsic alterations.

4.6.3 Validation of staining technique for highlighting the MZ.

It was unexpected that the five-minute injection of anti-CD21 antibody would mark MZB cells inside the MZ but not directly outside it, as there is no tight endothelial barrier to the red pulp as marginal sinus is to the follicle.
To validate the approach, we titrated the amounts of the injected anti-CD21 to determine the extent of cells stained in five minutes. Using a lesser amount of anti-CD21 (0.5 μg), we detected areas of IgM-positive cells outside the anti-CD21-labelled zone. With more antibody (1 μg or 5 μg), these areas were no longer visible as the cells were fully stained on CD21. We also tested these amounts of anti-CD21 in αPix ko mice, which show strongly increased numbers of MZB outside the MZ. The same effect was evident, albeit with higher amounts of anti-CD21, the αPix ko MZB cells at the outside of the CD21 border were only stained when 5 μg of anti-CD21 was used. These results show that suboptimal amounts of anti-CD21 are preferentially taken up by staining of MZB cells in the MZ, and that MZB cells located at the border of the MZ and the RP and beyond are not stained unless the amount of anti-CD21 is increased.
We then co-injected mice with anti-CD21 antibody (1 μg) to highlight the MZ and anti-F4/80 antibody (1 μg), which binds a surface molecule only expressed by red pulp macrophages. We observed that the anti-F4/80 antibody could flow through the MZ to the RP and labelled the macrophages there, while the anti-CD21 antibody was bound only to the MZB located in the MZ (Fig. 20). However, in αPix ko spleens,

Figure 20: Evidence for iv-injected anti-CD21 antibody as a marker that delimits the MZ.

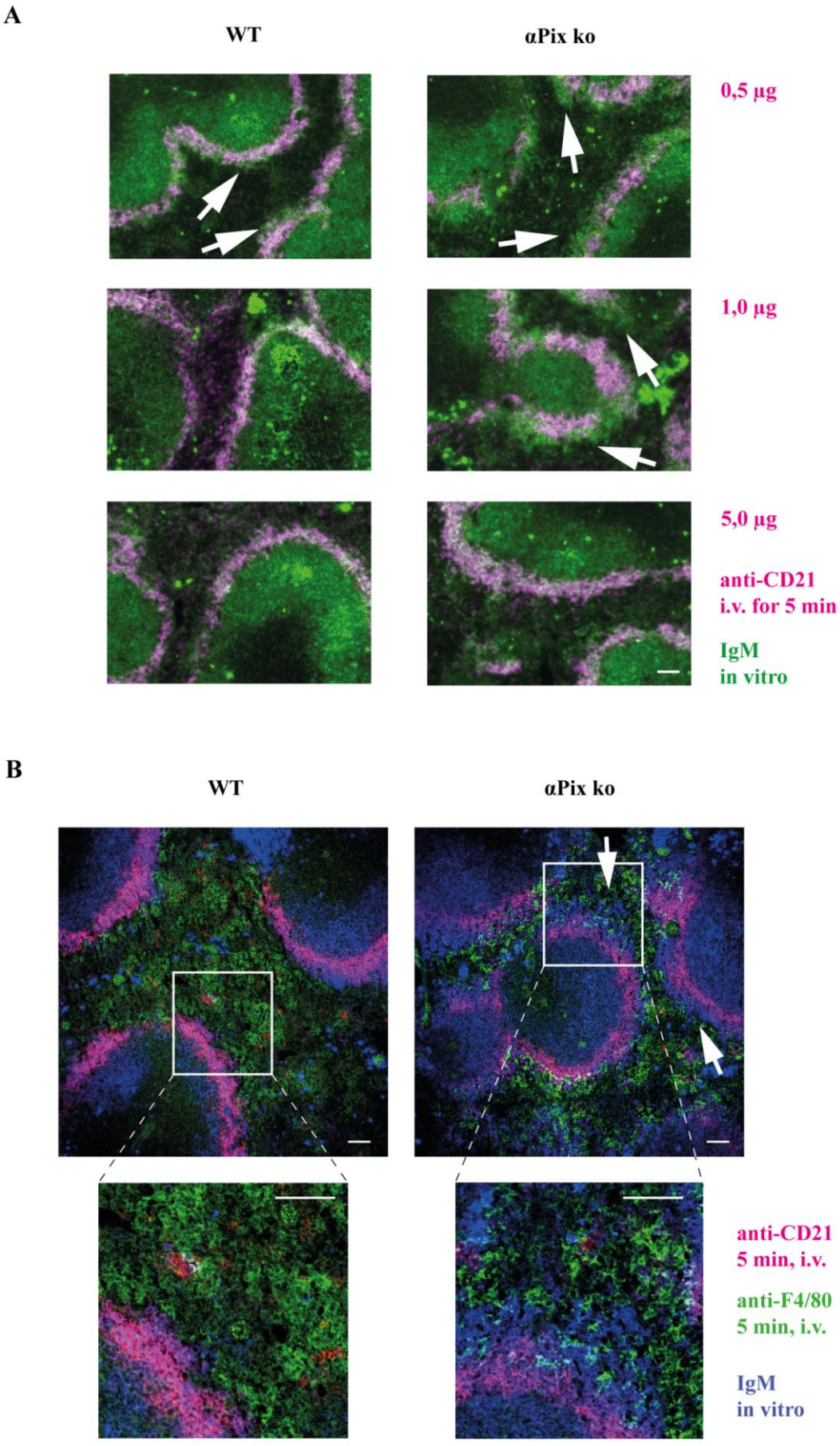

Fig. 20 (on previous page): *Data was kindly provided by Dr. Mark Korthals* ***(A)*** *Titration of iv-injected anti-CD21 in WT and αPix ko mice. Mice were injected i.v. with anti-CD21 (red) for 5 minutes in the indicated amounts (0.5, 1.0 and 5.0 µg). Spleen sections were stained in vitro for IgM (blue). Arrows indicate areas where B cells appear beyond the CD21-labelled marginal zone. WT: n = 3, αPix ko: n = 3, 1 mouse per condition. Scale bar: 50 µm.* ***(B)*** *Co-injection of both anti-CD21 and anti-F4/80 (1 µg each) stains MZB in the marginal zone and red pulp macrophages simultaneously. In vitro staining with IgM shows B cells in αPix ko mice beyond the CD21-labelled marginal zone (white arrow).* ***Inset****: note the interspersed IgM$^+$ and F4/80$^+$ cells in αPix ko spleen. Data represent independent 2 experiments with 1 spleen per genotype. Scale bars: 50 µm.*

unlabelled MZB which were found in direction to the RP were clearly co-localized with the RP macrophages. Therefore, the intermingling of the IgM positive cells with F4/80 positive red pulp macrophages in the αPix ko spleen revealed that the αPix ko MZB, which were not labelled by the 5 min injection of 1 µg antibody are localized in the red pulp (Fig. 20, insets).

4.6.4 Inhibition of LFA-1 causes a mis-localization of MZB into RP

Treating mice with blocking antibodies against VLA-4 and LFA-1 or blocking VLA-4 in ICAM-deficient mice, results in a near complete displacement of MZB cells from the spleen to the blood. However, treating mice with blocking antibodies against LFA-1 alone, and leaving the VLA-4 - VCAM-1 signalling axis intact, does not displace MZB cells into peripheral blood[68, 123]. It was hypothesized that MZB cells in anti-LFA-1-treated mice would not be able to shuttle from the marginal zone to the follicles and would be displaced over time from the MZ to the RP. To test this, WT mice were injected i.v. with control IgG or with anti-LFA-1 antibody. After 30 minutes of anti-LFA-1 incubation, mice were then injected as per the in vivo double labelling protocol with anti-CD35 for 15 minutes highlighted in green followed by anti-CD21 for 5 minutes highlighted in red. Spleens were processed accordingly for the read-out by flow cytometry and immunofluorescence microscopy.

Result of flow cytometry (Fig. 21A and Fig. 21B) showed that the LFA-1 blocking treatment caused a strong redistribution of double-labelled, “MZ-localized” MZB cells to the “shuttlers” population, a 2.5-fold increase in this single-labelled quadrant

Figure 21: Inhibition of LFA-1 causes mis-localization of MZB cells towards the red pulp.

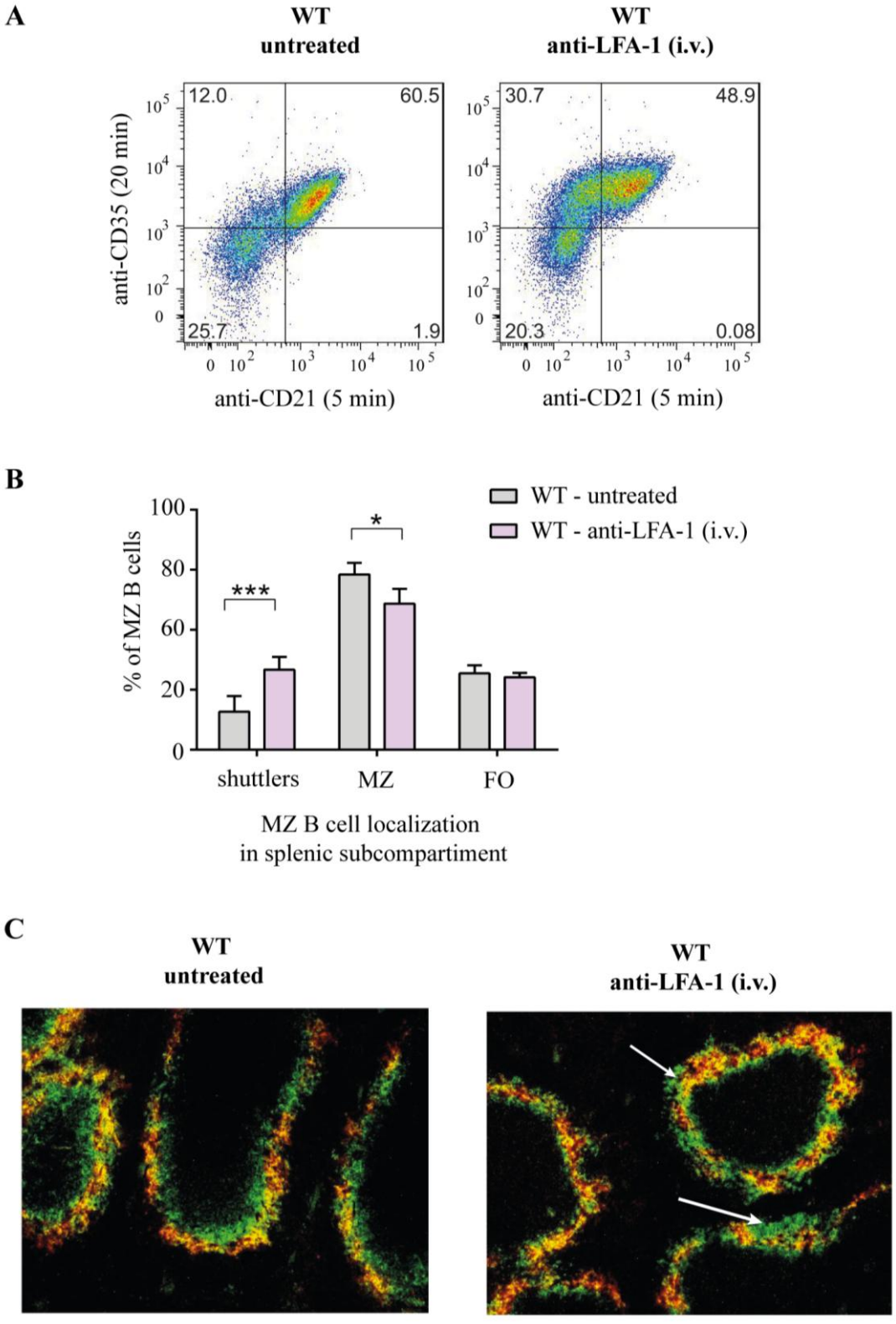

Fig. 21: (A) *Flow cytometry analysis of MZB cells after i.v. injection of anti-LFA-1 antibody to block interactions LFA-1 and ICAM-1 in the marginal zone. Numbers correspond to percentage of cells in each quadrant.* ***(B)*** *Quantification of shuttlers, MZ-localized and inside follicle MZB upon in vivo double labelling (n = 3). Bars show mean ± SEM. *P < 0.05, ***P < 0.001 by t-test.* ***(C)*** *IF microscopy of spleen sections*

from WT mice treated with i.v. injected anti-LFA-1 or control IgG (100 µg) for 30 minutes followed by in vivo double labelling. First antibody (anti-CD35, 20 min) shown in green, second antibody (anti-CD21, 5 min) shown in red, merged colours appear yellow.

(12% to 30% shuttlers, Fig. 21A), despite a reduction of MZ residing MZB (60% to 47%). Spleen sections from these mice showed an abnormal localization of MZB in the direction of the RP of the spleen (Fig. 21C). Thus, the effect of blocking LFA-1 was to induce the release of MZB cells from the ICAM-1 rich MZ, and their re-localization in direction to the VCAM-1-rich RP.

These data show that LFA-1 is required for MZB to shuttle from the MZ to the B cell follicle. They also confirm that the increased single-labelled "shuttler" population that was observed in the αPix ko mice, is located in the RP, since only VCAM-1 mediated adhesion could retain MZB in the LFA-1 treated mice. Finally, they strongly suggest that the force that propels the anti-LFA-1-treated MZB cells from the MZ into the RP is the shear stress caused by blood flow in the MZ. This was at least confirmed by additional experiments published in the journal Nature Communications[140].

4.7 Analysis of S1P treatment on αPix ko MZB under flow

Since S1P is produced by platelets, S1P is found in high concentration in blood but not in blood-empty tissues like lymph nodes or white pulp of the spleen consisting of B cell follicle and T cell zones[120]. S1P serves as an egress signal for immune cells to exit the tissue into the blood[130]. MZ residing MZB are exposed to the blood flow and therefore also to S1P. MZB express the S1P receptors S1PR1 and S1PR3[69]. S1P1 is essential for MZ positioning but becomes rapidly internalized upon S1P ligation in the MZ. S1P1 deficient MZB cannot locate in the MZ but become trapped in the B cell follicle[69]. In static transwell migration assays it was found that S1PR3 is essential for the S1P induced response[69, 70]. Beside this, S1P exerts many varied effects in multiple cell systems, often via controlling cell-cell and cell-matrix adhesion[125], [147].

Therefore, it was speculated that S1P would affect MZB cell migration against shear flow and the effect of S1P treatment on shear flow-induced migration of WT and αPix ko MZB cells was tested on ICAM-1 and VCAM-1.

4.7.1 On ICAM-1 S1P leads to decreased migration of MZB against the flow and this is enhanced in the absence of αPix

In Fig. 22A track plots of WT and αPix ko MZB migrated under flow (3 dyn cm^{-2}) on surfaces coated with 2,5 µg ml^{-1} ICAM-1 or 2,5 µg ml^{-1} VCAM-1 with or without S1P (200 nM) are shown. The migratory behaviour was analysed by the determination of the following parameters: velocity, migration index, straightness and percent displacement more than 10 µm. Statistics are shown in Fig. 22B.

On ICAM-1 S1P inhibited the migration up to the flow and this is enhanced in the absence of αPix. The track plots of the migration in Fig. 22A revealed that on ICAM-1 S1P-treated MZB showed more red tracks than untreated cells, indicating that S1P inhibits MZB migration up to the flow when ICAM-1 is present (Fig. 22A).

ICAM – Velocity. On ICAM-1 without S1P the mean velocity for MZB migrating up the flow was for WT MZB 6,5 µm min^{-1}. αPix ko MZB showed a velocity of 8 µm min^{-1} on ICAM-1 without S1P and was therefore increased compared to the velocity of WT MZB. The presence of S1P did not significantly affect the velocity under flow for both WT and αPix ko MZB (Fig 23B, ICAM-1).

ICAM – Migration index. The positive migration index shows that WT and αPix ko MZB migrate on ICAM-1 up to the flow. Without S1P αPix ko MZB showed an increased migration index compared to WT. In the presence of S1P the migration indices decreased modestly for WT and strongly for αPix ko MZB. This means that S1P induced a stop signal in MZB migrating under flow on ICAM-1. The effect of S1P induced reduction of the migration index was much higher in αPix ko MZB compared to WT. This resulted in a lower migration index for αPix ko MZB in the presence of S1P on ICAM-1 compared to WT MZB. This suggested a function of αPix in the regulation of the S1P induced migratory response of MZB on ICAM-1.

Figure 22: S1P inhibits MZB directional migration against flow but increases motility.

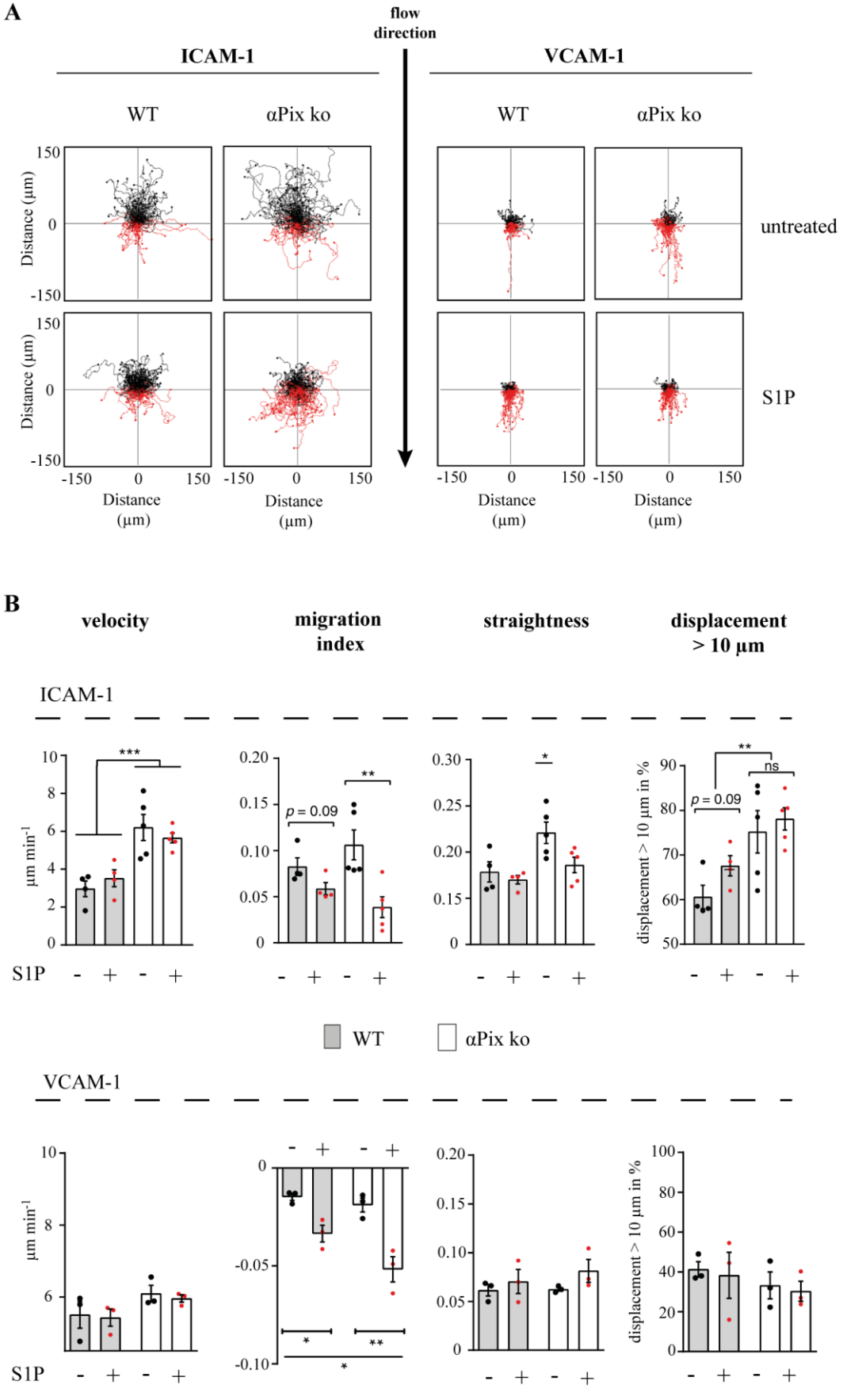

Fig. 22 (on previous page): *Data was kindly provided by Dr. Kerry Tedford and Dr. Mark Korthals.* ***(A)*** *Representative track plots of WT and αPix ko MZB, untreated or with treated with S1P (200 nM), migrating under flow (3 dyn cm^{-2}) on ICAM-1 (2.5 µg ml^{-1}) or VCAM-1 (2.5 µg ml^{-1}).* ***(B)*** *Quantification of velocity, migration index, straightness and percentage of cells with displacement greater than 10 µm for WT (grey bars) and αPix ko (white bars) MZB on ICAM-1 (upper panel) or VCAM-1 (lower panel). WT: n = 4, αPix ko: n = 5 mice with 5 experiments in total. Data are expressed as mean ± SEM. *P < 0.05, **P < 0.01, ***P < 0.001 by t-test for migration index and percentage displacement on ICAM-1, one-way ANOVA (for straightness and percentage displacement, comparison of values to WT), and two-way ANOVA (velocity on ICAM-1, migration index on VCAM-1).*

ICAM– Straightness. The straightness of WT MZB was not significantly affected by the presence of S1P. On ICAM-1 without S1P αPix ko MZB showed under flow an increased straightness compared to WT (WT: 0.175, αPix ko: 0.225, factor 1.3). In the presence of S1P, this increased straightness decreased almost to WT level on ICAM-1.

ICAM – Percent displacement more than 10 µm. On ICAM-1 without S1P 60% of WT MZB displaced more than 10 µm. In the presence of S1P the percentage increased to 68% (p = 0.09). This indicates that on ICAM-1 S1P increased the number of long-distance migrating cells. The percentage of αPix ko MZB migrated more than 10 µm on ICAM-1 without S1P was at 76%. This is an increase to WT by factor 1.3. When S1P was present αPix ko MZB tended also to an increase of the long-distance migrating cells but this was not significant (without S1P: 75%, to 78% with S1P). In summary, S1P had no significant effect on the displacement of αPix ko MZB, but αPix ko MZB migrated longer distances on ICAM-1 without S1P compared to S1P treated WT MZB.

4.7.2 On VCAM-1 S1P induced increased migration down to the flow and this is enhanced in the absence of αPix

VCAM – Velocity. On VCAM-1 the velocity of WT MZB was at 5.6 µm min^{-1} and for αPix ko MZB at 6.1 µm min^{-1}. Although the tendenz of increased speed is also visible, the difference was not significant. This means that on VCAM-1 the speed of

migrating MZB was not altered by the lack of αPix, suggesting that αPix has only a minor function in VCAM VLA-4 signalling of MZB. Velocity was not altered when WT and αPix ko MZB were treated with S1P compared to untreated MZB (Fig 23B, VCAM-1).

VCAM – Migration index. The negative migration index shows that WT and αPix ko MZB migrated in the direction with or down the flow on VCAM-1. The presence of S1P increased this negative migration index for both WT and αPix ko MZB. For αPix ko MZB this increase was higher compared to WT (WT: 2-fold, αPix ko: 3-fold).

VCAM – Straightness. On VCAM-1 the straightness was not altered by the presence of S1P or the lack of αPix.

VCAM – Percent displacement >10 µm. On VCAM-1 a fraction of 41% of WT MZB displaced more than 10 µm. For αPix ko MZB this percentage was reduced to 33%, but this was not a significant reduction. Although also not significant, the presence of S1P leads to a slight reduction of the numbers of cells displaced more than 10 µm in both WT (38%) and αPix ko (30%) MZB.

Summary – S1P effect. Summarized, these results show that MZB migration up the flow on ICAM-1 is inhibited by S1P, which likely acts on LFA-1 activation or its positioning in MZB during their polarisation (Fig. 22B). The data also suggest that in MZB αPix is involved in the ICAM-1 LFA-1 mediated adhesion. On VCAM S1P induced an increase of migration down the flow. Since on VCAM-1 the migration down the flow is further increased in the absence of αPix, αPix serves as ‚anti-loss factor' for MZB. All together this indicates that in the presence of S1P αPix deficiency leads to a reduced ability to migrate up the flow on ICAM-1 and a reduced ability to resist the shear stress on VCAM-1.

4.7.3 – S1P inhibition of MZB migration up the flow requires S1PR3

S1PR1 functions as egress sensor to shuttle from the B cell follicle back into the MZ. Upon S1P ligation in the MZ S1PR1 becomes rapidly internalized. S1PR3 is essential in S1P induced migration rates in static transwell assays. The role of S1PR3 in the follicular shuttling of MZB is still unknown. To investigate the role of S1PR3 in S1P-induced decrease of migration index of MZB on ICAM-1 (Fig. 22), additionally to αPix, the S1P receptor 3 was co-deleted by crossing αPix ko with S1PR3 ko mice (Fig. 23).

MZB were sorted out of spleens derived from WT, αPix ko, S1PR3 ko and αPix/S1PR3 dko mice. Migration of WT, αPix ko, S1PR3 ko, and αPix/S1PR3 dko MZB was analysed under flow (3 dyn cm^{-2}) on ICAM-1 (2.5 µg ml^{-1}) with or without S1P (200 nM). Track plots are shown in Fig. 23A. Statistics of velocity, migration index and straightness are shown in Fig. 23B.

As expected, αPix deficiency led to increased velocity of S1PR3 ko MZB (Fig. 23A and Fig. 23B). It was also observed again that S1P modestly inhibited the migration of WT MZB but strongly inhibited the migration of αPix ko MZB up the flow (Fig. 23A and Fig. 23B, migration index). Strikingly, the strong effect of S1P on αPix ko MZB was completely abolished in MZB lacking S1PR3 or both αPix and S1PR3 (Fig. 23A and Fig. 23B). With other words, MZB lacking S1PR3 were completely resistant to S1P induced reduction of the migration index.
Unexpectedly, there was a slight decrease in straightness in the S1PR3 ko MZB that was independent of S1P treatment (Fig. 23A and Fig. 23B). This finding suggested that S1PR3 also has a ligand-independent function in MZB, potentially in sensing shear stress leading to migration.
Together, these results showed that S1P inhibition of flow-directed migration proceeded via S1PR3. This is a new observation published for the first time by our research group[140].

Figure 23: S1P inhibition of MZB migration up the flow requires S1PR3.

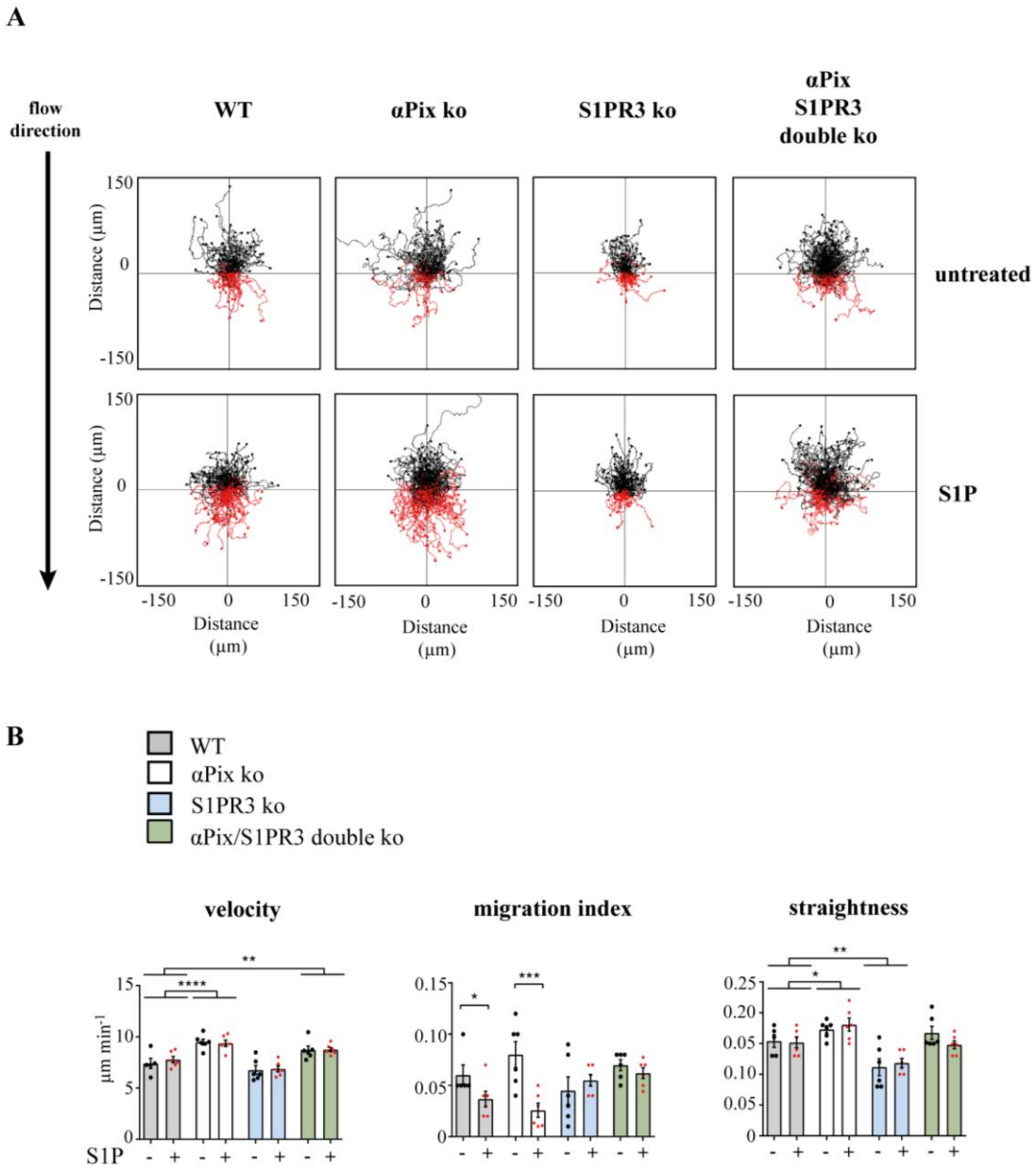

Fig 24: *Data was kindly provided by Dr. Kerry Tedford and Dr. Mark Korthals.* ***(A)*** *Representative track plots of WT, αPix ko, S1PR3 ko, and αPix/S1PR3 double ko MZB, untreated or treated with S1P (200 nM), migrating under flow (3 dyn cm^{-2}) on ICAM-1 (2.5 µg ml^{-1}).* ***(B)*** *Quantification of velocity, migration index, and straightness. Two-way ANOVA significance indicated with horizontal bars for genotype significance, brackets for Mann–Whitney test (migration index). Bars show mean ± SEM. *P < 0.05, **P < 0.01, ***P < 0.001, ****P < 0.0001. Data represent 12 experiments with two mice each, six mice per genotype total. Symbols in one condition group denote the replicates and represent the average of 100 - 200 cells from each individual mouse.*

4.7.4 Translocation of αPix ko MZB towards the red pulp is rescued by co-deletion of S1P-receptor 3

To investigate the effect of the missing stop signal in αPix/S1PR3 dko MZB, the positioning of MZB was analysed in αPix ko, S1PR3 ko, αPix/S1PR3 dko bone marrow chimeric mice compared to WT bone marrow chimera.

MZB numbers from these BM chimeric mice were increased in αPix ko and αPix/S1PR3 dko, consistent with the αPix ko phenotype (Fig. 24). As shown in Fig. 24 mice reconstituted with bone marrow lacking S1PR3 only develop normal relative numbers of MZB in the spleen. However, the co-deletion of αPix and S1PR3 lead to increased relative numbers of MZB in the spleen (WT: 6%, αPix ko: 10%, S1PR3 ko: 5%, αPix/S1PR3 double ko: 11%).

Figure 24: Increased numbers of αPix ko MZB in spleen.

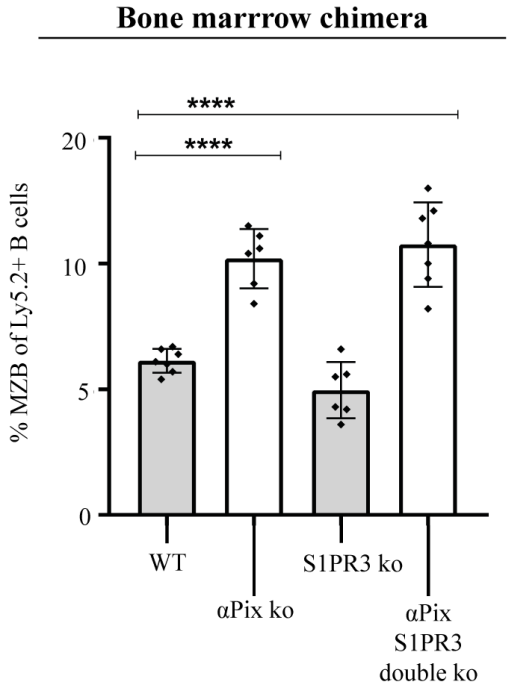

Fig. 24: *Quantification of Ly5.2$^+$ MZB numbers in Ly5.1$^+$ recipient mice, which were lethally irradiated and reconstituted with bone marrow of genotypes as indicated. Splenocytes of reconstituted mice were analysed by flow cytometry and MZB were identified as follows: Ly5.2$^+$B220$^+$CD21^{hi}CD23^{lo}. WT, αPix ko, S1PR3 ko: n = 6; αPix ko/S1PR3 dko: n = 7. Bars show mean ±SEM. **** p <0.001 by one-way ANOVA.*

Figure 25: Translocation of αPix ko MZB toward the red pulp is rescued by co-deletion of S1PR3.

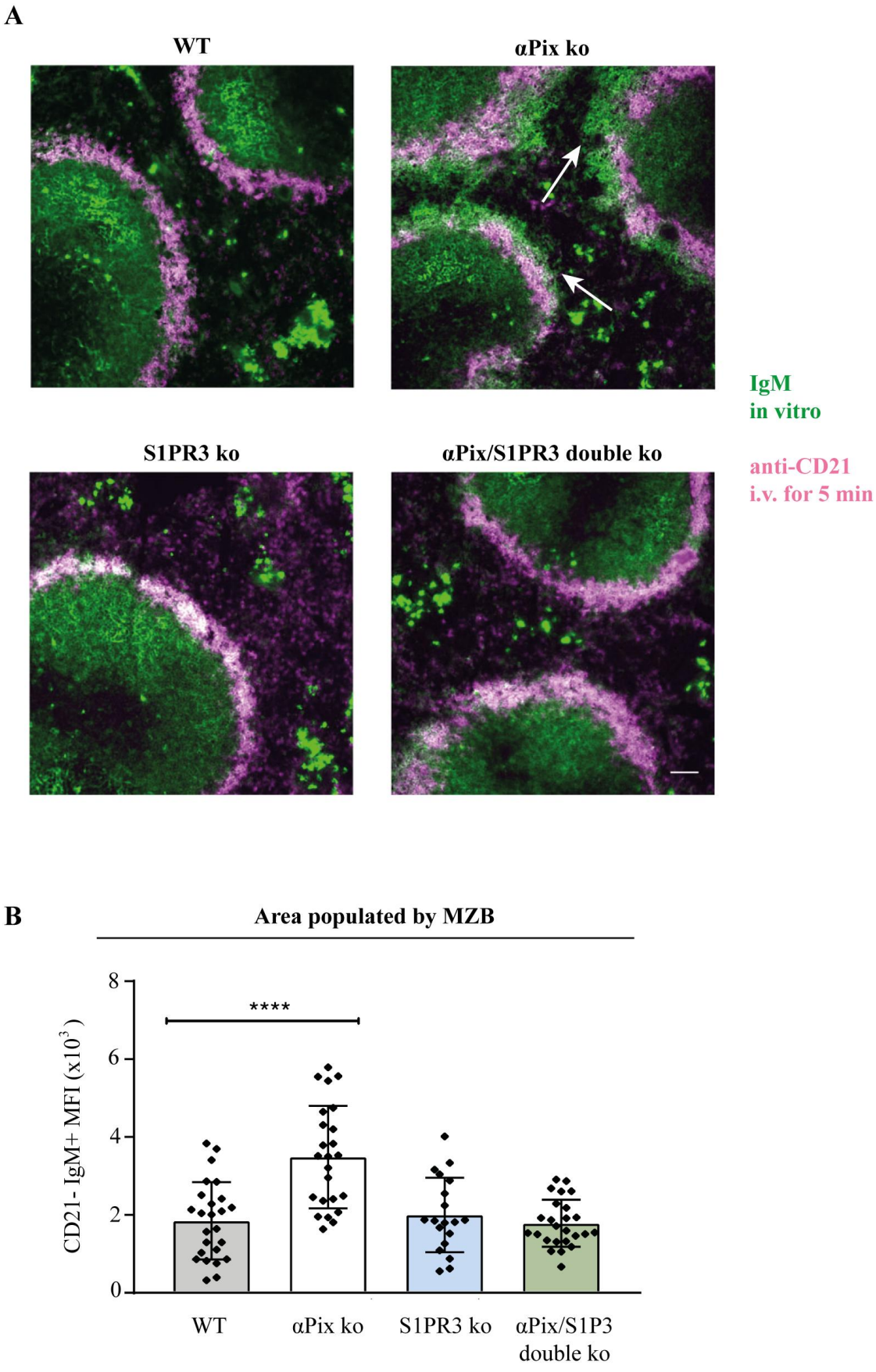

Fig. 25 (on previous page): (A) *Immunofluorescence microscopy of IgM positive cells located beyond the anti-CD21-positive boundary of the marginal zone (white arrows) in wildtype (WT), αPix ko, S1PR3 ko, and αPix/S1PR3 dko BM chimeric spleens. Scale bar, 50 µm.* ***(B)*** *Quantification of mean fluorescence intensity (MFI) of $CD21^{-}$ IgM^{+} cells inside a band of 60 µm beyond the marginal zone, itself calculated as a band of 60 µm outside of MAdCAM-1 staining. Bars show mean ± SEM. Data represent two independent experiments with three bone marrow chimeric mice per genotype. Symbols in one condition group denote individual follicles (WT, αPix ko and αPix/S1PR3 dko: n = 5 mice; S1PR3 ko: n = 4 mice). ****P < 0.0001, one way ANOVA with Dunnett post hoc test relative to WT.*

The MZ was visualized using the 5 min anti-CD21 injection method and merged with the in vitro IgM staining to identify MZB beyond it. There were bone marrow-reconstituted mice used because the deletion of αPix may affect stroma cell types and S1PR3 ko mice have a defective MAdCAM-1+ endothelial layer on the marginal sinus[70], which could potentially affect the shuttling of MZB into the B cell follicle by making the barrier more porous.

In WT and in S1PR3 ko spleens from chimeric mice, no areas of IgM-positive cells were located just outside the border of the MZ (Fig. 25A). As expected in spleens populated by αPix ko cells, large areas of IgM-positive MZB were found outside the anti-CD21-marked zone (Fig. 25A), reflecting the defect in adhesion of αPix ko MZB observed in the detachment under flow assay (Fig. 17C). In spleens of αPix/S1PR3 dko BM chimeric mice the mis-localization of MZB into RP could not be observed anymore. Patches of strong green staining in the middle of the red pulp likely represent plasma B cells (Fig. 25A).

The bar graph in Fig. 25B shows the quantification of IgM positive cells 60 µm beyond the marginal sinus. The level of the mean fluorescence intensity (MFI) was similar for WT, S1PR3 and αPix/S1PR3 dko MZB but increased by factor 2 for αPix ko MZB.

Taken together S1PR3 exerts a downward directional force on MZB towards the RP. If S1P stop signal is abolished in αPix/S1PR3 dko MZB, MZB overcome RP mis-localization by migration up the flow.

5. Discussion

In this study the role of the RhoGEF αPix in MZB regarding their development and positioning in the murine spleen was investigated. Due to limitations of experimental setups to answer the questions underlying the hyper-motile phenotype of αPix deficient lymphocytes, a live-cell imaging system was combined with a innovative pump to generate constant flow and was published in the ‚Journal of Visualized Experiments'[141]. This innovative setup enabled the investigation of migrational behaviour of MZB under flow for the first time, which was published in the journal ‚Nature Communications'[140]. At least this study discovered that αPix is involved in the regulation of integrin-mediated adhesion and shear stress-induced migration of MZB under flow. It was demonstrated that the loss of αPix leads to a drift of MZB out of the MZ in direction to the RP triggered by the blood-flow. This is caused by a decreased attachment in the MZ and a defect S1P induced stop signal transduced through S1PR3 in αPix deficient MZB. Blood flow induced shear stress was identified as new directional force guiding MZB in direction to the B cell follicle and S1P and VCAM-1 as counteracting forces. In conclusion an extended model for the process of MZB positioning in the MZ was proposed[140] (Fig. 26).

5.1 The role of αPix in the development of MZB

In αPix deficient mice an increased population of MZB can be observed compared to the WT (Fig. 10). A role of αPix in signalling of the B cell receptor of B cells was described[42]. The influence of the BCR defect on the increased MZB population in αPix ko mice was not discussed. Mouse models with reduced signal strength or defects in the BCR signalling pathway, such as the QM (quasi monoclonal) mouse[76] or the Btk ko mouse[77], show enlarged MZB populations. Therefore, it is possible that in the absence of αPix the reduced BCR signal could result in an increase of the αPix ko MZB population. Since no detailed data sets regarding the differentiation stages of the progenitor cells of αPix ko MZB were available so far, a detailed analysis of the MZB progenitor cells in bone marrow and spleen was performed in the course of this study. The analysis of the different developmental stages of MZB progenitor cells in the bone marrow and spleen of αPix ko mice showed no significant differences to WT (Fig. 7

and 9). Thus, the already published data[42] was reproduced. Nevertheless, αPix ko mice produce spleens magnified 1.8 times (Fig. 8A), which is reflected in the increase in the total number of all B cell subpopulations (Fig. 10A). This means that an αPix deficiency leads to an increased colonization of the spleen by all lymphocyte subtypes. The increase of the absolute number of αPix ko MZB is an exception within the splenic lymphocytes, since all B cell subpopulations showed a global increase by factor 1.8 but MZB showed almost a doubling of the factor to 3.5 (Fig. 14). MZB develop from T2 B cells and T2 B cells develop from T1 B cells. The slight decrease of the αPix induced global increase by 1.8 for T1 B cells (factor 1.6), the slight increase for T2 B cells (factor 2.0) but constant increase for the T3 B cell population (factor 1.8) (Fig. 9D), could indicate a shift B cell differentiation towards MZB, which could result in an increased MZB population. This observation suggests an influence of αPix-deficiency induced defects in BCR B-cell signalling on MZB development. The analysis of purified MZB progenitor cells could give insight into the αPix involvement in BCR signalling during MZB differentiation. However, the processing of those approaches is very limited, due to the low cell count of MZB T progenitor cell with about 3 - 5 x 10^5 per MZB T progenitor subtype per spleen (Fig. 9D, left). This low number will be further reduced during the purification process. For further detailed investigations purification processes with increased effectivity would be needed.

The MZB populations in S1PR1 ko[69] and in αPix/S1PR3 double ko bone marrow reconstituted mice (Fig. 24) are also enlarged compared to WT. In MZB, S1P receptors play a role in migration processes and their correct localization in the MZ. S1PR1 deficient MZB localize abnormally inside the B cell follicle because they are not able to localize or shuttle into the MZ[69, 126]. S1PR3 ko MZB localize normal in the MZ of BM reconstituted mice (Fig. 25A) but show an increased migration into the B cell follicle upon S1PR1 inhibition[126] and LPS activation[70]. That observation remained elusive in the literature but can now be explained, since it was demonstrated here that S1P inhibits MZB migration up the flow via S1PR3 signalling and S1PR3 deficient MZB are not responsive to S1P induced stop signal. Therefore, S1PR3 deficient MZB show an increased ‚S1PR1 inhibition'-induced migration into B cell follicle, since the S1PR3 mediated counterforce or the S1P induced stop signal of up-flow migration is missing (Fig. 23B, migration index). It further enables MZB with a lack of αPix and S1PR3 simultaneously to localize normally in the MZ in contrast to αPix single ko MZB (Fig. 25). However, mice reconstituted with αPix/S1PR3 double ko bone

marrow cells develop also an increased MZB population (Fig. 23). As in αPix/S1PR3 double ko BM chimeric mice MZB localize normal in the MZ but develop also an increased relative number of MZB, the RP mis-localization of MZB can be excluded as factor contributing to increased MZB populations in αPix deficient mice. In summary, according to the presented data, the increased population of MZB in αPix ko mice cannot be explained by an altered differentiation of MZB precursors or an altered localization of αPix ko MZB. Consequently, further mechanisms for the regulation of MZB homeostasis must exist but are still unknown.

It could be shown that αPix plays a role in the regulation of the basal and chemokine induced motility of MZB (Fig. 11). The increased motility of αPix deficient MZB was not due to altered expression levels of chemokine receptors or integrins (Fig. 12A and 13B) but could be the effect of increased βPix expression (Fig. 12C), by which MZB likely compensate the lack of the αPix expression as proposed for αPix deficient thymocytes[54]. βPix is involved in the regulation of cellular protrusion formation[135, 136, 138, 139, 142]. Increased βPix levels lead to increased Rac activity, which correlates with multiple peripheral lamellae or protrusions and increased random motility[144]. The observation of more frequently occurring shape changes and protrusion formation of αPix ko MZB as described for αPix deficient thymocytes[54] supported this model. As shown in the figures 12, 18, 23 and 24 the lack of αPix expression in MZB leads to increased motility. In T cells αPix deficiency is associated with inefficient conjugate formation with antigen presenting cells[42]. Furthermore, in αPix ko mice the maturation of thymocytes at the stage of positive selection is disturbed, due to reduced interactions with stroma cells in the thymus[54]. MZB interact via the CD1d molecule with iNKT cells that express an invariant T cell receptor specific for CD1d. This interaction regulates the MZB population in a negative way[87]. Since the interaction of MZB and iNKT cells results in a reduction of the MZB population, an inefficient interaction and communication of MZB and iNKT cells could lead to an increase in MZB numbers in mice with αPix deficiency. Another theoretically conceivable possibility would be a reduced iNKT population in the spleen of αPix ko mice, which could lead to the same effect. Therefore, a possible mechanism for the increased MZB population in αPix ko mice could be a disturbed interaction with iNKT cells.

In summary, the regulation of the homeostasis of the MZB population is still not understood in detail, due to a very complex process influenced by a variety of factors. This is illustrated by the high number of factors which are involved in a wide spectrum

of cellular functions (Tab. 1 and Tab. 2). The data of this study indicate the possibility that during MZB development αPix is involved in signalling pathways like BCR and chemokine receptors and/or in cell-cell interactions like iNKT cells which results in an increased MZB population.

5.2 The role of αPix on the motility of MZB under static conditions

For the biological function of MZB cells the chemokines S1P and CXCL13 are of utmost importance. Due to the finely tuned regulation of the corresponding chemokine receptors S1PR1, S1PR3 and CXCR5, MZB are able to shuttle between the marginal zone and the B cell follicle, two splenic sub-compartments separated by the marginal sinus[126] (Fig. 5). It is known that αPix deficient B and T cells show increased basal and CXCL12 induced motility rates in vitro[42]. However, a differential analysis of MZB responses to chemokine was still outstanding.

In the course of this study, it could be shown that the αPix deficiency leads to S1P-induced migratory responses that are increased by a factor of 1.6 to 2 (Fig. 11). S1PR1 does not play a role in the S1P-induced migration of WT MZB in vitro, since S1PR1 deficient MZB did not show any differences regarding their migration rate compared to WT[69]. Since S1P-induced migration in vitro is mainly mediated by S1PR3[69, 70], the result shown in Fig. 11 suggests an altered S1PR3 induced response of αPix ko MZB. However, this experimental approach does not allow differential conclusions regarding the contribution of S1PR1 or S1PR3 to the increased S1P-induced migration rate of αPix ko MZB. Therefore, a possible role of αPix in the ligand-induced inactivation or down-regulation of S1PR1 could not be excluded at this point. Since the CXCL13-induced migration rate of αPix ko MZB is also increased by a factor of 2.3 to 6 compared to WT, CXCR5-mediated response is also altered in the absence of αPix in MZB (Fig. 11). A possible explanation for the hypermotility of αPix ko MZB would be an increased expression of chemokine receptors on the cell surface. The flow cytometric analysis of S1P receptors 1 and 3, turned out to be very difficult and could not be performed precisely. On the one hand, the analysis of S1PR1 is not trivial due to its ligand-induced inhibition by internalization, since a high concentration of S1P is released from the red pulp of the spleen during processing of the spleen tissue for cell harvest and comes into contact with MZB. This leads to the internalization process of

S1PR1[132], which can make the detection on the cell surface difficult. On the other hand, only few antibodies are available for the detection of S1PR1 and S1PR3 and in most cases human receptor peptides have been used for immunization. This can compromise the specificity during the analysis of murine samples. Furthermore, the majority of antibodies have been used for receptor analysis in western blot assays and are only conditionally suitable for flow cytometric measurements of receptors on the cell surface. One reason is that western blot is an analysis of denatured or stretched proteins and flow cytometric measurements are an analysis of native or folded proteins in or on the cells. Thus, a measurable signal could be generated with a S1PR3 specific antibody, but the S1PR3 ko sample as negative control showed the same signal strength (not shown), which in turn shows the non-specificity of the anti-S1PR3 antibody used. The use of further S1PR1 and S1PR3 specific antibodies did not lead to a result, as they did not generate measurable signals (not shown). The analysis of the CXCR5 expression of αPix ko MZB showed that the αPix deficiency does not affect the exposure of CXCR5 on the cell surface of MZB (Fig. 12). Nevertheless, CXCL13-induced migration is increased (Fig. 11). Since cellular migration is mediated via integrins the expression of integrins was analysed but showed also no αPix deficiency related differences (Fig. 12B). In summary, this suggests in MZB an intracellular mechanism in which αPix is involved in the regulation of the signal transduction from chemokine receptors to integrin complexes needed for cellular adhesion and migration.

It could be shown that the absence of αPix leads to an increased expression of βPix in MZB (Fig. 12). It is known that βPix, which is homologous to αPix, can activate the GTPases Rac1 and Cdc42 as GEF[14], which in turn regulate cellular migration[135] (point 1.1.2.) and thus has a stimulating effect on processes underlying the migration of cells[136]. βPix is highly dynamic in the course of motion processes in focal adhesions. βPix activates Rac1 in lamellipodia and regulates the maturation of focal adhesions in a negative way, i.e. βPix localizes in newly forming focal adhesions[143] and dissociates again during their maturation[136]. With other words, cellular migratory processes are based on the dynamics of βPix. PIX proteins form the PIX/GIT complex by interaction with GIT proteins (point 1.1.6 and 1.1.7). The αPix deficiency leads to increased βPix expression in thymocytes[54] and to destabilization and functional loss of Git-2[42]. Therefore, the absence of αPix results in a PIX/GIT complex with an altered composition. It is conceivable that in the absence of αPix βPix replaces αPix in the

PIX/GIT complex. The same applies to Git-1, which could take the place of Git-2 in αPix ko. If the composition of the PIX/GIT complex is changed in such a way that the dynamics of βPix and thus the regulation of Rac1 activity can no longer be guaranteed, this could lead to morphological abnormalities of αPix deficient MZB, since protrusions resulting from increased Rac activation can no longer be destabilized or keep reappearing. The observation that activated Rac1 is involved in the reinforcement and stabilization of newly formed cellular protrusions[8] supports this model. Furthermore, it could be shown that the level of activity of Rac1 decides about directed or random migration processes of cells[144]. A low level of Rac1 activity led to directional migration and a high level of Rac1 activity was associated with random or undirected migration of cells. Since αPix ko MZB also showed morphological anomalies despite increased βPix expression levels, it is possible that these are also caused by increased Rac1 activity as in αPix deficient thymocytes[54].

5.3 Design of an innovative experimental setup for a flow chamber system to observe and study the adhesion and migration of living cells

Since the further research which could explain the enhanced motility by a probably altered intracellular complex composition (e. g. PIX/GIT complex) or complex activation status (e. g. Rac1-GTP level) was limited, the need of an innovative flow-chamber system was recognized. This was due to several parameters like to low numbers of MZB in murine spleens, the lack of detecting antibodies with needed specificity and sensitivity, the poor data described for MZB in the literature and the fact that MZB are exposed to blood flow in the MZ and the conventional static adhesion assays represent only poorly the conditions for a cell exposed to the blood flow. Therefore, a flow-system was designed and established to expose MZB to shear stress and this was combined with and installed into a live cell imaging system to have the possibility to analyse migratory responses of living MZB even on a single cell level. The setup and handling of this system was published in JoVE[141]. The innovation was the combination of the ibidi pump system into a live cell imaging system. The ibidi pump was the first pump producing a constant direction of flow without any fluctuations of low strength. This is needed to ensure constant condition in the flow chamber with only minimal fluctuations of flow strength over an unlimited time

window[159]. The ibidi pump was equipped with calibrated lines and slides which were programmed into the corresponding software. This enabled a very precise and sensitive adjustment of the flow conditions exposed to the cell to be analysed and a theoretically timely independent observation period. This was needed to ensure a high reproducibility of adhesion or migration assays under flow in order to compare different cells under similar conditions or the response of cells to different conditions. The combination with the live cell imaging system enabled the observation and tracking of single cells using the time lapse function as part of the software provided with the live cell imaging system (Fig. 13). Furthermore, with this flow chamber system it would be even possible to study the cellular molecule dynamics in the cell-surface interface during the migration of cells by TIRF microscopy.

5.4 Functionality of the designed flow chamber system

Since only poor data derived from static assays were available literature for MZB[68, 69] and those static assays cannot mimic conditions of a cell exposed to the blood flow, in this study the adhesion and migration of MZB were analysed under flow for the first time. The functionality of the designed system was shown by the observation or detection of the different behaviour of MZB compared to FOB. Under flow MZB stayed attached on ICAM-1 but FOB could not resist the shear stress and were washed out (Fig. 14). Although the conditions in the flow chamber system differ from that of static assays, this finding is in line with data derived from static adhesion assays: on ICAM-1 MZB are more adherent than FOB[68]. However, with the innovative flow chamber system setup used here a 2 - 3-fold amount of MZB were determined as adherent on ICAM-1 (Fig. 14B), when compared to the result of static assay reported by Lu et al.[68]. In the course of this study the static adhesion assay showed about 50% of MZB were adherent when exposed to an ICAM-1 coat of 2.5 µg ml^{-1} (Fig. 11C) in contrast to the 14% adherent MZB on 10 µg ml^{-1} ICAM-1 used by Lu et al.[68]. This increased value could be due to more gentle wash steps possible with the flow chamber system presented here (Fig. 13). This shows on one hand the fluctuations of results from static adhesion assay depending on the different protocols and experimentators in different labs. On the other hand, it shows the improvement of the sensitivity and reproducibility by the use of the flow system compared with static experimental

designs, since the shear force on the cells can be adjusted very precisely via software and is not dependent on the kind or way of wash steps in conventional dishes or plates. Interestingly, the adhesion rate of MZB on VCAM-1 was increased by factor 2 compared to ICAM-1 coated surfaces with 80% on VCAM-1 vs. 40% on ICAM-1 of initial loaded cells (Fig. 15B). This result is different as that reported before under static conditions: that the MZB adhesion on VCAM-1 was similar to the adhesion on ICAM-1[68]. Furthermore, after 30 min of flow almost all MZB stayed attached, which were adherent after 10 sec of flow (Fig. 14C below). These improvements of sensitivity and resolution highlight the new possibilities of the designed flow system regarding the investigation of adhesive and migratory responses of lymphocytes, which are essential for their biological function. It can be utilized to determine the shear stress induced adhesion capacity of a given cell population under precisely defined conditions like substate(s), cellular activation status and shear stress. The design of the flow chamber system opens further the possibility to investigate and understand MZB responses also upon antigen activation. With the TIRF microscopy option even an analysis of the cell-surface interface becomes possible. Therefore, this system enables the answering of many experimental questions, which could not be addressed before, due to limiting parameters of conventional experimental setups[141].

5.5 The migratory response of marginal zone B cells under flow conditions

In the next step the migratory response of MZB was investigated in more detail. It could be shown here for the first time that MZB migrate up the flow, if ICAM-1 was present as substrate on the flow chamber surface. The migration up the flow was increased with increasing strength of flow (Fig. 15). This shows that MZB can sense shear stress and are able to respond to it. The response was specific for ICAM-1, since this migratory behaviour of MZB up the flow could not be observed when the amounts of VCAM-1 exceeded those of ICAM-1 on the coated flow chamber surfaces (Fig. 16A and 17B). With other words, when ICAM-1 is exposed alone or in excess to MZB (like in the MZ, Fig. 16C) they migrate up the flow (in direction to the B cell follicle), if VCAM-1 amounts increase (like in direction to the RP, Fig. 16C) the adhesion of MZB increases also, which leads to decreased migration up the flow. When MZB are exposed to VCAM-1 alone, migration up the flow is aborted and MZB tend to migrate

down the flow (Fig. 16B, migration index). This is consistent with the high adhesiveness measured for MZB exposed to VCAM-1 (Fig. 14B). So in the MZ MZB would migrate up the flow, in contrast MZB would become more adherent, if they reach areas outside the MZ in direction to the RP, not to get washed out of the MZ. Taken together, all these observations are in line with the distribution of integrin ligands in the spleen (Fig. 16C) and the resulting localization of MZB in the MZ[68, 69, 74, 126]. Therefore, the detection of integrin ligand specific responses of MZB further confirms the functionality of the flow system and it was discovered here that MZB can sense shear stress and respond to it in a substrate-depending manner.

5.6 The role of αPix in the migratory response of marginal zone B cells under flow conditions

Since αPix deficiency leads to increased motility of MZB in static transwell assays (Fig. 11) and the directional motility is essential for positioning of MZB in the MZ[69] and for their shuttling between the MZ and the B cell follicle[126], the role of αPix in the migrational behaviour of MZB under flow was investigated in detail with the flow system designed in the course of this study.

The lack of αPix expression lead also to increased motility of MZB under flow. This was likely due to increased expression levels of βPix, which were also reported for αPix deficient thymocytes[54]. It is possible that lymphocytes compensate the lack of αPix with an increased expression of its homologue βPix. It is known that increased βPix expression goes along with increased Rac activity, leading to enhanced migratory activities of βPix overexpressing cells[18, 54, 144]. However, the attachment rate of αPix ko MZB was decreased over time when ICAM-1 was present but almost not altered on VCAM-1 alone coated surfaces (Fig. 14C). This strongly suggests a role for αPix in the regulation of ICAM-1 mediated adhesion and migration of MZB up the flow. This is in contrast to the result from the static adhesion assay as no adhesion defect could be measured for αPix ko MZB (Fig. 11C, right). This emphasizes the potential of the flow chamber system designed for this study, since even a mildly altered adhesion, which could lead to effects after prolonged time periods, are now detectable with this system (Fig. 13). As mentioned above, the migratory response of MZB on VCAM-1 coated surfaces was different from the ICAM-1 induced migration up the

flow. On VCAM-1 MZB are not able to migrate up the flow. Moreover, with increasing shear stress the presence of VCAM-1 induced a stop signal in WT MZB, indicated by the decrease of their velocity (Fig. 17D). This VCAM-1 stop signal could not be observed for αPix deficient MZB (Fig. 17D). This observation would also not be possible with conventional static adhesion assays and suggests a function of αPix in the regulation of shear-stress induced adhesion of MZB on VCAM-1.

Taken together these data suggested that αPix functions in the regulation of the integrin complexes LFA-1 and VLA-4 and therefore, in the coordination of the flow-induced migration of MZB. The presence and function of αPix leads to an increased ICAM-1 mediated attachment rate to retain the MZB in the MZ and to a VCAM-1 induced decrease of the velocity of MZB, not to be washed out of the MZ into the RP.

5.7 The role of αPix in the positioning of marginal zone B cells in the marginal zone

In the process of the follicular shuttling (Fig. 5), MZB have to respond to various signals to home and locate in the MZ, to shuttle from MZ into the B cell follicle and to find the way back from the B cell follicle into the MZ[69, 126]. Since the loss of αPix increases the basal and chemokine induced migration of MZB (Fig. 11, Fig. 17A and 18B), decreases the attachment rate on ICAM-1 under flow (Fig. 17C) and leads to the loss of the VCAM-1 induced stop signal under flow (Fig. 17D), the impact of αPix deficiency on the positioning and follicular shuttling of MZB was analysed in vivo.

To address this question an in vivo double staining technique was established to show the localization MZB and their motility between the MZ and B cell follicle[126]. Briefly, an antibody injection in the tail vein labels the MZB residing the MZ, since exposed to blood. Those MZB which migrate from the MZ through the marginal sinus into the blood-less B cell follicle are protected against the second antibody injection. Those MZB which stayed in the MZ are labelled with both antibodies (Fig. 18). The quantitative read-out with the flow cytometer showed, that in vivo almost the double amount of αPix deficient MZB was motile compared to WT MZB (Fig. 18B). This increase was consistently correlated to a decrease of MZ residing MZB (Fig. 18B, statistic). The visualization of the in vivo labelling of MZB by immunofluorescence (IF) microscopy delivered the spatio-temporal information and revealed that αPix

deficient MZB residing the MZ not only migrate into the follicle but also as expected were found outside the MZ in direction to the RP (Fig. 18C). This phenotype of mis-localized MZB in the direction to the RP was discovered here for the first time. The mis-localization was intrinsic to MZB and not induced by the αPix deficient environment, since the effect was also observed in αPix heterozygous female mice, which develop WT and αPix ko MZB in the same mouse (Fig. 19). The hypothesis that αPix has a function in the regulation of ICAM-1 mediated adhesion was encouraged by the inhibition of the ICAM-1 - LFA-1 interaction of MZB as the anti-LFA-1 treated WT mice showed the similar MZB phenotype as αPix ko mice (Fig. 21). Therefore, together with the in vitro data generated with the flow chamber system (point 5.6), it could be shown here that the function of αPix has an impact on the integrin-mediated positioning of MZB in the MZ.

A similar phenotype of defective MZB retention in the spleen was observed upon CD97 depletion in the lab of J. Cyster and published very recently[163]. There it could be shown that another RhoGEF called Lsc is involved in a pathway needed for the homeostasis and function of MZB. This pathway is triggered by CD97 expressed by MZB which binds and interacts with CD55 on RBC. It was reported that this cell-cell interaction of MZB and RBC is needed to ensure a proper retention of MZB in the spleen and an intact IgM response to T cell-independent antigens. CD97 is an adhesion G-protein-coupled receptor and induces a signal pathway via $G\alpha_{13}$ and Lsc which leads to the activation of the small GTPase RhoA promoting cell membrane retractions. Evidence was provided that MZB use mechano-sensing by CD55-mediated extraction of the extracellular NTF unit of CD97 to find an optimal position for an intact immune response.

The observations reported by Liu et al.[163] and the data presented in this study suggest that an intact positioning and function of MZB is a result of a number of fine regulated processes which interfere with each other with the involvement of RhoGEFs in order to control the activity of small Rho GTPases. However, in MZB the mechanisms of interactions of and within the involved signal complexes are still not known in detail. In the future more research is needed to increase the understanding of the processes and their interferences underlying correct location of MZB and their intact immune response. Since integrins are essential for MZB retention in the MZ[68, 163] and it could be shown here that αPix is involved in the regulation of integrin function, it cannot be excluded that in MZB αPix plays also a role in the signalling pathway of CD97

reported by Liu et al.[163]. However, the impact of CD97 deficiency on the function of integrins was not investigated. The use of the laminar flow chamber system established in the course of this study (point 4.4) could be an effective tool to gain increased understanding of the underlying mechanisms for the intact retention and function of MZB in the MZ.

5.8 Validation of the method used to define the extent of the MZ

To exclude an interfering of staining artefacts of in vivo labelling during the IF microscopy, two validating experiments were done additionally (Fig. 20). The titration of the injected anti-CD21 antibody showed that suboptimal amounts of injected anti-CD21 are preferentially taken up by staining of MZB cells in the MZ, and that MZB cells located at the transition from the MZ to the RP and beyond are not stained (Fig. 20A). It is unclear why the antibody would not diffuse fully around the cells just outside the marginal zone if there is no physical barrier. One possible explanation is that VCAM-1 levels are high enough in this area to cause MZB cells to adhere strongly. This could inhibit coating of the cells with the anti-CD21 antibody, as they would be constrained from rotating or moving around. With suboptimal amounts, the MZB cells that can move freely in the antibody containing blood would have an advantage in becoming stained. Another hypothesis would be that the binding conditions are optimal in the MZ. Antigen binding and the in vivo staining of MZB becomes more difficult in the direction to the RP, due to decrease of vessel volume which goes along with increased flow strength[63, 110]. Since exposure time of MZB to blood-borne antigens becomes decreased with increasing flow strength more antigens would be needed to get the same amount of antibody bound to MZB. Therefore, MZB that localize outside the MZ in the direction to RP stay unstained. The second experiment was the co-injection of anti-CD21 with anti-F4/80 (F4/80 = red pulp macrophage marker). The result clearly showed that anti-CD21 injection stains only MZ residing MZB, since MZB, which could not be labelled with the anti-CD21 injection in αPix ko spleens co-localized with red pulp macrophages.

5.9 Shear stress as novel force, that contributes to correct positioning of MZB in the MZ, which is counteracted by S1P signalling through S1PR3

During this study it could be shown that αPix ko MZB have normal static adhesion (Fig. 12C, right) but defective adhesion under flow (Fig. 17). The loss of adhesion and the faster migration under flow enabled it to exploit αPix ko MZB as a tool to reveal the effects of S1P treatment, which are less apparent on WT MZB. S1P treatment inhibited both WT and αPix ko MZB from migrating up the flow, but the effect was much more pronounced when αPix was not expressed in MZB (Fig. 22, migration index). This S1P-induced drift with the flow of αPix ko MZB, coupled with increased detachment under flow (Fig. 17C) and increased migration with the flow on VCAM-1 (Fig. 17D), acted to lodge αPix ko MZB in the RP as shown in Fig. 18C. These effects were mostly reversed in αPix/S1PR3 double ko MZB (Fig. 25), showing that S1PR3 is the principal S1P receptor for counteracting migration up the flow (Fig. 23). S1P receptors are an important target for immunosuppressive drugs because they promote lymphocyte exit from lymph nodes by counteracting chemokine signaling[129, 130, 145, 146, 147]. The role for S1P in mobilizing lymph node T cells into circulation is in interesting contrast to the role for it identified here in keeping MZB cells positioned in the MZ. However, if shear force-induced directional migration is considered as analogous to chemotaxis, then the similarities in S1P signalling in other cell systems and MZB cell migration become apparent. For example, S1P signalling through S1PR1 opposes the actions of CCR7 for T cells[148], and S1P signalling through S1PR3 opposes the response of germinal centre B cells to CXCL13[149].

Why would S1P impede the migration of MZB cells towards the B cell follicle, if this is needed for MZB to shuttle through the MS into the B cell follicle? One possible reason is that S1P increases the transit time in the MZ so that naïve MZB cells have a better chance of being exposed to blood-borne antigens in order to get activated and shuttle into the B cell follicle for antigen presentation via FDC. Although S1PR1 is downregulated on MZB exposed to S1P, it is possible that S1PR3 is also downregulated[69], since the MZB that need to migrate up the flow towards the follicle would not otherwise be able to overcome the drag force of S1PR3 signalling. It could be shown that an activation of MZB by LPS or BCR-specific antigen leads to a reduction of S1PR3 mRNA level and S1P-induced migration[69] and S1PR3 deficient MZB show faster entry into the B cell follicle[70, 126], implicating a downregulation of

S1PR3 on the surface of MZB. Supporting this possibility, there is evidence for ligand-induced internalization of S1PR3 in other cell types[152, 153]. Even it was reported that MZB activation leads to a migration of MZB from the MZ into the B cell follicle, due to the down regulation of S1PR3[69, 70], the detailed mechanisms and effects of such a MZB activation on their migratory response, e.g. the modulation of surface receptors, the adhesion and chemokine responsiveness, were not described yet, therefore, still unknown. Alternatively, there was an unexpected ligand-independent function observed for S1PR3 on MZB (Fig. 23B, straightness). It is possible that flow-induced shear stress activates S1PR3, as it activates S1PR1 on endothelial cells, even when S1P binding is not possible[154]. Another possible explanation is that S1P may act to increase productive contacts between MZB and other immune cells in the MZ, such as macrophages, iNKT cells, and neutrophils[113, 150, 151]. In the findings presented here, S1P-treated MZB are less capable of migrating against the flow than the untreated, but they are just as fast (Fig. 22B and 24B, velocity vs. migration index). Therefore, the net result would be lateral migration within the confines of the MZ, allowing the MZB to increase the interaction with blood-borne antigens and other immune cells until the S1P receptors become internalized, at which point the MZB cells would be free to migrate up the flow towards the MS and the B cell follicle.

The effects of S1P treatment on MZB, the increased motility of stuck cells (Fig. 22B and 24B, displacement > 10 µm) and the redirection of MZB migrating up the flow (Fig. 22B and 24B, migration index), strongly suggest that S1P acts on integrin adhesion complexes and that αPix is involved in their regulation. Shear stress likely directs MZB migration up the flow by polarizing integrin complexes to the edge of the cell that senses the most force. The defects of αPix ko MZB may also be related to altered regulation of integrins[136, 155] and an additive effect of deregulated S1P signalling which could explain why the effects of S1P treatment were stronger with αPix ko MZB than with WT. For both WT and αPix deficient MZB, however, migration up the flow was only possible when ICAM-1 and not VCAM-1 was present as substrate (Fig. 22). The MZB actually migrated with the flow, if the concentration of VCAM-1 was high. A similar result has been reported for T cells[156]. These differences are most likely due to the 10-fold higher rate of ligand binding for VLA-4 than for LFA-1[157]. The MZ contains mainly ICAM-1 while the RP is high in VCAM-1 expression (Fig. 16C). Thus, MZB residing the MZ will either stay there or migrate up the flow, while an MZB in the VCAM-1-rich red pulp will likely adhere there or

be pushed away from the MZ by blood flow. This could be a mechanism to ensure that only robust MZB cells with normal adhesion and migration can reside in the MZ and shuttle into the B cell follicle. All other MZB would be shunted to the RP for eventual destruction.

As discussed already above (point 5.7) another example for the ability of mechano-sensing by MZB was recently reported for CD97[163]. The extraction of the extracellular NTF unit of CD97 by binding of CD55 on RBC under shear stress lead to RhoA activation via $G\alpha_{13}$ and Lsc signalling. However, the research group could only estimate the applied shear force. The usage of the flow system designed for this study (point 4.4) would provide a more flexible and precise approach. For example, by possibility of the adjustment and modification of distinct shear forces and the possibility to design defined surfaces and/or stimuli to the cells. CD97 depletion caused a loss of MZB from spleen and a defective IgM response to T cell-independent antigens[163]. Since the impact of CD97 depletion on the function of integrins was not investigated, Lsc is a RhoGEF for RhoA and αPix for Cdc42 and Rac1 it is difficult to discuss a possible involvement of αPix in this pathway. However, with the use of the system designed for this study (point 4.4) the impact of the CD97-CD55 interaction on the regulation of the activation of integrins in MZB could be investigated in detail.

5.10 Extended model for MZB positioning in MZ

Based on the experiments and results presented in this study a number of further validating experiments were done within our research group. All results were published together[140] and in conclusion a model describing the underlying molecular mechanisms of MZB positioning in the MZ was extended by flow-induced shear stress and S1P as novel counterforces (Fig. 26).

According to the conventional model MZB shuttle in the spleen from the B cell follicle (FO) surrounding marginal zone (MZ) into the inside of the FO, to carry antigens from blood into the blood-less B cell follicle and migrate back into the MZ. CXCL13 is produced by FDC and is required to attract MZB for the entry into the B cell follicle. For the exit of MZB from B cell follicle back into the MZ the function of S1PR1 is required. The MZ is rich in ICAM-1 while the red pulp contains both ICAM-1 and

Figure 26: Model of MZB migration up the flow with S1P as counterforce.

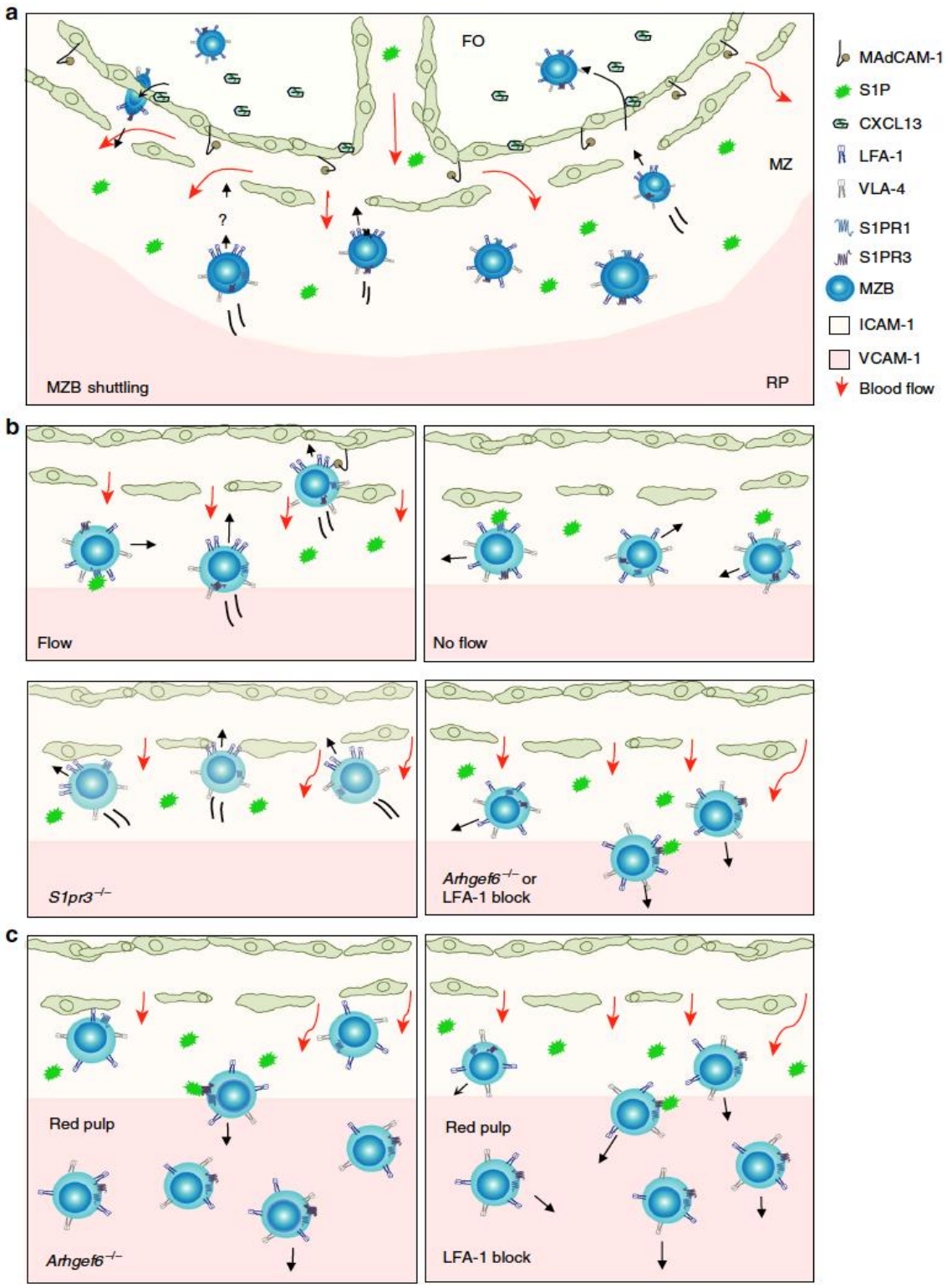

Description of Fig. 26: on next page.

Fig. 26 (on previous page):

a) ***MZB shuttling:*** *MZB in spleen migrate from the marginal zone (MZ) surrounding the B cell follicle (FO) to the inside of the follicle, to carry antigens from blood to the follicular dendritic cells and shuttle back into MZ again. CXCL13 is required for MZB entry into the follicle, while S1PR1 is required for MZB exit from the follicle and localization in the MZ. The marginal zone is rich in ICAM-1 while the red pulp contains both ICAM-1 and high levels of VCAM-1. An unknown force drives MZB toward the B cell follicle.*
b) ***Flow:*** *ICAM-1 is present in the MZ. Shear flow induces MZB migration up the flow. S1P signalling through S1P receptors inhibits MZB migration up flow and may trigger LFA-1 integrin redistribution. S1PR1 is rapidly internalized, thus S1PR3 may be the main counterforce. Upon eventual internalization of S1PR3, MZB would migrate up the flow. MZB that reach the sinus (elongated green cells) would bind strongly to MAdCAM-1 and CXCL13, preventing their migration against flow but protecting them from washing out. MZB would then transmigrate through the sinus into the follicle.* ***No flow:*** *without flow, MZB migrate for shorter distances in random directions and MZB follicular shuttling is impaired.* ***S1pr3−/− (S1PR3 ko):*** *without S1PR3, MZB do not respond to S1P and are not inhibited from migrating up the flow toward the follicle.* ***Arhgef6−/− (αPix ko) or LFA-1 block:*** *MZB that undergo a loss of adhesion, through Arhgef6 (αPix) mutation or LFA-1 blockade, are susceptible to washing out of the marginal zone toward the red pulp. S1P binding to receptors would accelerate this process. Impaired migration up flow causes reduced shuttling into the follicle.*
c) VCAM-1 in the red pulp. MZB can adhere to VCAM-1 under flow but do not migrate on it up the flow. MZB with reduced adhesion via LFA-1 are conveyed by flow to the red pulp. ***Left panel:*** *Arhgef6−/− (αPix ko) MZB that reach the red pulp can adhere to it and resist being washed out by flow.* ***Right panel:*** *MZB with blocked LFA-1 are only able to partially resist the force of the flow by adhering via VLA-4 to VCAM-1. Published Nature Communications*[140].

high levels of VCAM-1. In the conventional model the force that drives MZB within the MZ toward the MS and B cell follicle is unknown (Fig. 26A).

If ICAM-1 is present flow-mediated shear stress induces MZB migration up the flow. S1P signalling through S1P receptors 1 and 3 may trigger LFA-1 integrin redistribution and inhibits MZB migration up the flow. S1PR1 is rapidly internalized, thus S1PR3 may exert the main counterforce. Upon the internalization of S1PR3, MZB migration up the flow will be increased. MZB that reach the marginal sinus (elongated green cells) would bind strongly to MAdCAM-1 and CXCL13, preventing their migration against flow but protecting them from washing out[140]. MZB would then transmigrate through the marginal sinus into the B cell follicle (Fig. 27B, flow). Without flow, MZB migrate for shorter distances in random directions and follicular

shuttling of MZB is impaired[140] (Fig. 27B, no flow). Without S1PR3, MZB do not respond to S1P and are not inhibited from migrating up the flow toward the B cell follicle (Fig. 27B, S1PR3-/-). MZB that undergo a loss of adhesion, through αPix (Arhgef6) mutation or LFA-1 blockade, are susceptible to washing out of the MZ toward the red pulp by blood flow. S1P binding to receptors would accelerate this process, due to defective adhesion. Impaired migration up the flow causes reduced migration into the B cell follicle (Fig. 27B, αPix-/- or LFA-1 block). MZB can adhere to VCAM-1 under flow but do not migrate on it up the flow. MZB with reduced adhesion via LFA-1 are conveyed by blood flow in direction to the red pulp. αPix ko MZB that reach the red pulp can adhere to it and resist being washed out by flow (Fig. 27C, left panel). MZB with blocked LFA-1 are only able to partially resist the force of the flow by adhering to VCAM-1 only (Fig. 27C, right panel).

5.11 Model for the molecular function of αPix in MZB

The function and composition of the PIX-GIT complex in lymphocytes is intensively studied but is still largely unknown. The investigations suggest that in lymphocytes, the PIX-GIT complex is a cooperative action of αPix and Git-2, since they interact and stabilize each other[42, 54, 55]. In the course of coordinated migration processes, they play a role in the negative regulation of cytoskeletal dynamics. If α4 integrins are activated and then phosphorylated, the interaction of α4 integrins with paxillin is prevented. In other words, Paxillin interacts with non-activated α4 integrins. It is hypothesized that the PIX-GIT complex is recruited by the interaction with Paxillin at sites on the cell membrane where the dynamics of the cytoskeleton have to be
inhibited in the course of directed movement processes, e.g. at the lateral sides and ends of migrating cells[29]. It is speculated whether αPix, in addition to its function as a RhoGEF, also assumes recruiting functions with respect to PAK and GIT to enable localized regulation of the cytoskeleton[53]. In the course of morphological changes for directed cell movement a cooperative action of αPix as GEF and Git-2 as GAP could regulate the activity of Rho GTPases at those sites of the cellular complexes[25, 145]. The results suggest a function of αPix in the negative regulation of the migrational response

during motility processes of MZB. In this context, αPix could enable or support the coordinated dynamics of the promigratory-acting βPix.

5.12 Possible dual function of αPix in MZB

The data of this study show that the deletion of αPix expression leads to an increase of the MZB population and to altered migratory behaviour of MZB. Since αPix has GEF activity towards the RhoGTPases Rac1 and Cdc42 depending on its interaction partners (point 1.1.6 and 1.1.7), it is possible that the observations of increased motility and enlarged MZB population are not related directly. The B cell specific deletion of Cdc42 has no impact on migratory responses of B cells but on the development of all B cell subtypes[161] and Rac activity controls cellular motility by regulating the formation of protrusions and lamellopodia[144]. Therefore, the αPix deficiency induced alterations, which lead to the defective migration and adhesion of αPix ko MZB might be the effect of deregulated Rac1, while the αPix deficiency induced increase of the MZB population could be the effect of deregulated Cdc42. Therefore, it is possible that αPix has dual function in MZB by regulating on one hand Rac1 activity for actin remodelling processes during MZB migration and on the other hand signalling to Cdc42 during MZB differentiation processes. Since Cdc42 is involved in the antibody secretion of plasma cells[161], the attenuated immune response in αPix ko mice despite the increased MZB population[42] would be also in line with this hypothesis. However, it is unclear, if αPix is involved directly by the regulation of the GTPases by its GEF activity or if αPix is involved indirectly by a recruiting activity into the scaffold-like PIX-GIT complex also towards other factors to ensure the complex composition needed for proper signal transduction in cellular responses to receptor-induced signals.

5.13 Further perspectives

The correct localization of immune cells in their respective niches is fundamental for their biological function in order to gain activation signals or cell-cell interactions. Therefore, it is important to investigate the mechanisms underlying the interactions of cells with other cells or their environment.

In the presented study it could be shown with αPix ko MZB as an example how small alterations of adhesive responses can lead to the displacement from the biological niche as a long-term effect. It would be very interesting to study the migratory behaviour of immune cells after their activation by e.g. chemokines, antigens, interferons, interleukins, etc..

To confirm if Rac1 activity is increased in MZB would be needed to confirm the thesis, that increased Rac1 activity leads to increased motility of MZB, due to increased βPix expression in the absence of αPix.

It is speculated that αPix has not only GEF activity towards Rac1 and Cdc42 but also recruiting functions of factors into functional protein complexes like integrin-complexes. The analysis of the composition of αPix containing protein complexes and the investigation of the alterations of the protein complexes if αPix is not present could help to understand the dynamic and the fine regulation of migratory processes.

In order to understand the underlying adhesion and migratory processes, it is now possible to study the migratory behaviour of immune cells under defined flow conditions. This flow-system enables the investigation of new parameters important during adhesive and migratory responses of immune cells. Since the system is highly sensitive and precise adjustable, the resolution of known analysis systems can be increased, and new scientific question can be addressed.

This could include the investigations of isolated/purified immune cells out of patients suffered from diseases caused by defects in cellular adhesion or the developing or proofing applied gene therapies intended to improve adhesion defects or the investigations of cell-cell interaction interfaces like the immunological synapse by the use of artificial conditions to mimic the interaction partner. The investigation of the molecular dynamics of interaction interfaces by TIRF microscopy would give insights into the molecular dynamic within the cellular membrane of immune cells during their adhesion and migratory processes under flow conditions.

6. Summary

Cellular motility is regulated by the spatiotemporal coordination of the Rho GTPases Cdc42 and Rac1, which act on PAK. αPix is a GEF for Rac1 and Cdc42 and is expressed almost exclusively by hematopoietic cells. The absence of αPix expression in mice results in an increased population of marginal zone B cells (MZB) in the spleen and an increased motility of lymphocytes was reported. Therefore, the first part of the present study investigated the role of αPix in the development and the second part in the motility of MZB.

In this study, it could be shown that the absence of αPix leads to a dislocation of MZB from the marginal zone to the red pulp. However, the data from this study suggest that this mis-localization from the marginal zone to the red pulp is not the cause of the increased MZB population in αPix-deficient mice. However, a slight shift of precursor populations within the MZB from T1 to T2 could be measured. The shift of MZB progenitor cells from the T1 to the T2 population is an indication that αPix may be involved in the Cdc-42-regulated differentiation processes of MZB. Although this was a small shift, long-term effects of αPix deficiency could lead to an increased MZB population. MZB population development and homeostasis are regulated by complex mechanisms involving a variety of different factors. Further research is needed to fully understand MZB development and homeostasis.

In the past, increased motility has been reported in αPix-deficient lymphocytes. In the course of this work, it was shown that the absence of αPix expression also leads to increased motility in MZB. αPix-deficient MZB show increased βPix expression to compensate for the loss of αPix. We speculate that increased βPix expression may in turn lead to increased Rac1 activity, which could be the cause of the increased motility. Increased expression of chemokine receptors on the surface of MZB could be excluded.

As described above, the examination of αPix ko MZB with conventional experimental setups showed clear effects of αPix deficiency on MZB, but further detailed analysis of αPix ko MZB was unfortunately not readily available. One reason for this was, for example, a difficult cell sorting procedure with the eventual availability of only low cell numbers of MZB for in vitro analyses. Furthermore, conventional adhesion assays, both static and flow-through, showed insufficient resolution or sensitivity. Due to these limitations of conventional experimental setups, an innovative setup was developed to

investigate the increased motility of αPix ko MZB in more detail. For this purpose, a constant flow chamber system was combined with a live cell imaging system with time-lapse capability. This system was used for the first time to investigate the migration behaviour of MZB under laminar flow. The functionality of this system was demonstrated and proven by showing that MZB migrate upward on ICAM-1 under flow and tend to stick to VCAM-1 and have a tendency to migrate with the flow. This behaviour differed from the adhesion behaviour of follicular B cells and thus previously described observations could be reproduced. Furthermore, the present work demonstrated that αPix is involved in the regulation of shear force- and S1P-induced migration responses of MZB, probably through the regulation of integrin complexes. The absence of αPix leads to flushing or mis-localization of MZB from the MZ toward the red pulp, and this drift is triggered by blood flow.

Finally, the present study identified and described other factors that regulate MZB migration under blood flow: Shear Force, S1P, ICAM-1, and VCAM-1. These were used to propose a model for MZB cell positioning. The opposing forces of ICAM-1 and flow on the one hand, and VCAM-1 and S1P signalling through S1PR3 on the other, determine whether an MZB cell remains in the marginal zone, migrates toward the follicle, or is washed out into the red pulp. These data were published in Nature Communications[140]. The experimental setup of the flow system developed in this study provides a new and wide range of possibilities to study the adhesive and migratory behaviour of immune cells. The design and handling of this innovative system was published in Journal of Visualized Experiments[141].

7. Zusammenfassung

Die zelluläre Motilität wird durch die räumlich-zeitliche Koordination der Rho-GTPasen Cdc42 und Rac1 reguliert, die auf PAK wirken. αPix ist ein GEF für Rac1 und Cdc42 und wird fast ausschließlich von hämatopoetischen Zellen exprimiert. Das Fehlen der αPix-Expression in Mäusen führt zu einer vergrößerten Population von Marginalzonen B-Zellen (MZB) in der Milz und es wurde eine erhöhte Motilität von Lymphozyten berichtet. Daher wurde im ersten Teil der vorliegenden Studie die Rolle von αPix bei der Entwicklung und im zweiten Teil bei der Motilität von MZB untersucht.

Im Rahmen dieser Forschungsarbeit konnte gezeigt werden, dass die Abwesenheit von αPix zu einer Dislokation der MZB aus der Marginalzone in die Rote Pulpa führt. Die Daten dieser Studie deuten jedoch darauf hin, dass diese Dislokalisierung aus der Marginalzone in die Rote Pulpa nicht die Ursache für die vergrößerte MZB-Population in αPix-defizienten Mäusen ist. Es konnte aber eine leichte Verschiebung der Vorläuferpopulationen innerhalb der MZB von T1 zu T2 gemessen werden. Die Verschiebung von MZB-Vorläuferzellen von der T1- zur T2-Population ist ein Hinweis, dass αPix an der Cdc-42 regulierten Differenzierungsprozessen von MZB beteiligt sein könnte. Obwohl es sich nur um eine kleine Verschiebung handelte, könnten langfristige Effekte einer αPix-Defizienz zu einer vergrößerten MZB-Population führen. Die Entwicklung und Homöostase der MZB-Population wird durch komplexe Mechanismen unter Einbindung einer Vielzahl verschiedener Faktoren reguliert. Um die Entwicklung und Homöostase der MZB vollständig zu verstehen, sind weitere Forschungen erforderlich.

In der Vergangenheit wurde bei αPix-defizienten Lymphozyten eine erhöhte Motilität berichtet. Im Zuge dieser Arbeit konnte gezeigt werden, dass das Fehlen der αPix-Expression auch bei MZB zu einer erhöhten Motilität führt. αPix-defiziente MZB zeigen eine erhöhte ßPix-Expression, um den Verlust von αPix zu kompensieren. Wir vermuten, dass die erhöhte ßPix-Expression wiederum zu einer erhöhten Rac1-Aktivität führen könnte, was die Ursache für die erhöhte Motilität sein könnte. Eine erhöhte Expression von Chemokin-Rezeptoren auf der Oberfläche von MZB konnte ausgeschlossen werden.

Wie oben beschrieben, zeigte die Untersuchung von αPix ko MZB mit konventionellen Versuchsanordnungen deutliche Effekte einer αPix-Defizienz auf MZB, aber eine

weitere detaillierte Analyse von αPix ko MZB war ohne Weiteres leider nicht möglich. Ein Grund dafür war z. B. ein schwieriges Zellsortierverfahren mit der letztendlichen Verfügbarkeit von nur geringen Zellzahlen von MZB für *in-vitro*-Analysen. Weiterhin zeigten herkömmliche Adhäsionsassays, sowohl statisch als auch im Durchfluss nur unzureichende Auflösung bzw. Empfindlichkeit. Aufgrund dieser Einschränkungen herkömmlicher Versuchsaufbauten wurde ein innovativer Aufbau entwickelt, um die erhöhte Motilität von αPix ko MZB genauer untersuchen zu können. Dazu wurde ein Durchflusskammersystem mit konstantem Fluss mit einem Live-Zell-Imaging-System mit Zeitrafferfunktion kombiniert. Mit diesem System wurde erstmals das Migrationsverhalten von MZB unter laminarer Strömung untersucht. Die Funktionalität dieses Systems konnte dadurch gezeigt und nachgewiesen werden, dass MZB unter Strömung an ICAM-1 aufwärts wandern und an VCAM-1 eher haften bleiben und eine Tendenz zur Wanderung mit dem Strom haben. Dieses Verhalten unterschied sich vom Adhäsionsverhalten der follikulären B-Zellen und somit konnten bereits beschriebene Beobachtungen reproduziert werden. Darüber hinaus konnte in der vorliegenden Arbeit gezeigt werden, dass αPix an der Regulierung der Scherkraft- und S1P-induzierten Migrationsreaktionen von MZB beteiligt ist, wahrscheinlich durch die Regulierung von Integrinkomplexen. Das Fehlen von αPix führt zu einem Ausspülen bzw. Dislokalisierung von MZB aus der MZ in Richtung der Roten Pulpa und dieser Drift wird durch den Blutfluss ausgelöst.

Schließlich konnten in der vorliegenden Studie weitere Faktoren identifiziert und beschrieben werden, die die MZB-Migration im Blutfluss regulieren: Scherkraft, S1P, ICAM-1 und VCAM-1. Diese wurden verwendet, um ein erweitertes Modell für die Positionierung von MZB-Zellen in der Marginalzone vorzuschlagen. Die gegensätzlichen Kräfte von ICAM-1 und Strömung auf der einen Seite und VCAM-1 und S1P-Signalisierung durch S1PR3 auf der anderen Seite bestimmen, ob eine MZB-Zelle in der Marginalzone verbleibt, dem Follikel entgegen wandert oder in die Rote Pulpa ausgewaschen wird. Diese Daten wurden in *Nature Communications*[140] veröffentlicht. Der experimentelle Aufbau des im Rahmen dieser Studie entwickelten Durchflusssystems bietet ein neues und weites Spektrum von Möglichkeiten zur Untersuchung des adhäsiven und migratorischen Verhaltens von Immunzellen. Der Aufbau und die Handhabung dieses innovativen Systems wurde in *Journal of Visualized Experiments*[141] veröffentlicht.

8. References

1 Mulloy, J. C. *et al.* Rho GTPases in hematopoiesis and hemopathies. *Blood* **115**, 936-947, doi:10.1182/blood-2009-09-198127 (2010).

2 Ridley, A. J. Rho GTPases and actin dynamics in membrane protrusions and vesicle trafficking. *Trends in cell biology* **16**, 522-529, doi:10.1016/j.tcb.2006.08.006 (2006).

3 Evers, E. E. *et al.* Rho family proteins in cell adhesion and cell migration. *European journal of cancer (Oxford, England : 1990)* **36**, 1269-1274 (2000).

4 Chimini, G. & Chavrier, P. Function of Rho family proteins in actin dynamics during phagocytosis and engulfment. *Nature cell biology* **2**, E191-196, doi:10.1038/35036454 (2000).

5 Etienne-Manneville, S. & Hall, A. Rho GTPases in cell biology. *Nature* **420**, 629-635, doi:10.1038/nature01148 (2002).

6 Raftopoulou, M. & Hall, A. Cell migration: Rho GTPases lead the way. *Developmental biology* **265**, 23-32 (2004).

7 Sahai, E. & Marshall, C. J. RHO-GTPases and cancer. *Nature reviews. Cancer* **2**, 133-142, doi:10.1038/nrc725 (2002).

8 Machacek, M. *et al.* Coordination of Rho GTPase activities during cell protrusion. *Nature* **461**, 99-103, doi:10.1038/nature08242 (2009).

9 Aspenstrom, P., Fransson, A. & Saras, J. Rho GTPases have diverse effects on the organization of the actin filament system. *The Biochemical journal* **377**, 327-337, doi:10.1042/bj20031041 (2004).

10 Ellis, S. & Mellor, H. The novel Rho-family GTPase rif regulates coordinated actin-based membrane rearrangements. *Current biology : CB* **10**, 1387-1390 (2000).

11 Murphy, G. A. *et al.* Cellular functions of TC10, a Rho family GTPase: regulation of morphology, signal transduction and cell growth. *Oncogene* **18**, 3831-3845, doi:10.1038/sj.onc.1202758 (1999).

12 Egea, G., Lazaro-Dieguez, F. & Vilella, M. Actin dynamics at the Golgi complex in mammalian cells. *Current opinion in cell biology* **18**, 168-178, doi:10.1016/j.ceb.2006.02.007 (2006).

13 Bader, M. F., Doussau, F., Chasserot-Golaz, S., Vitale, N. & Gasman, S. Coupling actin and membrane dynamics during calcium-regulated exocytosis: a role for Rho and ARF GTPases. *Biochimica et biophysica acta* **1742**, 37-49, doi:10.1016/j.bbamcr.2004.09.028 (2004).

14 Rossman, K. L., Der, C. J. & Sondek, J. GEF means go: turning on RHO GTPases with guanine nucleotide-exchange factors. *Nature reviews. Molecular cell biology* **6**, 167-180, doi:10.1038/nrm1587 (2005).

15 Boettner, B. & Van Aelst, L. The role of Rho GTPases in disease development. *Gene* **286**, 155-174 (2002).

16 Cherfils, J. & Zeghouf, M. Regulation of small GTPases by GEFs, GAPs, and GDIs. *Physiological reviews* **93**, 269-309, doi:10.1152/physrev.00003.2012 (2013).

17 Hart, M. J., Eva, A., Evans, T., Aaronson, S. A. & Cerione, R. A. Catalysis of guanine nucleotide exchange on the CDC42Hs protein by the dbl oncogene product. *Nature* **354**, 311-314, doi:10.1038/354311a0 (1991).

18 Manser, E. *et al.* PAK kinases are directly coupled to the PIX family of nucleotide exchange factors. *Molecular cell* **1**, 183-192 (1998).

19 Oh, W. K. *et al.* Cloning of a SH3 domain-containing proline-rich protein, p85SPR, and its localization in focal adhesion. *Biochemical and biophysical research communications* **235**, 794-798, doi:10.1006/bbrc.1997.6875 (1997).
20 Bagrodia, S., Taylor, S. J., Jordon, K. A., Van Aelst, L. & Cerione, R. A. A novel regulator of p21-activated kinases. *The Journal of biological chemistry* **273**, 23633-23636 (1998).
21 Kim, S. *et al.* Molecular cloning of neuronally expressed mouse betaPix isoforms. *Biochemical and biophysical research communications* **272**, 721-725, doi:10.1006/bbrc.2000.2845 (2000).
22 Kim, S., Lee, S. H. & Park, D. Leucine zipper-mediated homodimerization of the p21-activated kinase-interacting factor, beta Pix. Implication for a role in cytoskeletal reorganization. *The Journal of biological chemistry* **276**, 10581-10584, doi:10.1074/jbc.C000806200 (2001).
23 Koh, C. G., Manser, E., Zhao, Z. S., Ng, C. P. & Lim, L. Beta1PIX, the PAK-interacting exchange factor, requires localization via a coiled-coil region to promote microvillus-like structures and membrane ruffles. *Journal of cell science* **114**, 4239-4251 (2001).
24 Feng, Q., Albeck, J. G., Cerione, R. A. & Yang, W. Regulation of the Cool/Pix proteins: key binding partners of the Cdc42/Rac targets, the p21-activated kinases. *The Journal of biological chemistry* **277**, 5644-5650, doi:10.1074/jbc.M107704200 (2002).
25 Rosenberger, G. & Kutsche, K. AlphaPIX and betaPIX and their role in focal adhesion formation. *European journal of cell biology* **85**, 265-274, doi:10.1016/j.ejcb.2005.10.007 (2006).
26 Li, Z. *et al.* Directional sensing requires G beta gamma-mediated PAK1 and PIX alpha-dependent activation of Cdc42. *Cell* **114**, 215-227 (2003).
27 Baird, D., Feng, Q. & Cerione, R. A. The Cool-2/alpha-Pix protein mediates a Cdc42-Rac signaling cascade. *Current biology : CB* **15**, 1-10, doi:10.1016/j.cub.2004.12.040 (2005).
28 Feng, Q., Baird, D. & Cerione, R. A. Novel regulatory mechanisms for the Dbl family guanine nucleotide exchange factor Cool-2/alpha-Pix. *The EMBO journal* **23**, 3492-3504, doi:10.1038/sj.emboj.7600331 (2004).
29 Frank, S. R. & Hansen, S. H. The PIX-GIT complex: a G protein signaling cassette in control of cell shape. *Seminars in cell & developmental biology* **19**, 234-244, doi:10.1016/j.semcdb.2008.01.002 (2008).
30 Bokoch, G. M. Biology of the p21-activated kinases. *Annual review of biochemistry* **72**, 743-781, doi:10.1146/annurev.biochem.72.121801.161742 (2003).
31 Wehrle-Haller, B. & Imhof, B. The inner lives of focal adhesions. *Trends in cell biology* **12**, 382-389 (2002).
32 Carragher, N. O. & Frame, M. C. Focal adhesion and actin dynamics: a place where kinases and proteases meet to promote invasion. *Trends in cell biology* **14**, 241-249, doi:10.1016/j.tcb.2004.03.011 (2004).
33 Nayal, A., Webb, D. J. & Horwitz, A. F. Talin: an emerging focal point of adhesion dynamics. *Current opinion in cell biology* **16**, 94-98, doi:10.1016/j.ceb.2003.11.007 (2004).
34 Premont, R. T. *et al.* The GIT/PIX complex: an oligomeric assembly of GIT family ARF GTPase-activating proteins and PIX family Rac1/Cdc42 guanine nucleotide exchange factors. *Cellular signalling* **16**, 1001-1011, doi:10.1016/j.cellsig.2004.02.002 (2004).

35 Paris, S., Longhi, R., Santambrogio, P. & de Curtis, I. Leucine-zipper-mediated homo- and hetero-dimerization of GIT family p95-ARF GTPase-activating protein, PIX-, paxillin-interacting proteins 1 and 2. *The Biochemical journal* **372**, 391-398, doi:10.1042/bj20030047 (2003).
36 Premont, R. T., Claing, A., Vitale, N., Perry, S. J. & Lefkowitz, R. J. The GIT family of ADP-ribosylation factor GTPase-activating proteins. Functional diversity of GIT2 through alternative splicing. *The Journal of biological chemistry* **275**, 22373-22380 (2000).
37 Qin, Y., Capaldo, C., Gumbiner, B. M. & Macara, I. G. The mammalian Scribble polarity protein regulates epithelial cell adhesion and migration through E-cadherin. *The Journal of cell biology* **171**, 1061-1071, doi:10.1083/jcb.200506094 (2005).
38 Dow, L. E. *et al.* The tumour-suppressor Scribble dictates cell polarity during directed epithelial migration: regulation of Rho GTPase recruitment to the leading edge. *Oncogene* **26**, 2272-2282, doi:10.1038/sj.onc.1210016 (2007).
39 Zhao, Z. S., Manser, E., Loo, T. H. & Lim, L. Coupling of PAK-interacting exchange factor PIX to GIT1 promotes focal complex disassembly. *Molecular and cellular biology* **20**, 6354-6363 (2000).
40 Turner, C. E. *et al.* Paxillin LD4 motif binds PAK and PIX through a novel 95-kD ankyrin repeat, ARF-GAP protein: A role in cytoskeletal remodeling. *The Journal of cell biology* **145**, 851-863 (1999).
41 Haendeler, J. *et al.* GIT1 mediates Src-dependent activation of phospholipase Cgamma by angiotensin II and epidermal growth factor. *The Journal of biological chemistry* **278**, 49936-49944, doi:10.1074/jbc.M307317200 (2003).
42 Missy, K. *et al.* AlphaPIX Rho GTPase guanine nucleotide exchange factor regulates lymphocyte functions and antigen receptor signaling. *Molecular and cellular biology* **28**, 3776-3789, doi:10.1128/mcb.00507-07 (2008).
43 Zhang, H., Webb, D. J., Asmussen, H., Niu, S. & Horwitz, A. F. A GIT1/PIX/Rac/PAK signaling module regulates spine morphogenesis and synapse formation through MLC. *The Journal of neuroscience : the official journal of the Society for Neuroscience* **25**, 3379-3388, doi:10.1523/jneurosci.3553-04.2005 (2005).
44 Totaro, A. *et al.* Biochemical and functional characterisation of alphaPIX, a specific regulator of axonal and dendritic branching in hippocampal neurons. *Biology of the cell / under the auspices of the European Cell Biology Organization* **104**, 533-552, doi:10.1111/boc.201100060 (2012).
45 Nadif Kasri, N. & Van Aelst, L. Rho-linked genes and neurological disorders. *Pflugers Archiv : European journal of physiology* **455**, 787-797, doi:10.1007/s00424-007-0385-1 (2008).
46 Ramakers, G. J. Rho proteins, mental retardation and the cellular basis of cognition. *Trends in neurosciences* **25**, 191-199 (2002).
47 Kutsche, K. *et al.* Mutations in ARHGEF6, encoding a guanine nucleotide exchange factor for Rho GTPases, in patients with X-linked mental retardation. *Nature genetics* **26**, 247-250, doi:10.1038/80002 (2000).
48 Gringel, A. *et al.* PAK4 and alphaPIX determine podosome size and number in macrophages through localized actin regulation. *Journal of cellular physiology* **209**, 568-579, doi:10.1002/jcp.20777 (2006).
49 Tarone, G., Cirillo, D., Giancotti, F. G., Comoglio, P. M. & Marchisio, P. C. Rous sarcoma virus-transformed fibroblasts adhere primarily at discrete

protrusions of the ventral membrane called podosomes. *Experimental cell research* **159**, 141-157 (1985).

50 Zambonin-Zallone, A. *et al.* Immunocytochemical distribution of extracellular matrix receptors in human osteoclasts: a beta 3 integrin is colocalized with vinculin and talin in the podosomes of osteoclastoma giant cells. *Experimental cell research* **182**, 645-652 (1989).

51 Xu, J. *et al.* Divergent signals and cytoskeletal assemblies regulate self-organizing polarity in neutrophils. *Cell* **114**, 201-214 (2003).

52 Mazaki, Y. *et al.* Neutrophil direction sensing and superoxide production linked by the GTPase-activating protein GIT2. *Nature immunology* **7**, 724-731, doi:10.1038/ni1349 (2006).

53 Phee, H., Abraham, R. T. & Weiss, A. Dynamic recruitment of PAK1 to the immunological synapse is mediated by PIX independently of SLP-76 and Vav1. *Nature immunology* **6**, 608-617, doi:10.1038/ni1199 (2005).

54 Korthals, M. *et al.* alphaPIX RhoGEF Supports Positive Selection by Restraining Migration and Promoting Arrest of Thymocytes. *Journal of immunology (Baltimore, Md. : 1950)* **192**, 3228-3238, doi:10.4049/jimmunol.1302585 (2014).

55 Phee, H. *et al.* Regulation of thymocyte positive selection and motility by GIT2. *Nature immunology* **11**, 503-511, doi:10.1038/ni.1868 (2010).

56 Hayakawa, K., Hardy, R. R., Herzenberg, L. A. & Herzenberg, L. A. Progenitors for Ly-1 B cells are distinct from progenitors for other B cells. *The Journal of experimental medicine* **161**, 1554-1568 (1985).

57 Hastings, W. D., Gurdak, S. M., Tumang, J. R. & Rothstein, T. L. CD5+/Mac-1- peritoneal B cells: a novel B cell subset that exhibits characteristics of B-1 cells. *Immunology letters* **105**, 90-96, doi:10.1016/j.imlet.2006.01.002 (2006).

58 Hardy, R. R. & Hayakawa, K. A developmental switch in B lymphopoiesis. *Proceedings of the National Academy of Sciences of the United States of America* **88**, 11550-11554 (1991).

59 Berland, R. & Wortis, H. H. Origins and functions of B-1 cells with notes on the role of CD5. *Annual review of immunology* **20**, 253-300, doi:10.1146/annurev.immunol.20.100301.064833 (2002).

60 Hardy, R. R. B-1 B cell development. *Journal of immunology (Baltimore, Md. : 1950)* **177**, 2749-2754 (2006).

61 Oliver, A. M., Martin, F., Gartland, G. L., Carter, R. H. & Kearney, J. F. Marginal zone B cells exhibit unique activation, proliferative and immunoglobulin secretory responses. *European journal of immunology* **27**, 2366-2374, doi:10.1002/eji.1830270935 (1997).

62 Pillai, S. & Cariappa, A. The follicular versus marginal zone B lymphocyte cell fate decision. *Nature reviews. Immunology* **9**, 767-777, doi:10.1038/nri2656 (2009).

63 Zandvoort, A. & Timens, W. The dual function of the splenic marginal zone: essential for initiation of anti-TI-2 responses but also vital in the general first-line defense against blood-borne antigens. *Clinical and experimental immunology* **130**, 4-11 (2002).

64 Weill, J. C., Weller, S. & Reynaud, C. A. Human marginal zone B cells. *Annual review of immunology* **27**, 267-285, doi:10.1146/annurev.immunol.021908.132607 (2009).

65 Allman, D. *et al.* Resolution of three nonproliferative immature splenic B cell subsets reveals multiple selection points during peripheral B cell maturation. *Journal of immunology (Baltimore, Md. : 1950)* **167**, 6834-6840 (2001).
66 Lindsley, R. C., Thomas, M., Srivastava, B. & Allman, D. Generation of peripheral B cells occurs via two spatially and temporally distinct pathways. *Blood* **109**, 2521-2528, doi:10.1182/blood-2006-04-018085 (2007).
67 Cariappa, A., Chase, C., Liu, H., Russell, P. & Pillai, S. Naive recirculating B cells mature simultaneously in the spleen and bone marrow. *Blood* **109**, 2339-2345, doi:10.1182/blood-2006-05-021089 (2007).
68 Lu, T. T. & Cyster, J. G. Integrin-mediated long-term B cell retention in the splenic marginal zone. *Science (New York, N.Y.)* **297**, 409-412, doi:10.1126/science.1071632 (2002).
69 Cinamon, G. *et al.* Sphingosine 1-phosphate receptor 1 promotes B cell localization in the splenic marginal zone. *Nature immunology* **5**, 713-720, doi:10.1038/ni1083 (2004).
70 Girkontaite, I. *et al.* The sphingosine-1-phosphate (S1P) lysophospholipid receptor S1P3 regulates MAdCAM-1+ endothelial cells in splenic marginal sinus organization. *The Journal of experimental medicine* **200**, 1491-1501, doi:10.1084/jem.20041483 (2004).
71 Ziring, D. *et al.* Formation of B and T cell subsets require the cannabinoid receptor CB2. *Immunogenetics* **58**, 714-725, doi:10.1007/s00251-006-0138-x (2006).
72 Wang, H. *et al.* The CXCR7 chemokine receptor promotes B-cell retention in the splenic marginal zone and serves as a sink for CXCL12. *Blood* **119**, 465-468, doi:10.1182/blood-2011-03-343608 (2012).
73 Chopin, M., Quemeneur, L., Ripich, T. & Jessberger, R. SWAP-70 controls formation of the splenic marginal zone through regulating T1B-cell differentiation. *European journal of immunology* **40**, 3544-3556, doi:10.1002/eji.201040556 (2010).
74 Martin, F. & Kearney, J. F. Marginal-zone B cells. *Nature reviews. Immunology* **2**, 323-335, doi:10.1038/nri799 (2002).
75 Cascalho, M., Ma, A., Lee, S., Masat, L. & Wabl, M. A quasi-monoclonal mouse. *Science (New York, N.Y.)* **272**, 1649-1652 (1996).
76 Kanayama, N., Cascalho, M. & Ohmori, H. Analysis of marginal zone B cell development in the mouse with limited B cell diversity: role of the antigen receptor signals in the recruitment of B cells to the marginal zone. *Journal of immunology (Baltimore, Md. : 1950)* **174**, 1438-1445 (2005).
77 Cariappa, A. *et al.* The follicular versus marginal zone B lymphocyte cell fate decision is regulated by Aiolos, Btk, and CD21. *Immunity* **14**, 603-615 (2001).
78 Samardzic, T. *et al.* Reduction of marginal zone B cells in CD22-deficient mice. *European journal of immunology* **32**, 561-567, doi:10.1002/1521-4141(200202)32:2<561::aid-immu561>3.0.co;2-h (2002).
79 Kuroda, K. *et al.* Regulation of marginal zone B cell development by MINT, a suppressor of Notch/RBP-J signaling pathway. *Immunity* **18**, 301-312 (2003).
80 Tan, J. B. *et al.* Lunatic and manic fringe cooperatively enhance marginal zone B cell precursor competition for delta-like 1 in splenic endothelial niches. *Immunity* **30**, 254-263, doi:10.1016/j.immuni.2008.12.016 (2009).

81 Sheng, Y. *et al.* Expression of Delta-like 1 in the splenic non-hematopoietic cells is essential for marginal zone B cell development. *Immunology letters* **121**, 33-37, doi:10.1016/j.imlet.2008.08.001 (2008).

82 Batten, M. *et al.* BAFF mediates survival of peripheral immature B lymphocytes. *The Journal of experimental medicine* **192**, 1453-1466 (2000).

83 Schiemann, B. *et al.* An essential role for BAFF in the normal development of B cells through a BCMA-independent pathway. *Science (New York, N.Y.)* **293**, 2111-2114, doi:10.1126/science.1061964 (2001).

84 Otipoby, K. L. *et al.* BAFF activates Akt and Erk through BAFF-R in an IKK1-dependent manner in primary mouse B cells. *Proceedings of the National Academy of Sciences of the United States of America* **105**, 12435-12438, doi:10.1073/pnas.0805460105 (2008).

85 Cariappa, A., Liou, H. C., Horwitz, B. H. & Pillai, S. Nuclear factor kappa B is required for the development of marginal zone B lymphocytes. *The Journal of experimental medicine* **192**, 1175-1182 (2000).

86 Adams, E. J. & Luoma, A. M. The yin and yang of CD1d recognition. *Nature immunology* **13**, 814-815, doi:10.1038/ni.2401 (2012).

87 Wen, X., Yang, J. Q., Kim, P. J. & Singh, R. R. Homeostatic regulation of marginal zone B cells by invariant natural killer T cells. *PloS one* **6**, e26536, doi:10.1371/journal.pone.0026536 (2011).

88 Martin, F. & Kearney, J. F. Positive selection from newly formed to marginal zone B cells depends on the rate of clonal production, CD19, and btk. *Immunity* **12**, 39-49 (2000).

89 Karlsson, M. C. *et al.* Macrophages control the retention and trafficking of B lymphocytes in the splenic marginal zone. *The Journal of experimental medicine* **198**, 333-340, doi:10.1084/jem.20030684 (2003).

90 Calamito, M. *et al.* Akt1 and Akt2 promote peripheral B-cell maturation and survival. *Blood* **115**, 4043-4050, doi:10.1182/blood-2009-09-241638 (2010).

91 Guinamard, R., Okigaki, M., Schlessinger, J. & Ravetch, J. V. Absence of marginal zone B cells in Pyk-2-deficient mice defines their role in the humoral response. *Nature immunology* **1**, 31-36, doi:10.1038/76882 (2000).

92 Girkontaite, I. *et al.* Lsc is required for marginal zone B cells, regulation of lymphocyte motility and immune responses. *Nature immunology* **2**, 855-862, doi:10.1038/ni0901-855 (2001).

93 Pearce, G. *et al.* Signaling protein SWAP-70 is required for efficient B cell homing to lymphoid organs. *Nature immunology* **7**, 827-834, doi:10.1038/ni1365 (2006).

94 Chen, Y. *et al.* A critical role of Rap1b in B-cell trafficking and marginal zone B-cell development. *Blood* **111**, 4627-4636, doi:10.1182/blood-2007-12-128140 (2008).

95 Croker, B. A. *et al.* The Rac2 guanosine triphosphatase regulates B lymphocyte antigen receptor responses and chemotaxis and is required for establishment of B-1a and marginal zone B lymphocytes. *Journal of immunology (Baltimore, Md. : 1950)* **168**, 3376-3386 (2002).

96 Bokoch, G. M. Regulation of innate immunity by Rho GTPases. *Trends in cell biology* **15**, 163-171, doi:10.1016/j.tcb.2005.01.002 (2005).

97 Henderson, R. B. *et al.* A novel Rac-dependent checkpoint in B cell development controls entry into the splenic white pulp and cell survival. *The Journal of experimental medicine* **207**, 837-853, doi:10.1084/jem.20091489 (2010).

98 Saito, T. *et al.* Notch2 is preferentially expressed in mature B cells and indispensable for marginal zone B lineage development. *Immunity* **18**, 675-685 (2003).
99 Muppidi, J. R. *et al.* Cannabinoid receptor 2 positions and retains marginal zone B cells within the splenic marginal zone. *The Journal of experimental medicine* **208**, 1941-1948, doi:10.1084/jem.20111083 (2011).
100 Beer, S. *et al.* Impaired immune responses and prolonged allograft survival in Sly1 mutant mice. *Molecular and cellular biology* **25**, 9646-9660, doi:10.1128/mcb.25.21.9646-9660.2005 (2005).
101 Makowska, A., Faizunnessa, N. N., Anderson, P., Midtvedt, T. & Cardell, S. CD1high B cells: a population of mixed origin. *European journal of immunology* **29**, 3285-3294, doi:10.1002/(sici)1521-4141(199910)29:10<3285::aid-immu3285>3.0.co;2-p (1999).
102 Shao, W. H. *et al.* Disrupted Mer receptor tyrosine kinase expression leads to enhanced MZ B-cell responses. *Journal of autoimmunity* **35**, 368-374, doi:10.1016/j.jaut.2010.08.001 (2010).
103 Chen, J., Limon, J. J., Blanc, C., Peng, S. L. & Fruman, D. A. Foxo1 regulates marginal zone B-cell development. *European journal of immunology* **40**, 1890-1896, doi:10.1002/eji.200939817 (2010).
104 Hart, G. T., Wang, X., Hogquist, K. A. & Jameson, S. C. Kruppel-like factor 2 (KLF2) regulates B-cell reactivity, subset differentiation, and trafficking molecule expression. *Proceedings of the National Academy of Sciences of the United States of America* **108**, 716-721, doi:10.1073/pnas.1013168108 (2011).
105 Winkelmann, R. *et al.* B cell homeostasis and plasma cell homing controlled by Kruppel-like factor 2. *Proceedings of the National Academy of Sciences of the United States of America* **108**, 710-715, doi:10.1073/pnas.1012858108 (2011).
106 Turchinovich, G. *et al.* Programming of marginal zone B-cell fate by basic Kruppel-like factor (BKLF/KLF3). *Blood* **117**, 3780-3792, doi:10.1182/blood-2010-09-308742 (2011).
107 Vu, T. T. *et al.* Impaired B cell development in the absence of Kruppel-like factor 3. *Journal of immunology (Baltimore, Md. : 1950)* **187**, 5032-5042, doi:10.4049/jimmunol.1101450 (2011).
108 Martin, F., Oliver, A. M. & Kearney, J. F. Marginal zone and B1 B cells unite in the early response against T-independent blood-borne particulate antigens. *Immunity* **14**, 617-629 (2001).
109 Cerutti, A., Cols, M. & Puga, I. Marginal zone B cells: virtues of innate-like antibody-producing lymphocytes. *Nature reviews. Immunology* **13**, 118-132, doi:10.1038/nri3383 (2013).
110 Kraal, G. Cells in the marginal zone of the spleen. *International review of cytology* **132**, 31-74 (1992).
111 Willems, L. *et al.* IL-7 is required for the development of the intrinsic function of marginal zone B cells and the marginal zone microenvironment. *Journal of immunology (Baltimore, Md. : 1950)* **187**, 3587-3594, doi:10.4049/jimmunol.1004012 (2011).
112 Basu, S., Ray, A. & Dittel, B. N. Cannabinoid receptor 2 is critical for the homing and retention of marginal zone B lineage cells and for efficient T-independent immune responses. *Journal of immunology (Baltimore, Md. : 1950)* **187**, 5720-5732, doi:10.4049/jimmunol.1102195 (2011).

113 You, Y. *et al.* Marginal zone B cells regulate antigen capture by marginal zone macrophages. *Journal of immunology (Baltimore, Md. : 1950)* **186**, 2172-2181, doi:10.4049/jimmunol.1002106 (2011).

114 Balazs, M., Martin, F., Zhou, T. & Kearney, J. Blood dendritic cells interact with splenic marginal zone B cells to initiate T-independent immune responses. *Immunity* **17**, 341-352 (2002).

115 Whipple, E. C., Shanahan, R. S., Ditto, A. H., Taylor, R. P. & Lindorfer, M. A. Analyses of the in vivo trafficking of stoichiometric doses of an anti-complement receptor 1/2 monoclonal antibody infused intravenously in mice. *Journal of immunology (Baltimore, Md. : 1950)* **173**, 2297-2306 (2004).

116 Attanavanich, K. & Kearney, J. F. Marginal zone, but not follicular B cells, are potent activators of naive CD4 T cells. *Journal of immunology (Baltimore, Md. : 1950)* **172**, 803-811 (2004).

117 Gatto, D., Ruedl, C., Odermatt, B. & Bachmann, M. F. Rapid response of marginal zone B cells to viral particles. *Journal of immunology (Baltimore, Md. : 1950)* **173**, 4308-4316 (2004).

118 Ferguson, A. R., Youd, M. E. & Corley, R. B. Marginal zone B cells transport and deposit IgM-containing immune complexes onto follicular dendritic cells. *International immunology* **16**, 1411-1422, doi:10.1093/intimm/dxh142 (2004).

119 Hoek, K. L. *et al.* Follicular B cell trafficking within the spleen actively restricts humoral immune responses. *Immunity* **33**, 254-265, doi:10.1016/j.immuni.2010.07.016 (2010).

120 Mebius, R. E. & Kraal, G. Structure and function of the spleen. *Nature reviews. Immunology* **5**, 606-616, doi:10.1038/nri1669 (2005).

121 Fort, P. & Blangy, A. The Evolutionary Landscape of Dbl-Like RhoGEF Families: Adapting Eukaryotic Cells to Environmental Signals. Genome Biol. Evol. 9(6):1471–1486.

122 Cinamon, G., Shinder, V., Alon, R. Shear forces promote lymphocyte migration across vascular endothelium bearing apical chemokines. *Nature Immunology* **2**, 515–522 (2001).

123 Song, J. et al. Extracellular matrix of secondary lymphoid organs impacts on B cell fate and survival. *Proc. Natl Acad. Sci. USA* **110**, E2915–E2924 (2013).

124 Cyster, J. G. *et al.* Follicular stromal cells and lymphocyte homing to follicles. *Immunological reviews* **176**, 181-193 (2000).

125 Mendelson, K., Evans, T. & Hla, T. Sphingosine 1-phosphate signalling. *Development (Cambridge, England)* **141**, 5-9 (2014).

126 Cinamon, G., Zachariah, M. A., Lam, O. M., Foss, F. W., Jr. & Cyster, J. G. Follicular shuttling of marginal zone B cells facilitates antigen transport. *Nature immunology* **9**, 54-62, doi:10.1038/ni1542 (2008).

127 Forster, R. *et al.* A putative chemokine receptor, BLR1, directs B cell migration to defined lymphoid organs and specific anatomic compartments of the spleen. *Cell* **87**, 1037-1047 (1996).

128 Ansel, K. M. *et al.* A chemokine-driven positive feedback loop organizes lymphoid follicles. *Nature* **406**, 309-314, doi:10.1038/35018581 (2000).

129 Marsolais, D. & Rosen, H. Chemical modulators of sphingosine-1-phosphate receptors as barrier-oriented therapeutic molecules. *Nature reviews. Drug discovery* **8**, 297-307, doi:10.1038/nrd2356 (2009).

130 Schwab, S. R. & Cyster, J. G. Finding a way out: lymphocyte egress from lymphoid organs. *Nature immunology* **8**, 1295-1301 (2007).

131 Cyster, J. G. & Schwab, S. R. Sphingosine-1-phosphate and lymphocyte egress from lymphoid organs. *Annual review of immunology* **30**, 69-94, doi:10.1146/annurev-immunol-020711-075011 (2012).
132 Arnon, T. I. *et al.* GRK2-dependent S1PR1 desensitization is required for lymphocytes to overcome their attraction to blood. *Science (New York, N.Y.)* **333**, 1898-1903, doi:10.1126/science.1208248 (2011).
133 Miltenyi, S., Muller, W., Weichel, W. & Radbruch, A. High gradient magnetic cell separation with MACS. *Cytometry* **11**, 231-238, doi:10.1002/cyto.990110203 (1990).
134 Allman, D. & Pillai, S. Peripheral B cell subsets. *Current opinion in immunology* **20**, 149-157, doi:10.1016/j.coi.2008.03.014 (2008).
135 Cau, J. & Hall, A. Cdc42 controls the polarity of the actin and microtubule cytoskeletons through two distinct signal transduction pathways. *Journal of cell science* **118**, 2579-2587, doi:10.1242/jcs.02385 (2005).
136 Kuo, J. C., Han, X., Hsiao, C. T., Yates, J. R., 3rd & Waterman, C. M. Analysis of the myosin-II-responsive focal adhesion proteome reveals a role for beta-Pix in negative regulation of focal adhesion maturation. *Nature cell biology* **13**, 383-393, doi:10.1038/ncb2216 (2011).
137 Za, L. *et al.* betaPIX controls cell motility and neurite extension by regulating the distribution of GIT1. *Journal of cell science* **119**, 2654-2666, doi:10.1242/jcs.02996 (2006).
138 Zhang, H., D. J. Webb, H. Asmussen, and A. F. Horwitz.. Synapse formation is regulated by the signaling adaptor GIT1. *J. Cell Biol.* **161**: 131–142 (2003).
139 Kuo, J. C., X. Han, C. T. Hsiao, J. R. Yates, III, and C.M.Waterman.. Analysis of the myosin-II-responsive focal adhesion proteome reveals a role for b-Pix in negative regulation of focal adhesion maturation. *Nat. Cell Biol.* **13**: 383–393 (2011).
140 Tedford, K., Steiner, M, Koshutin, S. Richter, K. Tech. L Eggers, Y., Jansing, I., Schilling K., Hauser, A. E., Korthals, M. Fischer, K. D. The opposing forces of shear flow and sphingosine-1-phosphate control marginal zone B cell shuttling. *Nature Communications* **8** (1):2261. doi: 10.1038/s41467-017-02482-4 (2017).
141 Tedford, K., Tech, L., Steiner, M., Korthals, M., Fischer, K. D. Analysis of Shear Flow-induced Migration of Murine Marginal Zone B Cells In Vitro. *Journal of Visualized Experiments* **141**, e58759, doi:10.3791/58759 (2018).
142 Za, L., C. Albertinazzi, S. Paris, M. Gagliani, C. Tacchetti, and I. de Curtis.. betaPIX controls cell motility and neurite extension by regulating the distribution of GIT1. *J. Cell Sci*. **119**: 2654–2666 (2006).
143 Nayal, A. *et al.* Paxillin phosphorylation at Ser273 localizes a GIT1-PIX-PAK complex and regulates adhesion and protrusion dynamics. *The Journal of cell biology* **173**, 587-589, doi:10.1083/jcb.200509075 (2006).
144 Pankov, R. *et al.* A Rac switch regulates random versus directionally persistent cell migration. *The Journal of cell biology* **170**, 793-802, doi:10.1083/jcb.200503152 (2005).
145 Baeyens, A., Fang, V., Chen, C. & Schwab, S.R. Exit Strategies: S1P Signaling and T Cell Migration. *Trends in immunology* **36**, 778-787 (2015).
146 Chun, J. & Brinkmann, V. A mechanistically novel, first oral therapy for multiple sclerosis: the development of fingolimod (FTY720, Gilenya). *Discovery medicine* **12**, 213-228 (2011).
147 Hla, T. & Brinkmann, V. Sphingosine 1-phosphate (S1P): Physiology and the effects of S1P receptor modulation. *Neurology* **76**, S3-8 (2011)

148 Pham, T.H., Okada, T., Matloubian, M., Lo, C.G. & Cyster, J.G. S1P1 receptor signaling overrides retention mediated by G alpha i-coupled receptors to promote T cell egress. *Immunity* **28**, 122-133 (2008).
149 Muppidi, J.R., Lu, E. & Cyster, J.G. The G protein-coupled receptor P2RY8 and follicular dendritic cells promote germinal center confinement of B cells, whereas S1PR3 can contribute to their dissemination. *The Journal of experimental medicine* **212**, 2213-2222 (2015).
150 Bialecki, E. *et al.* Role of marginal zone B lymphocytes in invariant NKT cell activation. *Journal of immunology* **182**, 6105-6113 (2009).
151 Puga, I. *et al.* B cell-helper neutrophils stimulate the diversification and production of immunoglobulin in the marginal zone of the spleen. *Nature immunology* **13**, 170-180 (2012).
152 Harris, G.L., Creason, M.B., Brulte, G.B. & Herr, D.R. In vitro and in vivo antagonism of a G protein-coupled receptor (S1P3) with a novel blocking monoclonal antibody. *PloS one* **7**, e35129 (2012).
153 Licht, T., Tsirulnikov, L., Reuveni, H., Yarnitzky, T. & Ben-Sasson, S.A. Induction of pro-angiogenic signaling by a synthetic peptide derived from the second intracellular loop of S1P3 (EDG3). *Blood* **102**, 2099-2107 (2003).
154 Jung, B. *et al.* Flow-regulated endothelial S1P receptor-1 signaling sustains vascular development. *Developmental cell* **23**, 600-610 (2012).
155 Rosenberger, G. & Kutsche, K. AlphaPIX and betaPIX and their role in focal adhesion formation. *European journal of cell biology* **85**, 265-274 (2006).
156 Dominguez, G.A., Anderson, N.R. & Hammer, D.A. The direction of migration of T-lymphocytes under flow depends upon which adhesion receptors are engaged. *Integrative biology : quantitative biosciences from nano to macro* **7**, 345-355 (2015).
157 Chigaev, A. & Sklar, L.A. Aspects of VLA-4 and LFA-1 regulation that may contribute to rolling and firm adhesion. *Frontiers in immunology* **3**, 242 (2012).
158 Ishii, I. *et al.* Selective loss of sphingosine 1-phosphate signaling with no obvious phenotypic abnormality in mice lacking its G protein-coupled receptor, LP(B3)/EDG-3. *The Journal of biological chemistry* **276**, 33697-33704 (2001).
159 ibidi. *ibidi Pump System.* https://ibidi.com/perfusion-system/112-ibidi-pump-system.html. (2018).
160 Sixt, M. & Raz, E. Editorial overview: Cell adhesion and migration. *Current opinion in cell biology* **36**, iv-vi (2015).
161 Guo F, Velu C, Grimes H, Zheng Y. Rho GTPase Cdc42 is essential for B-lymphocyte development and activation. *Blood* **114** (14):2909-2916 (2009).
162 Burbage, M. *et al.* Cdc42 is a key regulator of B cell differentiation and is required for antiviral humoral immunity. *The Journal of experimental medicine* **212 (1)**, 53-72 (2015).
163 Liu D, Winer B, Chou M, Tam H, Xu Y, An J, Gardner J, Cyster J. Dynamic encounters with red blood cells trigger splenic marginal zone B cell retention and function. *Nature Immunology* **25** (1):142-154 (2024).

9. Abbreviations

%	percent
°	degree
°C	degree Celsius
αPix	alpha-Pix or Cool-2 (clone out of library-2) or ARHGEF6
αPix/S1P3 dko	alpha-Pix / S1P-receptor-3 double knock-out
anti-	Designation for the specificity of an antibody
Arhgef6	gene for Rho guanine nucleotide exchange factor 6 = αPix or Cool-2
APC	Allophycocyanin
βPix	beta-Pix (Cool-1: clone out of library-1) or ARHGEF7
B220	Protein tyrosine phosphatase, receptor type C = CD45R = LCA
BAFF	B cell activating factor
BAFFR	BAFF receptor
BCA	B cell attracting protein = CXCL13
Bcl-xL	B cell lymphoma-extra large
BCR	B cell receptor
Bio	Biotin
BM	bone marrow
BSA	bovine serum albumin
BrdU	Bromodeoxyuridine
c-Rel	subunit of NF-kappaB complex
CCR	C-C chemokine receptor type
CD	cluster of differentiation
CD45.1	Tyrosine phosphatase = Ly5.1
CD45.2	Tyrosine phosphatase = Ly5.2
Cdc42	cell division cycle-42
CLP	common lymphoid progenitor
Cool	cloned out of library = Pix
CXCL	chemokine-(C-X-C motif)-ligand
CXCR	chemokine-(C-X-C motif)-receptor
Cy3	cyanin3
Dbl	diffuse B cell lymphoma

dko	double knock-out
DL-1	Delta-like-1
dyn	Dyne
EDTA	Ethylenediaminetetraacetic acid
et al.	Latin = „et alia“ = and others
FACS	fluorescence activated cell sorting
FAK	focal adhesion kinase
FCS	foetal calf serum
FDC	follicular dendritic cells
Fig.	figure
Fitc	Fluorescein isothiocyanate
FO	B cell follicle
FOB	follicular B cells
FSC	forward scatter
GDP	Guanosine diphosphate
GAP	GTPase activating protein
GDI	Guanosine nucleotide dissociation inhibitor
GEF	Guanine nucleotide exchange factor
GIT	G protein-coupled receptor kinase interacting (proteins)
Git-1	G protein-coupled receptor kinase interacting ArfGAP-1
Git-2	G protein-coupled receptor kinase interacting ArfGAP-2
GmbH	German: „Gesellschaft mit beschränkter Haftung“ = Company with limited liability
GRK	G-protein coupled receptor kinase
GTP	Guanosine triphosphate
GTPase	GTP hydrolysing enzyme
h	hour
HBSS	Hanks' Balanced Salt Solution
HEPES	4-(2-hydroxyethyl)-1-piperazineethanesulfonic acid
HSC	hematopoietic stem cell
iNKT	invariant natural killer T cells
i.e.	Latin: „id est“ = that means
ICAM	intercellular adhesion molecule 1
IF	immune fluorescence

IgA	Immune globulin
IM	immature
kDa	kilodalton
kg	kilogram
ko	knock-out
LFA-1	Lymphocyte function-associated antigen 1
LPS	Lipopolysaccharide
Ly5.1	= CD45.1
Ly5.2	= CD45.2
µg	microgram
µl	microliter
µm	micrometre
M	molar = mol/Liter
mAb	monoclonal antibody
MadCAM	mucosal vascular addressing cell adhesion molecule
MEF	mouse embryonic fibroblasts
MFI	mean fluorescence intensity
mg	milligram
MHC	major histocompatibility complex
MINT	Msx2-interacting nuclear target protein
min	minute
ml	millilitre
mm	millimetre
mM	millimolar
mRNA	messenger ribonucleic acid
MS	marginal sinus
MZ	marginal zone
MZB	marginal zone B cells
MZM	marginal zone macrophages
MZP	marginal zone precursor
n	count
NaCl	Sodium chloride
$NaHCO_3$	Sodium hydrogen carbonate
NH_4Cl	Ammonium chloride

NF-kappaB	nuclear factor kappa-light-chain-enhancer of activated B cells
nm	nanometre
nM	nanomolar
Nm	newton meter
Notch-2	neurogenic locus notch homolog protein 2
NTF	N-terminal fragment
p50	subunit of NF-kappaB complex
p50-REL	heterodimeric transcription factor of NK-kappaB pathway
p50-RELa	heterodimeric transcription factor of NK-kappaB pathway
p65	subunit of NF-kappaB complex, RELA
PALS	periarteriolar lymphoid sheath
PAK	p21 activated kinase
PBS	phosphate buffered saline
PE	Phycoerythrin
PeCy7	Phycoerythrin-cyanin7-conjugate
PerCP	Peridinin chlorophyll protein-Cyanine5.5
PIX	PAK interacting exchange factor
Rac	Ras related C3 botulinum toxin substrate
Ras	Rat Sarcoma Protein
RBC	Red blood cells
REL	c-Rel, subunit of NF-kappaB complex
RELA	p65, subunit of NF-kappaB complex
Rho	Ras homologue
RP	red pulp
RPMI	Rosswell Park Memorial Institute
S1P	Sphingosine-1-phosphate
S1PR1	Sphingosine-1-phosphate-receptor-1
S1PR3	Sphingosine-1-phosphate-receptor-3
SA	Streptavidin
SEM	standard error of the mean
SPF	specific pathogen free
SSC	sidewards Scatter
SDF-1α	stromal cell-derived factor 1 = CXCL12
sec	second

SIGN-R1	C-type lectin, CD209b
Src	sarcoma (oncogene)
SWAP70	switch-associated protein 70
t	time
Tab.	table
TCR	T cell receptor
TD	thymus dependent
TI-1	thymus independent-1
TI-2	thymus independent-2
TIRF	total internal reflection fluorescence
VCAM	vascular cell adhesion molecule 1
VLA-4	very late antigen-4
w/v	weight per volume
WT	wildtype

10. Declaration of honour

I hereby declare that I prepared this thesis without impermissible help of third parties and that none other than the indicated tools have been used; all sources of information are clearly marked, including my own publications.

In particular I have not consciously:

- Fabricated data or rejected undesired results
- Misused statistical methods with the aim of drawing other conclusions than those warranted by the available data
- Plagiarized external data or publications
- Presented the results of other researchers in a distorted way

I am aware that violations of copyright may lead to injunction and damage claims of the author and also to prosecution by the law enforcement authorities.

I hereby agree that the thesis may be reviewed for plagiarism by mean of electronic data processing.

This work has not yet been submitted as a doctoral thesis in the same or a similar form in Germany or in any other country. It has not yet been published as a whole.

Bad Liebenstein, 10-Feb-2025

Michael Steiner